To the Graduate Council:

I am submitting herewith a dissertation written by Su-Ming Chan entitled "Vaporization of Moving Water Droplets in Air at High Temperatures." I have examined the final copy of this dissertation for form and content and recommend that it be accepted in partial fulfillment of the requirements for the degree of Doctor of Philosophy, with a major in Chemical Engineering.

George C. Frazier

George C. Frazier, Major Professor

We have read this dissertation
and recommend its acceptance:

Joseph J. Perona

H. W. Haw

J. W. Hodgson

Zach D. Watson

Accepted for the Council:

Lew Minkel

Vice Provost
and Dean of The Graduate School

VAPORIZATION OF MOVING WATER DROPLETS IN AIR AT HIGH TEMPERATURES

A Dissertation

Presented for the

Doctor of Philosophy

Degree

The University of Tennessee, Knoxville

Su-Ming Chan

March 1986

ACKNOWLEDGEMENTS

The author wishes to acknowledge his major professor, Dr. G. C. Frazier, whose constant assistance and numerous helpful suggestions make this work possible.

The author also wishes to thank the dissertation committee, Dr. J. W. Hodgson, Dr. H. W. Hsu, Dr. J. J. Perona and Dr. J. S. Watson for their suggestions and revisions of the final edition.

ABSTRACT

The vaporization rate of small droplets may control processes as diverse as the combustion of liquid fuels, spray-drying, and humidification operations. However, there are very few experimental data in the literature for the vaporization of small, freely moving droplets in the ambient temperature range above a few hundred degrees centigrade. This investigation was therefore undertaken to obtain vaporization data on water droplets in the temperature range of 500°C-850°C. These data are used to evaluate certain vaporization models that previously have been tested primarily in the moderately low temperature range with data obtained principally from vaporization experiments on suspended droplets. A subsidiary objective was to determine whether or not dissolved gases affect the vaporization rate.

A uniformly sized water droplet stream was directed through an elevated temperature air stream, and droplet size was evaluated photographically. The droplets are about 260 μm to 300 μm in diameter, spaced within two to three diameters of one another. Reynolds numbers range from 7 to 17.

Experimentally determined vaporization rates are compared with results computed according to the modified Froessling model and the Large Flux model, each with different coefficient on the ventilation factors. Although data scatter precludes an unambiguous choice of vaporization model and ventilation factor, the Large Flux model

containing the ventilation factor correlation of Rowe, Claxton and Lewis gives the best agreement with the experimental results, the mean error in this case being only 0.6%. The extent of the agreement between the data and the model predictions suggests that droplet-droplet interaction effects are not important, even with the relatively close droplet spacings of these experiments. This result may be a consequence of the droplet train-air stream, cross-flow arrangement.

TABLE OF CONTENTS

CHAPTER		PAGE
1.	INTRODUCTION	1
2.	REVIEW OF LITERATURE	4
	2.1 Theory and Vaporization Models	4
	2.1.1 Vaporization under Stationary Conditions	
	2.1.2 Influence of Forced Convection	
	A. Froessling Model	
	B. Large Flux Model	
	2.1.3 Influence of Free Convection	
	2.1.4 Effect of Pressure	
	2.2 Experimental Investigations	21
	2.2.1 Stationary Droplets	
	2.2.2 Moving Droplets	
	2.2.3 Summary of Experimental Conditions	
3.	EQUIPMENT AND PROCEDURE	39
	3.1 Experimental Equipment	39
	3.1.1 Droplet Generating System	
	3.1.2 Water Storage and Delivery System	
	3.1.3 Air Supply System	
	3.1.4 Heating System	
	3.1.5 Photographic System	
	3.2 Experimental Procedures	46
	3.2.1 Droplets with Dissloved Gases	
	3.2.2 Droplets Formed from Degassed Water	
4.	RESULTS AND INTERPRETATION	49
	4.1 Characterization of the Experimental System	49
	4.1.1 The Hot Air Jet	
	A. Air Stream Temperature	
	B. Air Stream Velocity	
	4.1.2 The Droplet Train	
	4.2 Experimentally Determined Vaporization Rates	57
	4.2.1 Photographic Results	
	4.2.2 Vaporization Rate Evaluation	
	4.3 Comparison with the Modified Froessling Model	62
	4.3.1 Calculated Results	
	4.4 Comparison with the Large Flux Model	81
	4.5 Prediction of Vaporization Rates at Elevated Pressures	87
5.	DISCUSSION OF RESULTS	99
	5.1 Comparison of the Froessling and Large Flux Model Predictions, with Different Ventilation Factors	99

CHAPTER PAGE

5.2 Droplet-Droplet Interaction 100
5.3 Droplet Oscillation 103
5.4 Effect of Outgassing 103

6. SUMMARY AND CONCLUSIONS 105

7. RECOMMENDATIONS 109

LIST OF REFERENCES 111

APPENDIXES 117

A. DROPLET SIZE HISTORIES IN STILL AIR AND AT ROOM TEMPERATURE 118

B. THE PLOTS OF D^2 VS. t OF THE COMPLETE SET 120

C. COMPUTER PROGRAM OF FROESSLING MODEL 138

D. COMPUTER PROGRAM OF LARGE FLUX MODEL 148

E. PROPERTY VALUE EXPRESSIONS FOR THE AIR-WATER VAPOR SYSTEM 154

F. RAW VAPORIZATION DATA 158

VITA 192

LIST OF TABLES

TABLE PAGE

1. Comparison of experimental results from Bhogte and Mason with model calculations 31
2. Summary of experimental work 37
3. Correction of air temperature readings by the measurement of two sizes of thermocouple 53
4. Correlation coefficients of three regression equations for D^2 vs. t curves 63
5. Experimental results of present investigation 64
6. Calculated results 67
7. Summary of vaporization rates from Froessling model predictions 73
8. Errors between experimental vaporization rates and rates calculated according to the modified Froessling model 83
9. Summary of vaporization rates from Large Flux model predictions 86
10. Errors between experimental vaporization rates and rates calculated according to the Large Flux model 91

LIST OF FIGURES

FIGURE PAGE

1. Newly formed droplets oscillate, as can be seen from the deviation of these drops from a spherical shape 34
2. Schematic of the experimental system 40
3. Apparatus of degassed water supply system 42
4. Calibration curve of the air flow rotameter 44
5. Representative hot air stream temperature profiles 50
6. Thermocouple junction of 5 mil wire with a bead diameter of 0.065 cm 52
7. Thermocouple junction of 1 mil wire with a bead diameter of 0.015 cm 52
8. Temperature measurement of two different size thermocouples 55
9. Photograph of a representative water droplet train with magnification of about 19X 56
10. Typical plot of D^2 vs. t 59
11. Diagram of view factor derivation 70
12. Calculated view factor from a sphere to a noncoaxial disk with a radius of 1.25 inches. Diameter of the sphere is 300 μm 71
13. Flow sheet of computer program for Froessling model calculation 75
14. Comparison of experimental results with the modified Froessling vaporization model using the Froessling ventilation factor (Eq.(4-15)) 77
15. Comparison of experimental results with the modified Froessling vaporization model using the Ranz and Marshall ventilation factor (Eq.(4-16)) 78

FIGURE PAGE

16. Comparison of experimental results with the modified Froessling vaporization model using the Rowe et al. ventilation factor (Eq.(4-17)) 79

17. Comparison of experimental results with the modified Froessling vaporization model using the Lee and Ryley ventilation factor (Eq.(4-18)) 80

18. Experimental sequence number of the data points for model calculations vs. experimental results 82

19. Flow sheet of computer program for Large Flux model calculation 85

20. Comparison of experimental results with the Large Flux vaporization model using the Ranz and Marshall ventilation factor (Eq.(4-16)) 88

21. Comparison of experimental results with the Large Flux vaporization model using the Rowe et al. ventilation factor (Eq.(4-17)) 89

22. Comparison of experimental results with the Large Flux vaporization model using the Lee and Ryley ventilation factor (Eq.(4-18)) 90

23. Flow sheet of computer program for calculating droplet dimension changes as a function of time using Froessling model 93

24. Comparison of experimental and calculated vaporization histories of a water droplet at one atmosphere 95

25. Comparison of experimental and calculated vaporization histories of a water droplet at ten atmospheres 96

26. Comparison of experimental and calculated vaporization histories of a water droplet at twenty atmospheres 97

27. Variation of ignition delay time with droplet spacing (from Sangiovanni and Kesten(69)) 101

FIGURE PAGE

28. Section of a droplet train, showing location of the wake axis relative to the direction of the droplet motion (Run No.8) 102

LIST OF SYMBOLS

A	droplet surface area ($=4\pi r_o^2$)
a	absorptivity of droplet
B	transfer number, $Cp_A(Ta-Ts)/(\lambda_A-q^r/m)$
C	gas phase total molar concentration
Cp	heat capacity of gas
Cp_A	heat capacity of vapor
D_{AB}	binary diffusion coefficient of the vapor relative to the gaseous medium
D,Do,Df	droplet diameter, initial and final diameter
F	ventilation factor
F_{12}	view factor
Gr	Grashof number, $g\,\rho^2\beta(Ta-Ts)Do^3/\mu_m^2$
g	acceleration of gravity
h	convection heat transfer coefficient
h_m	convection heat transfer coefficient of mixture
h_x	mean heat transfer coefficient
h_{xm}	mean heat transfer coefficient of mixture
Ka,Kg,Kv	thermal conductivity of air, gas and mixture
Km	thermal conductivity of vapor-gas mixture
k_x	mean mass transfer coefficient
k_{xm}	mean mass transfer coefficient of mixture
Le´	modified Lewis Number, $\overline{Km}/(\overline{D}_{AB}\ \overline{Cp}_A\ \overline{CM}_A)$
M_A	molecular weight of vapor
Mexp	droplet vaporization flux obtained from experiments

Ms,ML	droplet vaporization flux calculated by Froessling model and Large Flux model respectively
m	mass of the droplet
$\dot{m}$	droplet mass vaporization rate
$\dot{m}_{exp}$	mass vaporization rate obtained from experiment
$\dot{m}_s, \dot{m}_L$	mass vaporization rate predicted by Froessling model and Large Flux model respectively
$\dot{m}o$	droplet mass vaporization rate in stagnant medium
$\dot{m}o'$	droplet mass vaporization rate in stagnant medium, neglecting radiation
N_{As}	mean flux of A into the gas phase
Nuo	Nusselt Number for overall heat transfer in the absence of mass transfer perturbation
Nu	Nusselt Number for overall heat transfer, h_m D/Km
P_A, P_∞	liquid vapor pressure at the surface and far away, respectively
Pc	critical pressure
Pt	total system pressure
Pr	Prandtl Number, $\overline{Cp}_A \overline{\mu_m} / \overline{Km}$
q_r	radiant heat transfer from thermocouple bead
q_h	convective heat transfer at the surface of a thermocouple bead
q^r	net radiant heat flux to the drop
qs^c	conductive heat flux into gas phase
qs^r	net radiant heat flux from the drop
R	gas constant
Ra	radiation absorbed by drop per unit time

Re	Reynolds Number, Ur D μ_m/ρ
r, r_o, r_f	droplet radius, initial droplet radius and flame radius
Sc	Schmidt Number, $\mu_m/\rho\ D_{AB}$
Sh	Sherwood Number, $k_x\ M_A\ D(Pt-P_A)/D_{AB}$
Ta	absolute gas temperature far from the droplet
Tb	absolute droplet boiling temperature
Tc	absolute critical temperature
T_{do}, T_{df}	absolute initial and final droplet temperature
Tf	absolute flame front temperature
Ts	absolute droplet surface temperature
T_{tc}	absolute thermocouple temperature
t	time
Ua	air stream velocity
Ud	droplet velocity
Ur	resultant velocity
X	droplet spacing, center to center
X_A	vapor mole fraction
X_{As}	vapor mole fraction at droplet surface
$X_{A\infty}$	vapor mole fraction far from droplet
x	coordinate position in the direction of droplet motion
Z	ratio of droplet spacing to droplet diameter
$(\bar{})$	integrated mean value of property
α	nondimensional parameter, $Cp_A\ Tb/\lambda_A$
α_t	turbulence intensity
ε	emissivity of thermocouple

θ_a	normalized temperature far from the droplet, Ta/Tb
θ_s	normalized temperature evaluated at droplet surface, Ts/Tb
λ_A	latent heat of vaporization of the liquid
μ_o, μ_b, μ_m	gas phase viscosity evaluated at surface, bulk temperature and vapor-gas mixture
ρ	gas phase density
ρ_A	density of droplet
σ	Stefan-Boltzmann constant
σ_{AB}	collision diameter for molecules of A and B
σ_d	surface tension of liquid
τ	temperature function in vapor pressure equation

CHAPTER 1

INTRODUCTION

Numerous experimental or theoretical studies related to droplet vaporization processes have been conducted in order to improve the basic understanding of phenomena of heat and mass transfer from a spherical body under various conditions for a variety of application interests. The experimental results found by various investigators are not always consistent, and their empirical correlations for convection effects are not always verified by others. Discrepancies are due to different methods of conducting experiments and analyzing data, and unknown variables in the system. In deriving quantitative interpretations, restrictions and simplifications were very often made that make it difficult to get the same results even when using a similar approach.

Recently, high rate vaporization processes are of the most interest in the application of high temperature operations. It is difficult to reach an agreement on high rate vaporization processes in view of the significant temperature dependence of physical and transport properties of fluids, the effect of high vaporization rate on transfer processes, and the influence of free convection and radiation. Thus, to develop a theory for wide application, an adequate experimental approach and method of measurement have to be achieved in order to provide reliable data which can serve as a basis against which models derived from simple vaporization theory

may be tested. Freely moving, uniformly-sized droplets have been employed in this work to overcome the difficulties and disadvantages associated with suspended and sprayed droplets. The approach is to generate a uniform droplet stream by inducing the breakup of a liquid jet coming from a fine capillary tube, and then directing the resulting droplet train across a hot air stream. The rate of vaporization can be determined from measurements made on photomicrographs. Preliminary studies seem to indicate that higher vaporization rates can be obtained through this approach than through others. Vaporization rates calculated from existing models were considerably lower, up to about two to four times, than those measured experimentally. This deviation was attributed to factors such as droplet oscillation, natural convection, internal circulation and outgassing of dissolved gases.

In this investigation, care was used in equipment setup, data collection and reduction in order to minimize possible experimental errors and to provide a set of reliable data for vaporization model verification. The basic models tested are the Froessling model and the Large Flux model. Each of these requires a ventilation factor, and several forms of this factor appear in the literature. The form selected for test in this work is proportional to the square root of the Reynolds number, but contains different values for the coefficient. The basic Froessling model, developed in the 1930's and based on relatively low temperature vaporization data, requires modification for use in the relatively high temperature range of the

present investigation. Modifications introduced include a correction for radiation and a method of averaging the gas properties over the relatively wide temperature range between the droplet surface and the ambient air.

CHAPTER 2

REVIEW OF LITERATURE

2.1 Theory and Vaporization Models

As discussed by Ingebo(36), fuels are frequently injected in liquid droplet form at a point upstream of a combustion zone. The concentration of the fuel vapor in the fuel-air stream entering this zone is determined in part by the rate of evaporation of the droplets. A number of studies have been performed on the burning of small liquid droplets(25,30,42,43,59), and have shown that the combustion rate depends on the evaporation rate of the droplets. This section will review the previous works relating to droplet evaporation. For purposes of this review, prior works have been limited to vaporization in stationary media and vaporization with convection. This latter category is of greater interest in the context of combustion, but the calculation methods used begin with models for vaporization under stationary conditions. That is, aside from a purely empirical correlation for "evaporation constant," one proceeds to calculate the vaporization rate in a stagnant medium by one model or the other, and then applies an empirical correlation to correct for the convective effect.

The evaporation mechanism of a single droplet always serves as a first indicator of the behavior of a fuel droplet in a spray. Several analytical models have been proposed in the literature for droplet vaporization rates under atmospheric pressure or higher, and

in a stagnant environment or in a moving stream. The evaporation of a liquid drop is essentially an operation in which heat for evaporation is transferred by conduction and convection from hot gases to the drop surface, from which vapor is transferred by diffusion and convection back into the gas stream. A model developed under these conditions can then be analyzed. In view of the complexity of the vaporization process, it has been necessary to invoke certain assumptions and restrictions in order to derive tractable results from first principles.

2.1.1 Vaporization under Stationary Conditions

The first theoretical work on mass transfer from a stationary, spherical particle was that of Maxwell(57). The same result was derived independently by Langmuir(44), and has been known as the Langmuir equation:

$$mo = 4 \pi r_o D_{AB} M_A (P_A - P_\infty)/R\ Ta \qquad (2\text{-}1)$$

This result is based on the assumption of a diffusion controlled process and ideal gas behavior for vapors in the entire vapor phase with vapor pressure of the liquid at the gas-liquid interface taken at its equilibrium value. This simple result is valid only when the ambient temperature is substantially the same as that of the individual drops(35). The temperature should be low in relation to the boiling point of the material of the drop. However, when the difference in temperature between the drop and the surrounding atmosphere is considerable, as during the combustion of a drop in a

fuel spray, the rate of decrease in size is determined by the rate of heat transfer to the drop. Thus, the evaporation process may be governed more by heat flow than by mass diffusion. Therefore, when solving the droplet evaporation problem, both the mass diffusion and heat flow problem have to be solved simultaneously.

In a strict sense, the droplet vaporization problem is inherently unsteady. However, a simultaneous solution to the mass and energy conservation equations for the unsteady droplet vaporization problem is not known. Numerous investigators have therefore proceeded by considering the problem to be quasi-steady, and considerable in sight has been gained concerning vaporization rates from approximate solutions of the steady mass and energy balances.

Under these considerations, Godsave(25) developed a model based on a single burning droplet surrounded concentrically by a spherical surface at a high temperature, namely the flame front. An energy balance equation was written across a differential change in radius around the drop for quasi-steady state conditions, assuming an evaporation controlled combustion process.

$$Kg\left(\frac{d^2T}{dr^2} + \frac{2}{r}\frac{dT}{dr}\right) = \frac{\dot{m}o\ Cp}{4\pi r^2}\frac{dT}{dr} \qquad (2\text{-}2)$$

Temperature distribution around the drop can then be solved after introducing the relevant boundary conditions with appropriate average physical properties.

$$\frac{Tf - T}{Tf - Ts} = \frac{e^{-E/r_f} - e^{-E/r}}{e^{-E/r_f} - e^{-E/r_o}} \qquad (2\text{-}3)$$

where $E = \dot{m}o\ Cp/4\pi Kg$

The evaporation rate was evaluated by setting the energy balance at the surface of the drop. It can be written as

$$\lambda_A\ \dot{m}o = 4\pi Kg\ r_o^{\,2}(dT/dr)_{r=ro} + q^r \qquad (2\text{-}4)$$

where the effect of radiation is taken into account by term q^r. By differentiating Eq.(2-3), substituting for $(dT/dr)_{r=ro}$, and solving for the evaporation rate, Godsave obtained:

$$\dot{m}o = \frac{4\pi Kg\ r_o\ r_f}{Cp\ (r_f - r_o)} \ln\left[1 + \frac{Cp(Tf - Ts)}{\lambda_A - q^r/\dot{m}o}\right] \qquad (2\text{-}5)$$

This equation gives the rate of evaporation as a function of temperature, taking into account the effect of the radial mass transfer, which is counter to the direction of heat flow.

When $Cp(Tf-Ts)/(\lambda_A-a)$ is small ($\ll 1$), the effect of mass transfer can be neglected and Eq.(2-5) reduced to

$$\dot{m}o = \frac{4\pi Kg\ r_o\ r_f}{(r_f-r_o)(\lambda_A-a)} (Tf - Ts) \qquad (2\text{-}6)$$

where $a=q^r/\dot{m}o$. Thus, the ratio, f, of the vaporization rate including the mass transfer effect to the rate due to heat transfer can be obtained by dividing Eq.(2-5) by Eq.(2-6):

$$f = \frac{\lambda_A - a}{Cp_A(Tf - Ts)} \ln\left[1 + \frac{Cp_A(Tf - Ts)}{\lambda_A - a}\right] \qquad (2\text{-}7)$$

This equation points out that in high temperature surroundings,

radial mass flow has an important effect on evaporation rate, and the equation derived for low temperature operation should not be used.

Furthermore, if $r_f >> r_o$, Eq.(2-6) can be reduced to

$$mo = \frac{4 \pi Kg \, r_o}{\lambda_A - a} (Tf - Ts) \qquad (2\text{-}8)$$

This equation is analogous to Langmuir's equation, Eq.(2-1), which describes the rate of mass transfer for a spherical particle in still air under conditions that gives low evaporation rates.

In Godsave's(25) experimental work, he suspended small droplets on a fine quartz fiber and photographically examined the burning droplet and flame front as a function of time. There were some discrepancies between the experimental results and the predictions of Eq.(2-5) due to lack of symmetry of the burning droplets, and questionable values used for the physical properties. However, the calculated values are of the same order as the experimental results.

Other analyses(63,72) are similar to that of Godsave in his treatment of a single droplet. Goldsmith and Penner(26) extended and generalized Godsave's analysis by using integrated forms for the energy and continuity equations, and deleting the assumptions that the thermal conductivity and the specific heat of fuel vapor are independent of the temperature. They wrote the energy balance across the droplet surface by the following expression without taking into account the effect of heat transfer by radiation.

$$4\pi r_o^2 \, Kg(dT/dr) = \dot{m}o \, \lambda_A + \dot{m}o \int_{Ts}^{Tf} Cp \, dT \qquad (2\text{-}9)$$

If it is assumed that Kg and Cp are independent of temperature, then Eq.(2-9) can be integrated between r_o and r_f and leads directly to Godsave's equation, Eq.(2-5), except for the radiation term. Instead, they introduced the following approximate expressions for Kg and Cp:

$$Kg = Kgs \, (T/Ts) \qquad (2\text{-}10)$$

where Kgs is the thermal conductivity of the fuel vapor and air mixture at the droplet surface temperature Ts, and

$$Cp = a + b\,T \qquad (2\text{-}11)$$

where a and b are constants. Eq.(2-9) was then solved to obtain

$$\dot{m}o = \frac{4\pi Kgs \, r_o \, r_f}{b \, Ts(r_f - r_o)} \left(\ln\left[1 + \left(\frac{Tf-Ts}{\lambda_A}\right)(a + (b/2)(Tf+Ts))\right] - \frac{a}{\xi} \ln \frac{(a+b\,Tf-\xi)(a+b\,Ts+\xi)}{(a+b\,Tf+\xi)(a+b\,Ts-\xi)}\right) \qquad (2\text{-}12)$$

where

$$\xi = [a^2 - 2b(\lambda_A - (b/2)Ts^2 - a\,Ts)]^{1/2}$$

Reference to Eqs.(2-5) and (2-12) shows that $\dot{m}o$ is determined provided r_f, radius of flame front, Ts, droplet surface temperature, and Tf, flame temperature are known. Godsave used a measured value of r_f and a reasonable value of Tf and showed a good agreement with observed mo by using Eq.(2-5). On the other hand, Goldsmith calculated r_f and Tf by ignoring the distortion of the flame front

from natural convection, and also showed good agreement with Godsave's experimental results even though the calculated values of r_f and Tf were larger than those used by Godsave. However, these two values compensated for each other in the calculation of $\dot{m}o$ by using Eq.(2-12) and obtained satisfactory agreement between calculated and observed values of $\dot{m}o$.

The theoretical analyses from both authors have suggested that, under burning conditions or under high temperature evaporation, a heat transfer mechanism determines the rate of decrease in droplet size. Eq.(2-5) and Eq.(2-12) can be used to calculate the evaporation rate of pure compounds into still atmosphere by assigning Ts and Tf as the droplet and ambient temperatures respectively and assuming $1/r_f << 1/r_o$. Spalding(72) and Ranz(63) have derived similar expressions for a stationary drop undergoing steady state evaporation. The uncertainty in those analyses comes from the droplet temperature adopted in the calculations. For droplets undergoing combustion or droplets evaporating in high temperature surroundings, usually the boiling point of the liquid is used.

A more general model was developed by Frazier and Chang (10,18) by solving the conservation equations of mass and energy simultaneously for a single droplet vaporizing in stagnant surroundings. This approach has eliminated the difficulty in empirically assigning a droplet temperature in the calculation. The assumptions upon which the analysis was based are: (1) the droplet

is vaporized under quasi-steady state conditions, (2) droplet temperature is uniformly distributed, (3) convection effects can be neglected, (4) the droplet is spherical, and (5) the droplet is of pure liquid.

Under these considerations, the continuity equation for a single component vapor diffusing through a stagnant film surrounding the spherical droplet can be written as

$$-\frac{4\pi r^2 \overline{CD}_{AB} M_A}{(1 - X_A)} \frac{dX_A}{dr} = \dot{m}o \qquad (2\text{-}13)$$

The energy conservation equation at the droplet surface for this system is written in the following form, which is similar to what were derived by Godsave(25), Goldsmith et al.(26) and Ranz(63):

$$4\pi r^2 \overline{Km}(dT/dr) - \dot{m}o\ \overline{Cp}_A(T - Ts) + 4\pi r^2 q^r = \lambda_A \dot{m}o \qquad (2\text{-}14)$$

where q^r is the radiation heat from the surroundings to the droplet surface, X_A is the vapor mole fraction in gas phase, and M_A is the molecular weight of component A.

After introducing the integrated average thermal and transport properties between the surface and surrounding, Eq.(2-13) and Eq.(2-14) can be integrated between droplet surface, $r=r_o$ at T=Ts and $r=\infty$ at T=Ta, obtaining the following results:

$$\frac{1 - X_{As}}{1 - X_{A\infty}} = F(\dot{m}o)^{Le'} \qquad (2\text{-}15)$$

$$\exp\left(-\frac{\dot{m}o\ \overline{Cp}_A}{4\pi r_o\ \overline{Km}}\right) = F(\dot{m}o) \qquad (2\text{-}16)$$

where

$$F(\dot{m}o) = \frac{1 - (A\, q^r/\dot{m}o\, \lambda_A)}{1 - (A\, q^r/\dot{m}o\, \lambda_A) + \alpha(\theta_a - \theta_s)} \qquad (2\text{-}17)$$

θ_s and θ_a are normalized temperature of Ts and Ta respectively, α is $(\overline{Cp}_A\ Tb)/\ \lambda_A$, and Le´ is modified Lewis number defined as $\overline{Km}/(\overline{CD}_{AB}\overline{Cp}_A M_A)$.

The vapor mole fraction at the droplet surface, X_{As}, and the normalized droplet surface temperature, θ_s, appearing in Eq.(2-15) and (2-17) may be related to a good approximation for moderately low vapor pressures and for quasi-equilibrium vaporization, in terms of the droplet vapor pressure and the definition of mole fraction in ideal gas mixtures. By employing the water vapor pressure equation given by Keenan and Keyes(38) for water vaporizing in air, the mole fraction of vapor at the surface can be written:

$$X_{As} = \frac{P_A}{Pt} = \frac{Pc}{Pt} \exp(\tau(\theta_s)) \qquad (2\text{-}18)$$

where $\tau(\theta_s)$ is an empirical function for determining the vapor pressure of the liquid (see Appendix E, Eq.(E-1)). This model has been verified(18); it is valid and agrees very well with available moderately high temperature vaporization data for suspended droplets vaporizing in stationary media.

2.1.2 Influence of Forced Convection

When a difference in relative velocity exists between the droplet and the ambient gas, the rate of vaporization will be

enhanced to some extent. The vaporization rate under forced convection has been studied theoretically (20,28,64,68), but because of the complexity of the phenomena, more reliable estimates are provided by semi-empirical equations.

Two approaches have been used. The general one is to model the drop as a spherically symmetric flow field, and then correct the results with an empirical correlation for convection, as will be discussed in Section 2.1.2.A. An alternative approach involves the use of film theory. Film thickness is selected to yield the heat and mass transfer rate. This approach will be discussed in Section 2.1.2.B.

A. Froessling Model

The earliest reported work concerning convection effects was by Froessling(20), who treated the evaporation of droplets at finite air velocity theoretically and experimentally. He found that the vaporization rate under forced convection could be written in the following form:

$$\dot{m} = \dot{m}o(1 + F(Re,Sc)) \qquad (2\text{-}19)$$

where $\dot{m}o$ is the vaporization rate in the absence of convection and F(Re,Sc), called the ventilation factor, is a correction factor for the forced convection of the medium relative to the droplet. According to his experimental results, he proposed the following correlation:

$$\dot{m} = \dot{m}o(1 + 0.276\ Re^{1/2}\ Sc^{1/3}) \qquad (2\text{-}20)$$

The vaporizatiopn rate under stagnant conditions, $\dot{m}o$, in Froessling's expression was calculated by using Langmuir's equation, Eq.(2-1), which is commonly used for describing the evaporation rate of spherical particles in still atmosphere under conditions giving low evaporation rates. Under high temperature surroundings, a more accurate vaporization rate, $\dot{m}$, was found(25,36) using the model based on a heat transfer equation such as those developed by Godsave(25), Goldsmith and Penner(26), Ranz(63) and Frazier and Chang(18).

The correction factor used in Froessling's form was based on a semi-empirical approach. A more general form was written as

$$\dot{m} = \dot{m}o(1 + K\ Re^n\ Sc^m) \qquad (2\text{-}21)$$

Numerous authors(20,64,68) have suggested that the exponents $n=1/2$ and $m=1/3$ for laminar flow and $2<Re<2000$. However, the coefficient, K, obtained by various investigators is different. Among others, Ranz and Marshall(64) proposed $K=0.3$, which has been widely accepted in the literature instead of 0.276 proposed by Froessling.

The mass transfer rate from a body in a moving fluid medium is usually expressed in terms of the Sherwood number, Sh. Eq.(2-21) can then be written in the following form:

$$Sh = Sh_{Re=0}\ (1 + K\ Re^n\ Sc^m) \qquad (2\text{-}22)$$

where $Sh_{Re=0}$ has a theoretical value of 2 for radial diffusion from a sphere into a quiescent medium. Thus, Eq.(2-22) can be written as

$$Sh = 2(1 + K\ Re^n\ Sc^m) \qquad (2\text{-}23)$$

Such a correlation is also suggested from the analogy of the mass

transfer process to the heat transfer process. In terms of the dimensionless form of heat transfer, the equation corresponding to Eq.(2-23) is

$$Nu = 2(1 + K\ Re^{n}\ Pr^{m}) \qquad (2\text{-}24)$$

The difference between Eq.(2-23) and Eq.(2-24) is usually negligible, but for the gas mixture a Prandtl number, Pr, can sometimes be evaluated more easily and more unambiguously than an effective Schmidt number, Sc.

Various correlations published by many other investigators will be discussed in Section 2.2.2.

B. Large Flux Model

The effect of mass transfer on the film thickness has been considered by a number of investigators(1,11,48,58), and is summarized by Bird et al.(6). Based on film theory, it indicates the effect of high mass transfer rate on transfer coefficients and draws attention to using transfer coefficients correlated from systems with negligible mass transfer rates. They obtained the following results for computing the mean fluxes into the gas phase under steady state:

$$N_{As} = k_{xm}\ \ln\left(1 + \frac{X_{As} - X_{A\infty}}{1 - X_{As}}\right) \qquad (2\text{-}25)$$

$$q_s^{c} = \frac{N_{As}\ Cp_A(Ts - Ta)}{\exp\left(\frac{N_{As}\ Cp_A}{h_m}\right) - 1} \qquad (2\text{-}26)$$

where k_{xm}, mass transfer coefficient, and h_m, heat transfer coefficient, were taken from the correlation evaluated under the system with a low mass transfer rate such as proposed by Ranz and Marshall(64).

In the calculation of the vaporization rate, an interfacial energy balance was written for vaporization of pure component A from an isothermal droplet. That is:

$$N_{As}\,\lambda_A + qs^c + qs^r = 0 \qquad (2\text{-}27)$$

By using the results from Eq.(2-25) and Eq.(2-26), the calculation can be initiated by choosing a trial value of Ts, the droplet temperature. The interfacial composition, X_{As}, is approximated as $X_{As}=P_A/Pt$. After few trial values of Ts, a satisfactory convergence can be given to find a proper Ts consistent with Eq.(2-27).

The mass and heat transfer coefficients under the influence of a high evaporation rate can also be evaluated from Eq.(2-25) and Eq.(2-26) with the definition

$$k^*_{xm} = \frac{N_{As} - X_{As}\,N_{As}}{(X_{As} - X_{A\infty})} \qquad (2\text{-}28)$$

and

$$h^*_m = qs^c/(Ts - Ta) \qquad (2\text{-}29)$$

By the substitution of the above relations, the effect of mass transfer on the transfer coefficients is given by

$$\frac{k^*_m}{k_m} = \frac{\ln\left(1 + \dfrac{X_{As} - X_{A\infty}}{1 - X_{As}}\right)}{\dfrac{X_{As} - X_{A\infty}}{1 - X_{As}}} = \frac{\ln(1+B_X)}{B_X} \qquad (2\text{-}30)$$

$$\frac{h^*_m}{h_m} = \frac{\ln\left(1 + \dfrac{N_{As}\, Cp_A(Ts - Ta)}{qs^c}\right)}{\dfrac{N_{As}\, Cp_A(Ts - Ta)}{qs^c}} = \frac{\ln(1 + B_T)}{B_T} \qquad (2\text{-}31)$$

where B_X and B_T are Spalding transfer number of mass transfer and heat transfer processes respectively. Eq.(2-30) and Eq.(2-31) can be written in a general form in terms of Nusselt or Sherwood number

$$Nu\ (Sh) = \frac{\ln(1+B)}{B}\, Nuo(Sho) \qquad (2\text{-}32)$$

to indicate the variation by neglecting the mass transfer effect.

2.1.3 Influence of Free Convection

When a temperature difference exists between the droplet and the fluid, free convection effects arise from the varying buoyancy forces around the body, and the transfer rates increase accordingly. Under the similar consideration of forced convection, the velocity in Reynolds number can be taken as a velocity component due to free convection parallel to gravity. This velocity component is taken equal to $(D\ g\ \Delta T)^{1/2}$. Reasoning from dynamic similarity, the

empirical correlation, Eq.(2-23) and Eq.(2-24), can be extended to account for the effect of free convection:

$$Nu = 2(1 + K\ Pr^{1/3}\ Gr^{1/4}) \qquad (2\text{-}33)$$

$$Sh = 2(1 + K\ Sc^{1/3}\ Gr^{1/4}) \qquad (2\text{-}34)$$

These equations have been experimentally verified(64) with K at a value of 0.6 with uncertainty in the low range of Grashof number.

The same approaches as described in Section 2.1.2 for forced convection have been applied to the effect of free convection, using free convection correlations.

Frazier and Chang(18) took the data in Yuge's paper(83) and confirmed the analysis by Mahoney(51) that K depends on $Gr^{1/2}$ as Gr becomes small. The data were fitted by:

$$Nu = 2(1 + F(Gr,Pr)) \qquad (2\text{-}35)$$

$$F(Gr,Pr) = A(Gr\ Pr)^{1/n}$$

where

$A = 0.3$, $n = 2$; $Gr < 4.22/Pr$

$A = 0.43$, $n = 4$; $4.22/Pr \lesssim Gr < 10^5$

These correlations have been used with a proposed modified Froessling model in testing high temperature experimental results under the influence of free convection(18). They successfully computed results within 15% of Hoffman and Gauvin's(33) data on water droplets vaporizing at high temperature. The same procedure has also been applied to Kobayasi's(43) experimental work. The agreement is within 6% over the range of $100^{\circ}C$-$595^{\circ}C$. When computed results are tested against the data of Nishiwaki(59), the agreement

is somewhat less good. However, in view of the insufficient information provided in those papers and several approximations made in the test model, the agreement is considered relatively good. Hence it is concluded that the correlations are valid over the range of conditions used.

Frazier(17) also used this model to explain the curvature in Houghton's(35) data. The agreement between theory and experiment is good in most cases, and indicates further that free convection effects are appreciable around droplets of the order of 500 μm in diameter or larger, but should be negligible for diameters less than a few hundred microns. From the above review, it seems that for better prediction of the evaporation rate of a stationary droplet, free convection should be taken into account for a large droplet.

2.1.4 Effect of Pressure

In the previous review, investigators interested in engineering operations considered the process of droplet vaporization at atmospheric or near atmospheric pressure. Applied to internal combustion engine operation, droplet evaporation at elevated pressures and temperatures is important because it is assumed to be the rate controlling process. However, the results based on the evaporation rate controlled model at high chamber pressures is questionable, because there is a lack of understanding concerning the evaporation phenomena in super critical gas environments (above the critical temperature and pressure of the liquid). This problem

has been considered by some investigators(32,77). Vaporization under super critical conditions is outside the scope of this work; thus no further discussion will be given here. The following concerns only the effect of pressure on the vaporization rate at pressures below the liquid droplet critical pressure.

To predict the evaporation rate of a droplet at atmospheric pressure, the model based on quasi-steady state has been mentioned; however, this theory is questionable for environmental gas pressures greater than one-tenth the critical pressure of the vaporizing liquid(9,73). A theory which accounts for the transient character of the phenomena has been developed(56,73). Besides, when a droplet evaporates at high total pressure, the effect of non-ideal behavior of gas mixture may become significant. Manrique and Borman(53) showed that, although it is valid at low pressure, a simplified expression for the local equilibrium mole fraction given by

$$X_{As}(D,T) = P_A(T(D,T))/Pt \qquad (2\text{-}36)$$

fails to be correct at high pressure. The effect of the pressure of the inert gas on the equilibrium vapor pressure of pure component A at the droplet temperature, and the non-ideal gas mixture should be taken into consideration. Thus information on the chemical potential and fugacity of components in the system must be known. Furthermore the solubility of inert gas in the liquid may not be negligible at elevated pressure and temperature conditions(46,56). The effect of non-ideal behavior of the gas mixture on the energy requirements for vaporization also has to be considered.

Based on these considerations, Matlosz, Leipziger and Torda(56) have derived a model and compared predictions with their experimental results, obtained for n-hextane droplets evaporating in nitrogen and also argon gas environments, at a temperature of 548°K and in a range of pressure from 6.8 to 102 atm. The agreement was reported to be fairly close. They concluded that at high pressures molecular mass transport may not be the controlling mechanism for the evaporation process because the effective mass diffusion coefficients were greater than the formula-calculated molecular mass diffusion coefficients.

In the Matlosz et al.(56) study, no attempt was made to correlate the dependence of the vaporization rate on pressure. Some investigators(27,30) have indicated that the mass transfer rate increases with pressure raised to a power between 0.2 and 0.5. On the other hand, Ingebo(37) reported experimental results showing a decrease in the vaporization rate with increasing pressure for relatively low ambient temperature. The pressure dependence of the vaporization rate has been attributed to free convection(3,72,79), and related to the temperature dependence of the latent heat of vaporization and the increase in droplet temperature with increasing pressure(37,40,67).

2.2 Experimental Investigations

Experimental studies of droplet evaporation or combustion of liquid fuels have employed the following methods: (1) Suspended Droplet Technique: A single droplet is suspended at the end of a

filament, and the rate of vaporization is determined by following the decrease in droplet diameter with time photographically. (2) Porous Sphere Technique: Fluid is fed internally to a stationary porous sphere at a rate which is just sufficient to maintain a liquid film on the surface of the sphere during the study. The evaporation rate is determined by measuring the rate at which fluid is supplied to the system. (3) Free Fall Droplet or Droplet Stream Technique: This method is more complex and requires more care, and obtaining detailed photographic results is more involved. However, it offers the advantages of small droplet size, noninterference from a suspension fiber, and the capability of using volatile fuels.

Many workers conducted droplet evaporation or burning in an attempt to confirm vaporization models and to evaluate the effect of convection. A linear relationship of D^2 with time is found by many authors(30,33,59,64) when the influence of free convection and radiation is small. This confirms the D^2 - Law from a theoretical derivation(25,26,72,79) for an isolated, pure component droplet evaporating or burning under steady state. The slope of the plot of D^2 against time is defined as the evaporation constant, which is a function of fluid properties and ambient conditions. The rate of mass change of the vaporizing or burning droplet can be written in terms of droplet size by the following equation:

$$\dot{m} = -\frac{d}{dt}\left(\frac{1}{6}\pi D^3 \rho_A\right)$$

$$= -\frac{1}{4}\pi \rho_A D \frac{dD^2}{dt} \qquad (2\text{-}37)$$

It can be rearranged and becomes:

$$\frac{dD^2}{dt} = K = -\frac{4\dot{m}}{\pi \rho_A D} \qquad (2\text{-}38)$$

The parameter K is frequently called the evaporation or burning rate constant. Eq.(2-38) provides a method of estimating droplet evaporization rate from the observation of the rate of decrease in size of the drop. This relationship has been discussed extensively by Law(45), who points out the limitations of D^2 - Law.

2.2.1 Stationary Droplets

Godsave(25), in his theoretical and experimental study of the single burning droplet suspended on the silica filament, obtained the constant values of dD^2/dt for sixteen principal fuels. From Eq.(2-5), the burning rate derived by Godsave(25) can be expressed as

$$\frac{dD^2}{dt} = K = \frac{8Kg}{\rho_A Cp_A(1 - r_o/r_f)} \ln\left(1 + \frac{Cp_A \Delta T}{\lambda_A - a}\right)$$

$$= \alpha \ln(1 + B) \qquad (2\text{-}39)$$

where $\alpha = 8Kg/(\rho_A Cp_A(1-r_o/r_f))$ and $B = Cp_A \Delta T/(\lambda_A - a)$ are characteristic constants of the burning system. Similar expressions have been derived for the evaporation constant by Spalding(72), Williams(78) and Law(45).

In their experimental work, Hall and Diederichsen(30) also found that the mass burning rate was proportional to the drop

diameter for all the fuels used over a pressure range of 1-120 atm. The same conclusions were found for water drop evaporation under pressure. However, in the case of water drops vaporizing under an intense heat radiation beam, the rate of evaporation is proportional to the second power of the diameter. A deviation from linear dependence on drop diameter is sometimes revealed when there is significant interference from free convection or forced convection. Frazier(17) pointed out the effect of free convection on droplet vaporization histories and explained the curvature in the data obtained by Houghton(35).

2.2.2 Moving Droplets

Many investigators have attempted to correlate heat and mass rates in terms of convection effects. Those results were commonly written in the general form as indicated in Eq.(2-23) and Eq.(2-24):

$$Nu(Sh) = 2(1 + K\ Re^{n}\ Pr(Sc)^{m}) \qquad (2\text{-}40)$$

However, due to the uncertainties of physical properties, especially in high temperature surroundings, and with investigators using different techniques, numerous correlations have been published. Their validity is limited to the circumstances where the empirical equations were obtained.

Froessling(20) reported the earliest works on the evaporation of low volatility materials under diffusion controlled situations. He experimented with drops of water, aniline, and nitrobenzene suspended in an air flow, and obtained a K value of 0.276, and 1/2

and 1/3 for n and m respectively to describe droplet evaporation under his experimental conditions (refer to Eq.(2-21)).

Later, Ranz and Marshall(64) made an extensive study of the rate of heat and mass transfer from liquid drops under forced convection and proposed the same form as Froessling's correlations except for a slightly higher value of K, 0.3. Their study was restricted to a Reynolds number in a range of 0 to 200, with suspended droplets, and air temperature up to 220°C. As they stated, the results of their study could be extrapolated up to a Reynolds number of about 1000, but these equations must be used with care at air temperatures beyond 300°C. This correlation has been widely accepted in many applications.

Many experimental results(62) have been interpreted on the basis of the dimensional analysis of Ranz and Marshall(64), and a numerical value of K around 0.3 has been obtained(23,47,52,68). Rowe et al.(68), having analyzed many recent experimental data pertaining to heat and mass transfer of a sphere in a gas flow with Re<2000, obtained an even higher value of K, which is 0.345. However, several authors indicated that the simple expression of Eq.(2-40) does not always apply. Other more complex forms were also proposed(41,60,81), indicating that the simple expression of K can not be applied when droplet internal circulation, oscillation and deformation are significant.

Ingebo(36) based a model on heat transfer as the controlling process, and proposed a correlation from experimental values for

nine liquids in a temperature range of 30°C to 500°C. He gave the expression in terms of the Nusselt number:

$$Nu = (Kg/Kv)^{1/2} (2 + 0.303 (Re\ Sc)^{0.6}) \qquad (2\text{-}41)$$

where Kg is thermal conductivity of the medium evaluated at average film temperature, and Kv is the thermal conductivity of the vapor evaluated at average film temperature. Froessling's correlation was also tested in Ingebo's report, which showed that the agreement is fairly good at room temperature, but is poor at elevated temperatures.

Richardson(65) developed a theory of mass transfer in turbulent, separated flows, using the Reynolds number exponent, n=2/3 (see Eq.(2-40)), for the wake region transfer. In his theory, as developed by White and Churchill(76), he introduced two terms containing the Reynolds number. One term covers the contribution of the forward flow region, and the other the contribution of the wake region. The proposed equation is

$$Nu = C_1\ Re^{1/2} + C_2\ Re^{2/3} \qquad (2\text{-}42)$$

and it represents well the results of Yuge(83), using C_1=0.32 and C_2=0.043.

As predicted by Keey and Glen(39), Rowe et al.(68) plotted the exponent of Reynolds number, Re, in mass transfer correlations against the Reynolds number and showed that the trend to approach higher values of m at higher Reynolds numbers can be explained by a transition from potential flow, in which $Sh \propto Re^{1/3}$, to fully turbulent flow, in which $Sh \propto Re^{2/3}$. Thus, the correlations with

different values of n for the two regions achieve significantly more reliable fits to the data.

Another different form was presented by Galloway and Sage(22), counting the effect of turbulence based on the Froessling correlation, Eq.(2-40). They correlated the overall mass transfer rates from spheres and obtained

$$K = 0.281 + 0.09035\ D^{1/2} + 0.0336\ \alpha_t(\alpha_t + 0.05)\ Re^{1/2} \qquad (2\text{-}43)$$

where α_t is turbulence intensity in the oncoming gas stream, and D is the sphere diameter. The equation indicates that K depends on sphere diameter as well as turbulence intensity.

At high rates of mass transfer process, Agoston(2) found that the effect of intense mass transfer was to reduce the Nusselt number to about one-fourth of the value predicted from pure heat transfer. Under this situation, Nusselt and Sherwood numbers can not be adequately correlated with Reynolds and Prandtl or Schmidt numbers alone. The blowing parameter, B, has to be included in a non-dimensional analysis of heat and mass transfer equations, i.e.

$$Nu = Nu(\ Re,\ Pr,\ B) \qquad (2\text{-}44)$$

$$Sh = Sh(\ Re,\ Sc,\ B) \qquad (2\text{-}45)$$

where B is defined as $Cp_A\ \Delta T/(\lambda_A - q^r/\dot{m})$. This effect is more obvious in the evaporation of hydrocarbon fuel droplets in high temperature surroundings when B is in a order of 10. Usually the Nusselt number correlation was derived by starting with a Nusselt number relation believed to be correct for low temperature differences, evaluating

fluid properties in that correlation at a reference temperature and a reference composition, and multiplying by a correction factor which is a function of the transfer number B only,

$$Nu = Nuo\ f(B) \tag{2-46}$$

In correlating their data, those who have measured Nusselt numbers for droplets in high temperature flows have used a variety of shielding functions, f(B), as well as various heat transfer correlations obtained at low mass transfer effect, Nu .

Downing(13) showed that the correlation of Ranz and Marshall must be modified, and proposed the modified form:

$$Nu = M\ N(1/B)\ \ln(1+B)(2 + 0.6\ Re^{1/2}\ Pr^{1/3}) \tag{2-47}$$

$$Sh = M(2 + 0.6\ Re^{1/2}\ Sc^{1/3}) \tag{2-48}$$

where $M = 1 - 0.4(1-Ts/Ta)$, and $N = 1 - 0.4(1-(1/B)\ln(1+B))$. This correction permits the experimental data to be correlated to an average deviation of 6%. One of the empirical correction factors involves the group $(1/B)\ln(1+B)$, and thus accounts for the heat taken up by the outwardly diffusing vapor (see Eq.(2-31)). The second factor involves the group Ts/Ta, and thus accounts for the fact that the film properties are considered to be constant while they are functions of temperature in the actual system. Hoffman and Ross(34,66) found that shielding function, f(B), of the form,

$$f(B) = \ln(1+B)/B \tag{2-49}$$

or

$$f(B) = (1+B)^{-0.6} \tag{2-50}$$

were equally satisfactory. By fitting their data with various

correlations of Nu through regression analysis for $0 < B < 3.5$ and $20 < Re < 400$, they obtained

$$Nu = \ln(1+B)(1/B)(2+0.355\ Pr^{1/3}\ Re^{0.59}), \quad (2\text{-}51)$$

$$Nu = \ln(1+B)(1/B)(2+0.346\ Pr^{1/3}\ (Re^{0.59} +0.01\ Re^{0.54})), \quad (2\text{-}52)$$

and

$$Nu = (1+B)^{-0.6}\ (2+0.369\ Pr^{1/3}\ Re^{0.58}) \quad (2\text{-}53)$$

Eisenklam et al.(15) found the best equation for their experimental data was,

$$Nu = (1 + B)^{-1}\ (2 + 1.6\ Re^{1/2}) \quad (2\text{-}54)$$

Yuen and Chen(82) used a correction factor, $(1+B)^{-1}$ for evaporation of either water or methanol into air with Ranz and Marshall's correlation. Yuen and Chen fitted the results obtained into the following relationship:

$$Nu = (1 + B)^{-1}\ (2 + 0.6\ Re^{1/2}\ Pr^{1/3}) \quad (2\text{-}55)$$

Harpole(31) proposed:

$$Nu = (1 + a\ B)^{-0.7}\ (1.56 + 0.626\ Pr^{0.38}\ Re^{1/2}) \quad (2\text{-}56)$$

where a is weighting factor for blowing parameter defined as the ratio of the free stream molecular weight to the molecular weight of the injectant, and claimed better predictions for Yuen and Chen(82) and Downing(13)s' data than by using their own correlations. Harpole also pointed out the significance of radiative transfer, which some investigators did not take into the definition of B, and of the property dependence of reference temperature and composition, especially at high temperature surroundings.

In order to obtain sufficient information on the vaporization rate of droplets moving in a high temperature air stream, Frazier and Hellier(19), Bhogte(5) and Mason(54) performed the experiments using a similar setup to that used in this investigation to generate a well defined stream of small droplets and to measure the size changes photographically. Their results were not consistent with the existing simple model predictions.

Frazier and Hellier(19) carried out experiments to investigate Freon-113 droplets passing through a 699°C air stream, and showed that the mass transfer coefficient of these droplets was higher by a factor of about four than the value obtained from the low temperature correlation of Ranz and Marshall(64), which was based on vaporization data from suspended droplets. When the vaporization rate of Freon-113 droplets was recomputed under these conditions according to the Large Flux model, the difference between experiment and the calculated value was about 33% (12). This discrepancy points up the need for caution when using low temperature and fixed droplet correlations. Later, similar studies with water droplets was conducted by Bhogte(5) and by Mason(54). In both investigations, the results led to the same conclusion, and suggested that the vaporization rates of freely moving droplets may be greater than those predicted by either the Froessling model (see Eq.(2-19)) or the Large Flux model (see Eq.(2-27)). The comparison of those results and the model predictions is listed in Table 1.

In order to determine whether or not the extraordinarily high

Table 1. Comparison of experimental results from Bhogte and Mason with model calculations.

	Ta, C	Do, μm	Re	Vaporization Rate, $x10^4$ g/sec $\dot{m}_{exp}$	$\dot{m}_s$	$\dot{m}_L$
*	684	270	5.2	0.9020	0.2950	0.3450
	697	296	7.6	0.9790	0.3600	0.4270
	735	291	5.8	1.5000	0.3610	0.4230
	788	287	3.8	0.5500	0.3630	0.4170
	792	266	4.7	1.7400	0.3500	0.4050
	868	291	5.1	1.3400	0.4430	0.5250
**	760	204	2.8	0.7080	0.2230	0.2630
	770	210	4.4	1.0500	0.2590	0.3030
	800	228	4.4	1.8170	0.2880	0.3460
	847	208	3.4	2.2790	0.2700	0.3240

* from Mason(1975)

** from Bhogte(1972)

experimental vaporization rates are real, an analytical effort was made to formulate and test a model of the Froessling type against other high (and low) temperature vaporization data in the literature. The model formulated is basically an extension of the Froessling form, in which the vaporization rate, $\dot{m}$, under the influence of both radiation and convection is computed according to,

$$\dot{m} = \dot{m}o\left(1 + \frac{\dot{m}o'}{\dot{m}o} F(Re,Pr)\right) \qquad (2\text{-}57)$$

where $\dot{m}o$ is the vaporization rate under stationary conditions but with radiation, $\dot{m}o'$ is the vaporization rate under stationary conditions without radiation, and F(Re,Pr) is the forced or free convection "ventilation factor," given by an experimentally determined correlation. Eq.(2-57) was tested against the available data(18) for stationary droplets and has been shown to agree well for a wide range of experimental conditions. Thus the high vaporization rates obtained from moving droplets are accepted as real. It is therefore considered that an additional factor, or factors, producing the enhanced vaporization effect observed by Bhogte and Mason may be required in the standard calculation models and correlations in order to account for this effect.

A number of plausible causes were proposed that could be responsible for this discrepancy between experimental results and model calculations.

(1) Droplet Oscillation

Some investigators(24,81) observed that under forced convection droplets oscillate about a mean shape. Owing to this effect, a new surface is continually formed, and the fluid inside the drop is considerably agitated, leading to an increase in heat and mass transfer from the drop. In this investigation, droplet oscillation was observed in the early stage of ejection through the hot air nozzle. Figure 1 shows this motion in newly formed droplets.

A careful re-examination of the drop train photograph from Mason's experiment(54) shows no measurable deviations from sphericity. Besides, the vaporization rate data shows no statistically significant correlation with the Weber number. The possibility of appreciably increased vaporization of these droplets due to droplet oscillation is discounted.

(2) Wake Effect

The Reynolds number of the droplets in these experiments is of the order of 10, well below the range where turbulence or boundary layer separation should be produced. One therefore concludes that the wake effect in this series of experiments should reduce, not increase, the vaporization rate from that calculated according to the above simple models.

(3) Free Convection

According to Mason's calculation, free convection was estimated to contribute no more than 5% to the calculated valuse.

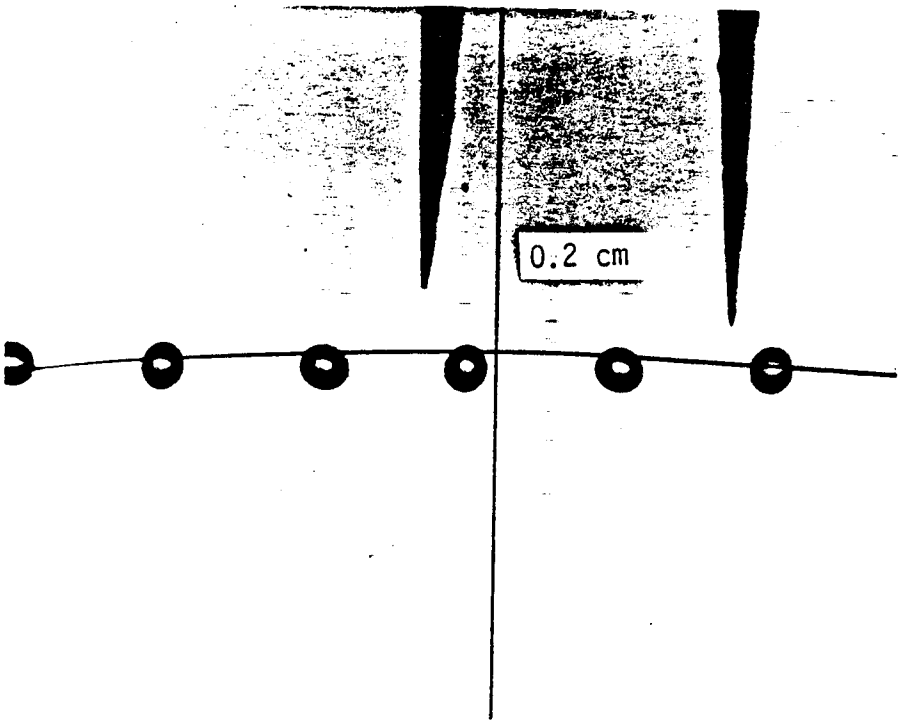


Figure 1. Newly formed droplets oscillate, as can be seen from the deviation of these drops from a spherical shape.

(4) Internal Circulation

Droplets circulate as they fall, as has been shown by Garner and Lane(24), and this circulation causes continual renewing of the surface, reduction of overall drag, thinning of the boundary layer and recession of the point of flow separation. Thus the internal circulation increases the values of the overall Nusselt and Sherwood numbers above those that would be expected in the absence of circulation. Downing(13) showed corrections ranging up to 8%. Whether an effect such as this is appreciable or not is unknown. Further analysis and experimentation is required to quantify this effect.

(5) Outgassing

In Bhogte(5) and Mason's(54) works, the distilled water was supplied to the capillary nozzle from a reservoir pressurized with nitrogen. Nitrogen pressures up to about one atmosphere gauge were required to produce the desired water flow rates through the nozzle. No effort was made to control or measure the amount of dissolved gas in the water during an experimental run.

In view of the nature of those experimental results, it was thought that outgassing of gases dissolved in the droplet might enhance evaporation. However, in the literature there appear to be no systematic theoretical or experimental investigations of the effect of dissolved gases on the vaporization rates of liquid droplets in high temperature gas streams. The present study is thus designed to investigate this effect with the considerations of other

possible factors listed above, and to provide a set of reliable data at temperatures sufficiently high ($500^{o}C$ to $860^{o}C$) so that the existing droplet data base is extended toward the direction of interest in various high temperature processes, such as liquid fuel combustion and drying in high temperature atmospheres.

2.2.3 Summary of Experimental Conditions

Some of the most representative experimental works of droplet evaporation discussed in Sections 2.2.1 and 2.2.2 are summarized in Table 2.

Table 2. Summary of experimental work.

Source	D, μm	Re	Ta, C	Method	Proposed Correlation
Houghton(35)	25-2600	0	3-32	S	
Hall & Diederichsen(30)	450-1000	0	coal gas temp.	S	
Godsave(25)	1400	0	combustion	S	
Nishiwaki(59)	700-900	0-30	250- 620	S	
Kobayasi(42)	700	0	100-600	S	
Hoffman & Gauvin(33)	400-1400	0	100-550	S	
Matlosz et al.(56)	720-1780	0	275	S	
Froessling(20)	100-2000	2-1300	20	S	$Sh=2(1+0.276\ Re^{1/2}Sc^{1/3})$
Ranz & Marshall(64)	600-1100	0-200	20-220	S	$Nu\ (Sh)=2(1+0.3\ Re^{1/2}Pr(Sc)^{1/3})$; $Nu\ (Sh)=2(1+0.3\ Gr^{1/4}Pr(Sc)^{1/3})$
Rowe et al.(68)	12500-38100	30-1800	20-26	P	$Nu\ (Sh)=2(1+0.345\ Re^{1/2}Pr^{1/3})$ (in air); $Nu\ (Sh)=2(1+0.395\ Re^{1/2}Pr^{1/3})$ (in water)
Lee & Ryley(47)	230-1130	64-250	superheated steam	S	$Nu=2(1+0.37\ Re^{1/2}Pr^{1/3})$
Beard & Pruppacher(4)	40-1200	0.2-370	0-40	F	$Sh=2(0.78+0.308\ Re^{1/2}Sc^{1/3})$ (for Re>2.5);
Kinzer & Gunn(41)	10-4200	0-2500	0-40	F	$Sh=2(1+0.108\ Re\ Sc^{2/3})$ (for Re<2.5)

Table 2. (continued)

Source	D, μm	Re	Ta, C	Method	Proposed Correlation
Ingebo(36)	6880	1100-2270	30-500	P	$Nu = 2(Ka/Kv)^{1/2}(1+0.152\ (Re\ Sc)^{0.6})$
Yao & Schrock(81)	3000-6000	10	23	F	$Nu\ (Sc) = 2(1+0.3\ Re^{1/2}Pr^{1/3}G(x))$; where $G(x) = 25(x/D)^{-0.7}$ for $10<x/D<600$; $3mm<D<6mm$
Downing(13)	1000	24-325	27-340	S	$Nu = 2MN(1/B)\ln(1+B)(1+0.3\ Re^{1/2}Pr^{1/3})$; $Sh = 2M(1+0.3\ Re^{1/2}Sc^{1/3})$; where $M = 1-0.4(1-Ts/Ta)$; $N = 1-0.4(1-(1/B)\ln(1+B))$
Ross & Hoffman(66)	500-2000	40-200	120-315	S	$Nu = 2\ \ln(1+B)(1/B)(1+0.1775\ Re^{0.59}Pr^{1/3})$; $Nu = 2\ \ln(1+B)(1/B)(1+0.173\ Pr^{1/3}(Re^{0.59}+0.01\ Re^{0.54}))$; $Nu = 2(1+B)^{-0.6}(1+0.1845\ Re^{0.58}Pr^{1/3})$
Eisenklan et al.(15)	25-500	0.01-15	200-600	F	$Nu = 2(1+B)^{-1}(1+0.8\ Re^{1/2})$ (for evaporation)
Yuen & Chen(82)	6500	200-2000	150-960	P	$Nu = 2(1+B)^{-1}(1+0.3\ Re^{1/2}Pr^{1/3})$
Harpole(31)	re-evaluate the data from (13), (66), (15) & (82)				$Nu = 2(1+aB)^{-0.7}(0.78+0.313\ Pr^{0.38}Re^{1/2})$; where a is weighting factor for blowing parameter

S = Suspended Droplet

P = Porous Sphere

F = Free Fall or Free Stream Droplet

CHAPTER 3

EQUIPMENT AND PROCEDURE

3.1 Experimental Equipment

A schematic diagram of the apparatus used in this study is shown in Figure 2. The purpose of this setup is to measure the diameter of a stream of free moving droplets vaporizing in a hot air stream. Essentially, the setup consists of a droplet generating system, a water storage and delivery system, an air supply system, a heating system and a photographic system. They will be discussed separately below.

3.1.1 Droplet Generating System

Water droplets are generated by the induced breakup of a water jet emanating from a fine capillary tube having 0.0065 inch I.D. that produced droplets of about 300 μm. The breakup is induced by longitudinal vibrations generated in the capillary by a sonic driver, Universat Sound model ID-30, having a frequency response range of 87-7500 HZ which is driven by an audio generator, Electrical Instrument Co. model 377, and an amplifier, Altec model 1570B. The signal from the audio generator is stabilized by a voltage regulator, Sorenson and Co. model 1000. A fine capillary tube is soldered into a standard injection needle, which can be carried by a standard injection needle holder soldered at the outlet end of the transmission chamber. A cooling coil is also soldered on

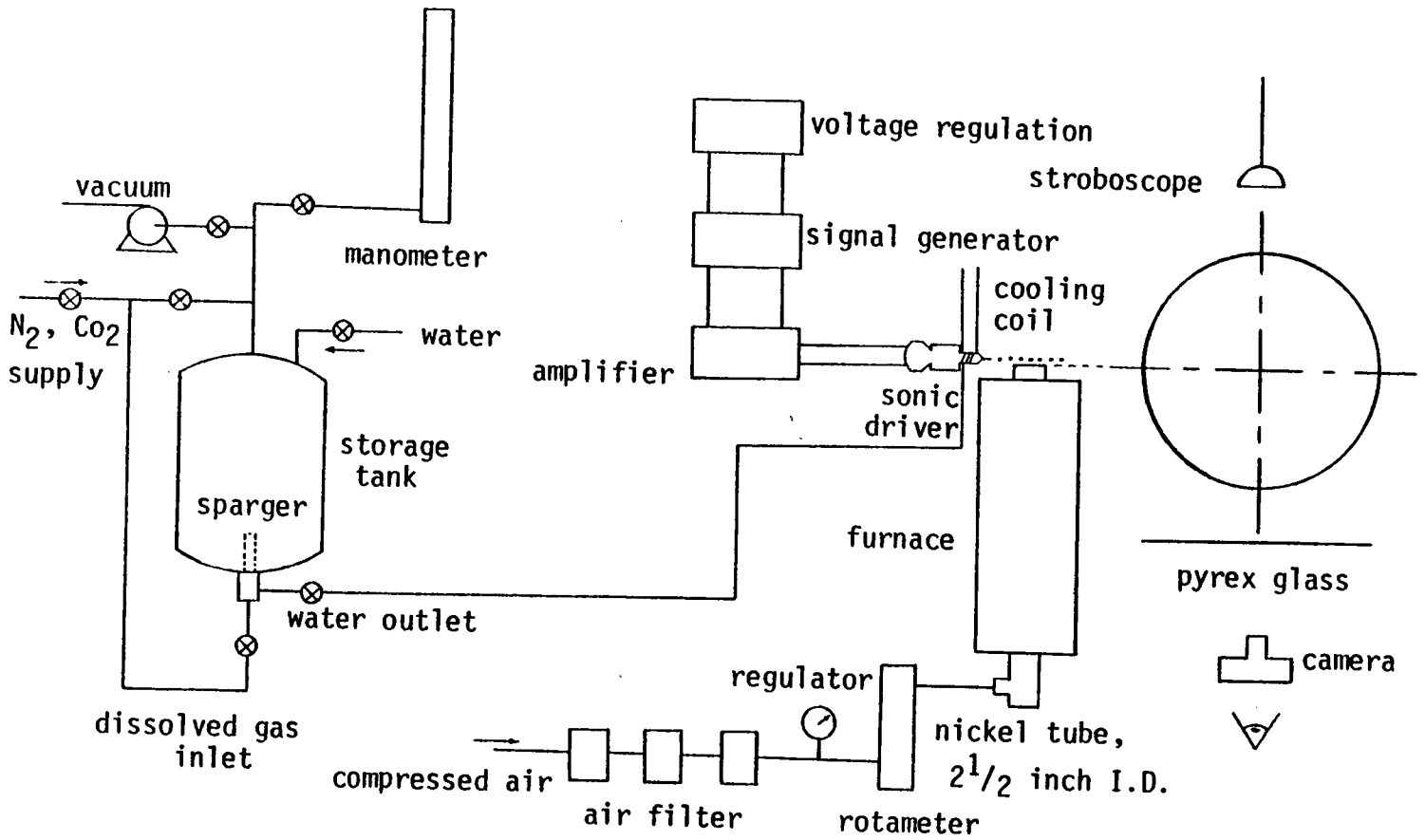


Figure 2. Schematic of the experimental system.

the outside of the transmission chamber to prevent heat from transferring to the liquid in the chamber.

3.1.2 Water Storage and Delivery System

Two types of water storage and delivery systems are provided, one for water with dissolved gases and one for degassed water. The storage tank for water with dissolved has a capacity of about 0.5 cubic foot, as shown in Figure 2, and is equipped with tube lines and valves to provide water inlet and outlet and a gas path for purging, vacuuming and pressurizing. Gases are dissolved by pressurizing the desired gases from the bottom of the tank through a porous ceramic sparger into the water phase. With this arrangement, water is delivered to the transmission chamber by pressurizing the tank with the same gas as that dissolved in the water.

For degassed water, another unit is made from a 9 15/16 inches O.D. and 9 7/16 inches I.D. acrylic cylinder having a capacity of 0.5 cubic foot, as shown in Figure 3, to replace the storage tank in Figure 2. In this unit, the bladder prevents the contamination of degassed water with gases while pressurizing the bladder to deliver water to the transmission chamber. Pressure is measured with a mercury manometer and held constant to provide a steady stream of droplets, which are ejected from the capillary and pass horizontally through a hot air stream near the exit of a vertically mounted tubular furnace.

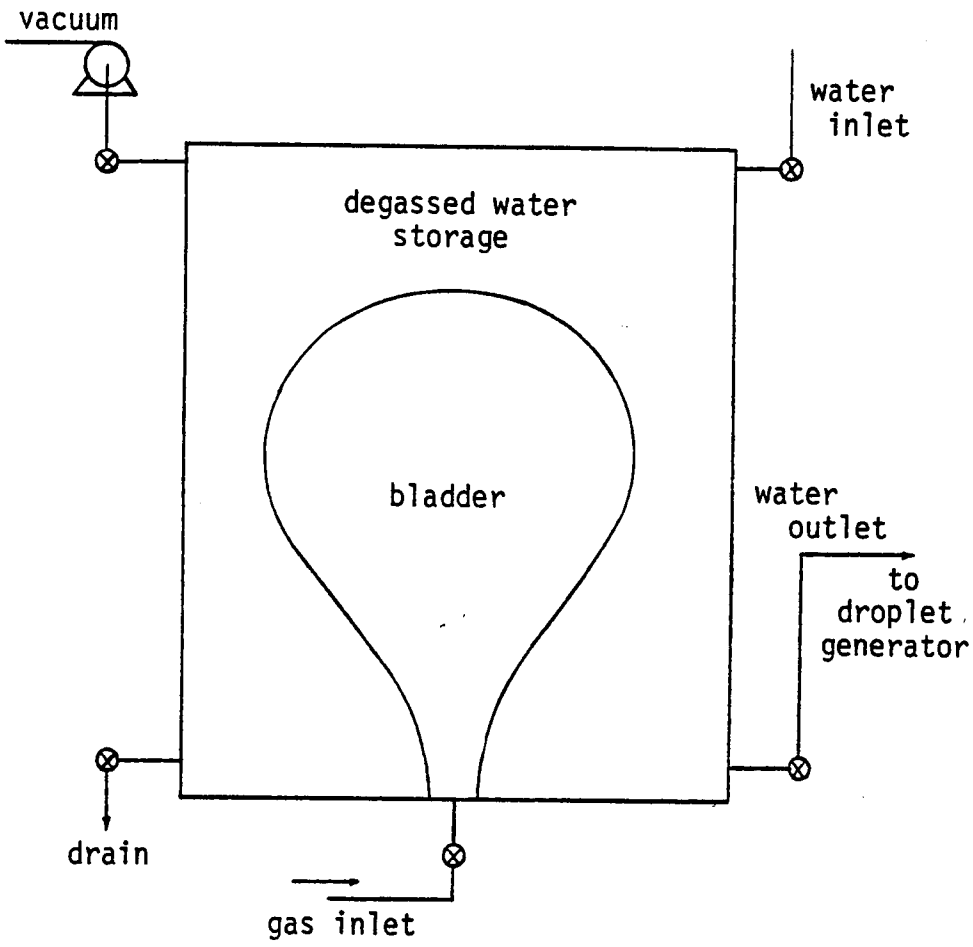


Figure 3. Apparatus of degassed water supply system.

3.1.3 Air Supply System

Compressed air at 120 psig is used for the air stream which, to knock off water and grease, passes through a Hannifin Crown Filter F-103, a pressure vessel packed with filter paper and a fine filter, Filter Manufacturing Company Style No.6. The air stream is regulated using a Moor nullmatic valve model 41-30F. Flow rate is measured by an inline rotameter, Brooks model 1111, which has been calibrated by a setup consisting of a Meriam Laminar Flow Element, model 50MC2-2F, and an inclined manometer, model Meriam 40HE35. Figure 4 shows the calibration curve of the flow rates read from the rotameter.

3.1.4. Heating System

The 2 1/2 inches I.D. nickel tube is heated by two 2575 watt furnaces, Electric Co. model Hevi Duty, which are individually controlled by two seven Kva variacs. In order to enhance the heat transfer between the tube and the air stream, the tube is filled with 1/2 inch ceramic Rashing rings for 2/3 of the tube and with 1/4 inch rings for rest of the space. To produce a uniform air velocity profile at the exit of the tube, three 100 mesh nickel screens, separated by three 2 1/2 inches I.D. nickel rings, are placed inside the tube normal to the air flow.

Air stream temperature is measured with a 5 mil Pt-Pt,13% Rh thermocouple mounted on a three-way sliding support stand fixed on the furnace support frame. Using an ice bath as the reference

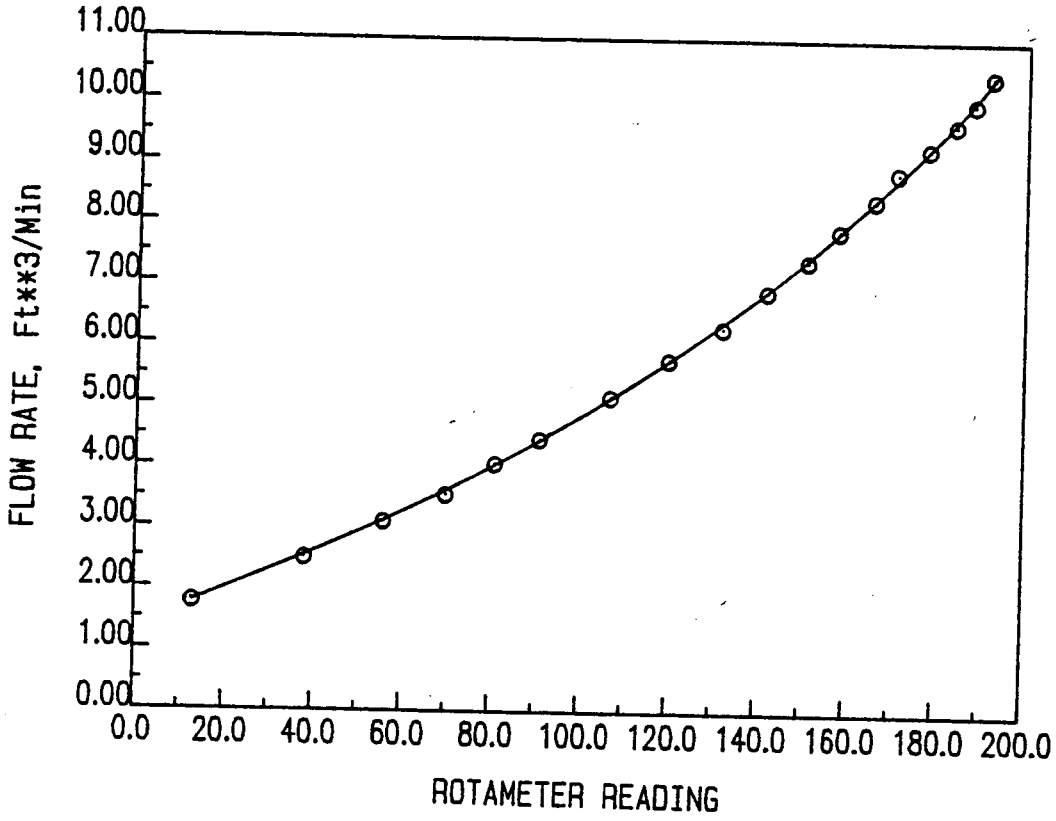


Figure 4. Calibration curve of the air flow rotameter.

junction, thermocouple potential difference is measured with a Leeds-Northrup potentiometer and recorded on a Heath chart recorder. A reference position indicator is also attached to the three-way sliding stand beside the thermocouple.

3.1.5 Photographic System

The changes in droplet diameter are recorded using a Graphic View camera mounted on a two-way sliding stand supported by the furnace frame. The lateral motion of the camera is parallel to the droplet stream and to the motion of the reference position indicator. By reading the scales attached to both the camera and the reference position indicator stands, it can be assured that the camera and the reference position indicator move in the same path. With the cross mark built in the microscope lens attached to the camera, the exact location of each droplet can be determined. A stroboscope, General Radio Company Type 1531 Strobotac, is located in front of the camera to stop the motion of droplets and to illuminate the film by a single flash. The camera lens is protected from heat by placing a piece of Pyrex glass between the lens and the hot air stream. Kodak Plus-X Pan professional film, 4147 ester thick, fine grain, is used in photographing.

3.2 Experimental Procedures

3.2.1 Droplets with Dissolved Gases

In this study, distilled water is the only liquid investigated. To release the gases dissolved in the water before a run, a degassing process is performed by a vacuum pump. Nitrogen or carbon dioxide is then sparged gradually into the tank from the bottom until the operation pressure is reached. In the meantime, air flow is set at a predetermined level and heated by increasing current in steps to both furnaces through two variacs. The temperature of the air stream is recorded on a chart recorder. When a desired temperature is reached and maintained constant, temperature profiles across the tube diameter at 0.25 inch and 0.5 inch above the tube rim are measured. The region of uniform temperature profile is then determined. This region is the working zone for taking droplet evaporation data. Air temperatures ranging from 500°C to 860°C are used in this study. Between 0.25 inch and 0.5 inch above the tube rim, the maximum temperature variation is no more than three degrees centigrade.

The storage tank is then pressurized by closing the gas valve to the sparger and opening the gas valve to the top of the tank to inject water into the transmission chamber and to introduce the water stream into the hot air stream through the capillary. Any air trapped in the transmission chamber is purged, and the water previously left in the connection tube is flushed through the purge

valve located at the top of the chamber. The water flow rate is determined by adjusting the gas pressure applied to the tank. In most cases, a pressure of about nine inches Hg generates a stream of uniform and stable droplets with a high degree of sphericity and sufficient residence time in the hot air stream.

The stream of water droplets is generated by adjusting the audio generator to a suitable frequency. In this investigation, frequency of about 3500 HZ is observed to produce the most stable and desirable droplet stream. The trajectory of the droplet stream is adjusted to 0.25 inch above the tube rim across the diameter of the tube and parallel to the lateral motion of the camera. The reference position indicator is set right on the top of the droplet stream so that both can be focused on each plate at same distance.

For taking pictures, on each run, the reference position indicator and camera are moved together and parallel at 0.5 cm intervals. The span of the indicator shown on each plate is also used to determine the magnification of the individual plate. The location of the droplets can be calculated from the sequence number of the plate and the position of the indicator on the film. Droplet motion is stopped and recorded photographically by opening the camera shutter for a single flash of the stroboscope. On each run a series of twelve photographs is made to cover the entire region of the hot air zone; however, only the plates taken at the location of uniform temperature profile are used to evaluate droplet size

changes. Besides, only the droplets on the center part of each plate that appeared to be clear and spherical were accepted.

3.2.2 Droplets Formed from Degassed Water

Except for using a different storage tank, the procedures are similar to that of the previous case. After filling the tank with distilled water preceeding a run, a vacuum process to prepare the degassed water is done which takes about five minutes. Afterward, water is delivered to the transmission chamber at a desired rate by pressurizing the bladder inside the tank. The bladder serves to separate the degassed water and gas while pressurizing the bladder to push water out of the tank.

Droplet diameters are measured from the photographic negatives using a Leeds-Northrup Microdensitometer. The reproducibility and reliability of this technique have been examined from the preliminary trials for both systems by ejecting a droplet stream across the tube diameter at room temperature without blowing air on droplet stream. Under this condition, droplet vaporization can be ignored and the accuracy of the analytical technique can be determined. Two sets of results plotted in terms of droplet diameter against time are collected in Appendix A. It can be found that the mean diameter of the droplets stay at an average value with a deviation of about 3%. This is due to the size variation of the droplets generated from the sonic driver and the techniques involved in analysis.

CHAPTER 4

RESULTS AND INTERPRETATION

4.1 Characterization of the Experimental System

4.1.1 The Hot Air Jet

A. Air Stream Temperature

Air stream temperature was measured by a Pt-Pt,13% Rh thermocouple constructed from 5 mil (0.005 inch) wire. The temperature profile across the furnace tube was thus obtained, as shown in Figure 5. In this figure, temperatures of three typical runs are plotted. It indicates that the temperature profiles are essentially uniform across the tube about 1 cm from the rim. The measured temperatures were then corrected for the effect of radiation transfering from the thermocouple junction.

Based on the energy balance on the surface of the thermocouple junction obtained by equating heat transfer from the hot air stream to the junction with heat radiated from the junction to the surrounding, and neglecting heat radiated from the screen inside the pipe,

$$q_h = q_r \qquad (4\text{-}1)$$

where

$$q_h = h(Ta - T_{tc}) \qquad (4\text{-}2)$$

and

$$q_r = \varepsilon \sigma T_{tc}^{4} \qquad (4\text{-}3)$$

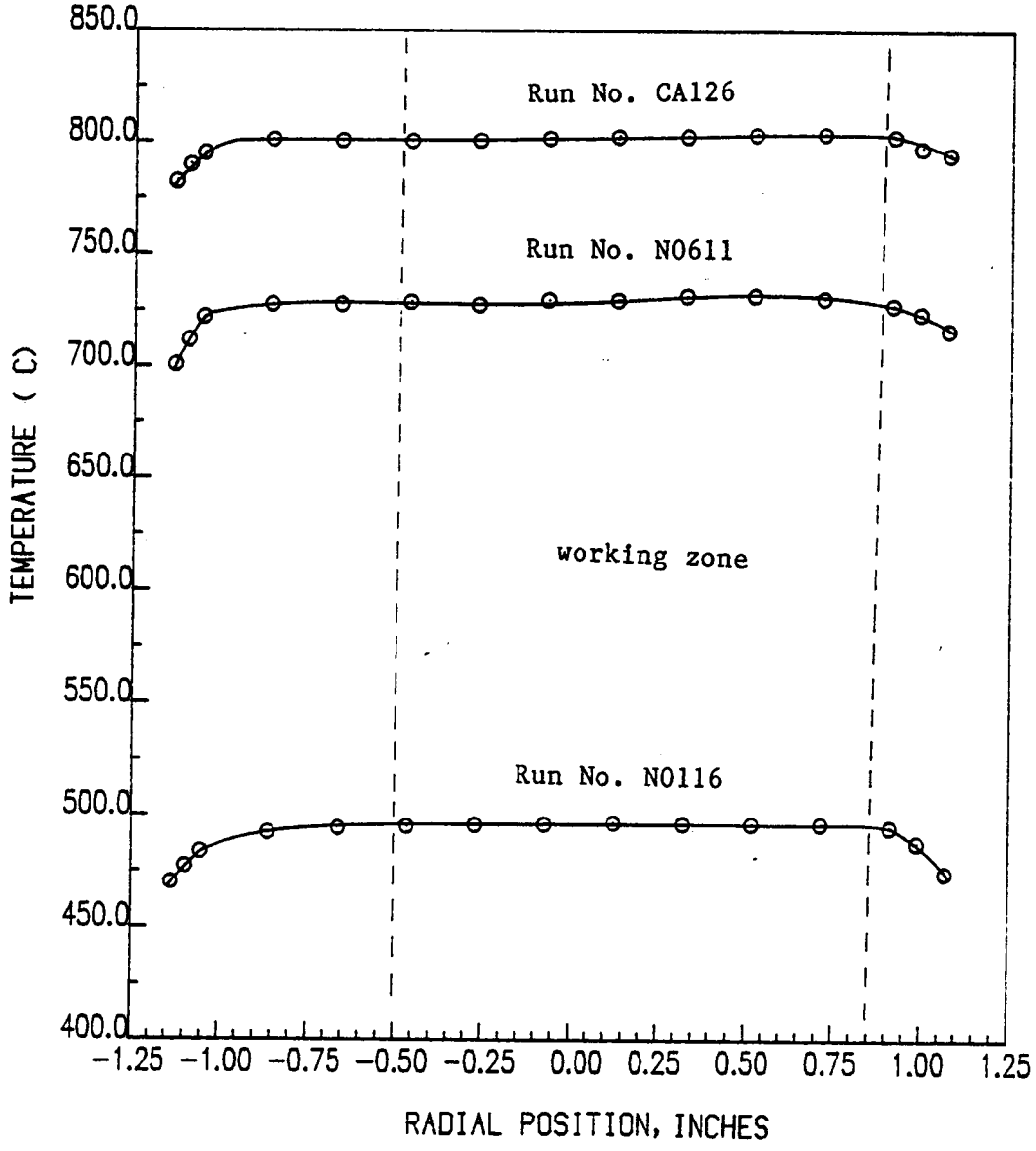


Figure 5. Representative hot air stream temperature profiles.

the following equation can be derived and used to calculate the corrected air temperature:

$$Ta = T_{tc} + \frac{\varepsilon \sigma}{h} T_{tc}^{4} \qquad (4\text{-}4)$$

where h, heat transfer coefficient, was determined from the correlation proposed by Whitaker(75):

$$Nuo = \frac{h\ D}{Ka}$$

$$= 2 + (0.4\ Re^{1/2} + 0.06\ Re^{2/3})\ Pr^{0.4}\ (\mu_b/\mu_o)^{1/4} \qquad (4\text{-}5)$$

One may consider the thermocouple junction as a spherical bead with a diameter D (see Figure 6). In view of the uncertainty of the emissivity of the thermocouple used in this study, 5 mil and 1 mil thermocouple wires with bead diameters of 0.065 cm and 0.015 cm respectively (see Figure 6 and 7) were used to measure a series of air stream temperatures simutaneously, and then the actual air stream temperatures, Ta, were calculated from Eq.(4-4) by searching for a value of ε until the results of both thermocouples reached the best agreement for the entire range of temperature measurements. The value of ε was found to be 0.3, compared with the literature value(61) of about 0.15 to 0.27 in this temperature range for a pure unoxidized platinum filament. This value of 0.3 gives fairly good agreement between the two thermocouples, as shown in Table 3, where T_{tc1} and T_{tc2} represent the measured temperatures from 1 mil and 5 mil wires respectively, and Ta_1 and Ta_2 represent the corresponding corrected air stream temperatures. The measured temperatures from

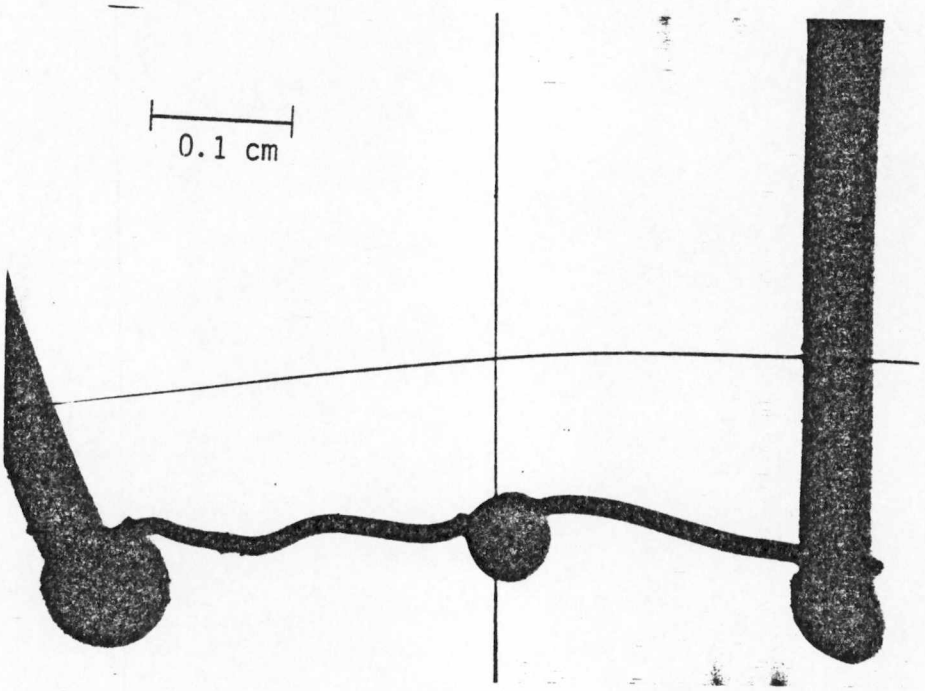


Figure 6. Thermocouple junction of 5 mil wire with a bead diameter of 0.065 cm.

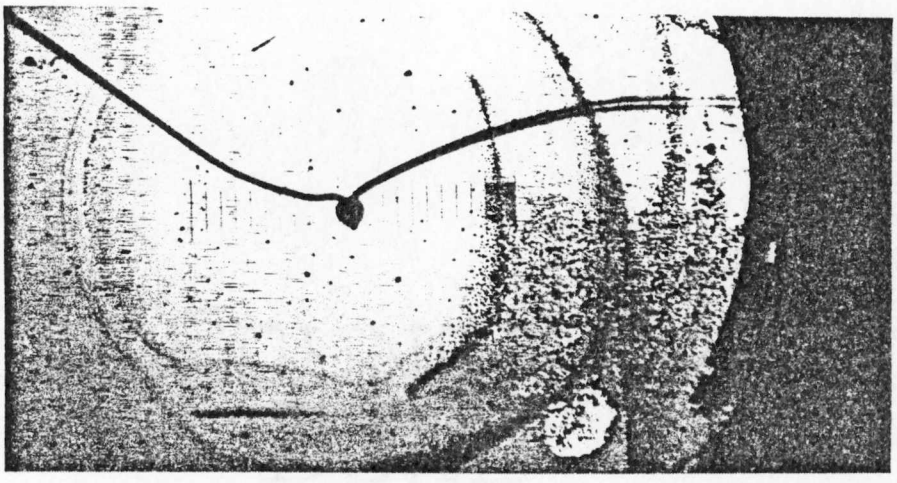


Figure 7. Thermocouple junction of 1 mil wire with a bead diameter of 0.015 cm.

Table 3. Correction of air temperature readings by the measurement of two sizes of thermocouple.[a]

Measured Air Temp., C		Corrected Air Temp.[b], C	
Ttc1	Ttc2	Ta1	Ta2
405	396	409.0	408.0
533	518	540.0	539.2
610	591	619.5	619.5
652	630	663.1	663.0
772	740	788.6	788.6
816	780	835.1	835.4

[a] Bead diameter of thermocouple 1 is 1 mil; that of thermocouple 2 is 5 mil.

[b] Using an emissivity of 0.3.

both thermocouples , T_{tc1} and T_{tc2}, which can be correlated in a straight line, are also plotted in Figure 8. The measured temperatures of 33 runs have been corrected and yielded a temperature range from 500°C to 860°C for the experimental work reported on here.

B. Air Stream Velocity

Air stream velocity, Ua, was determined from the reading of a calibrated rotameter mounted in the inlet of the air stream line. A uniform, laminar, air velocity profile at the exit of the furnace tube was produced by the use of a series of three 100 mesh nickel screens placed in the furnace tube normal to the air flow. The details of this technique of flow smoothing have been described by Walker and Westenberg(74). In this experiment, air velocity in a range of 136 to 205 cm/sec was obtained, and the Reynolds numbers based on the screen grid diameter at the corresponding air stream velocity were 1.9 and 3.1 respectively. These values are well below the critical value of 40 for the generation of turbulence by screens(71), so, in this investigation, the flow was laminar in the working zone.

4.1.2 The Droplet Train

Figure 9 shows a typical photograph, with a magnification of about nineteen, of a droplet train during a run. In this investigation, the frequency of the sonic driver was set at 3500 HZ to produce, through the entire working zone, the most stable droplet

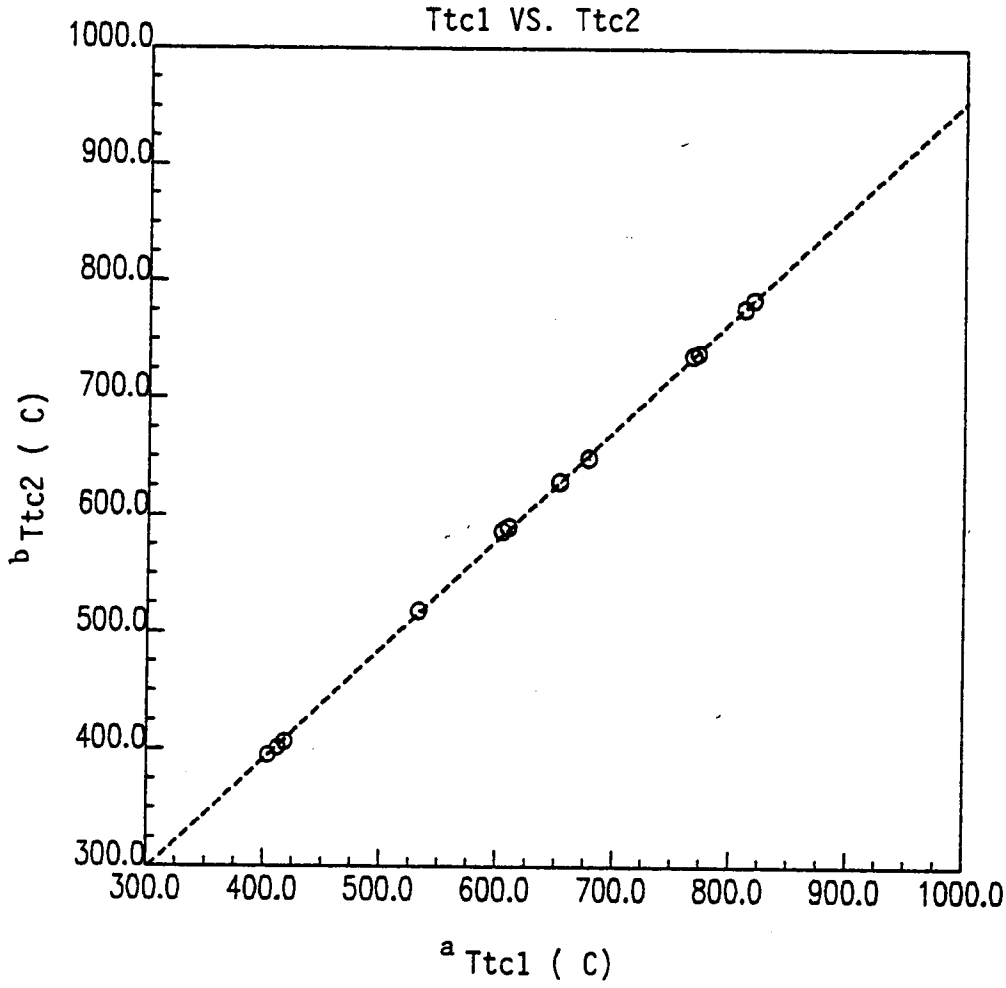
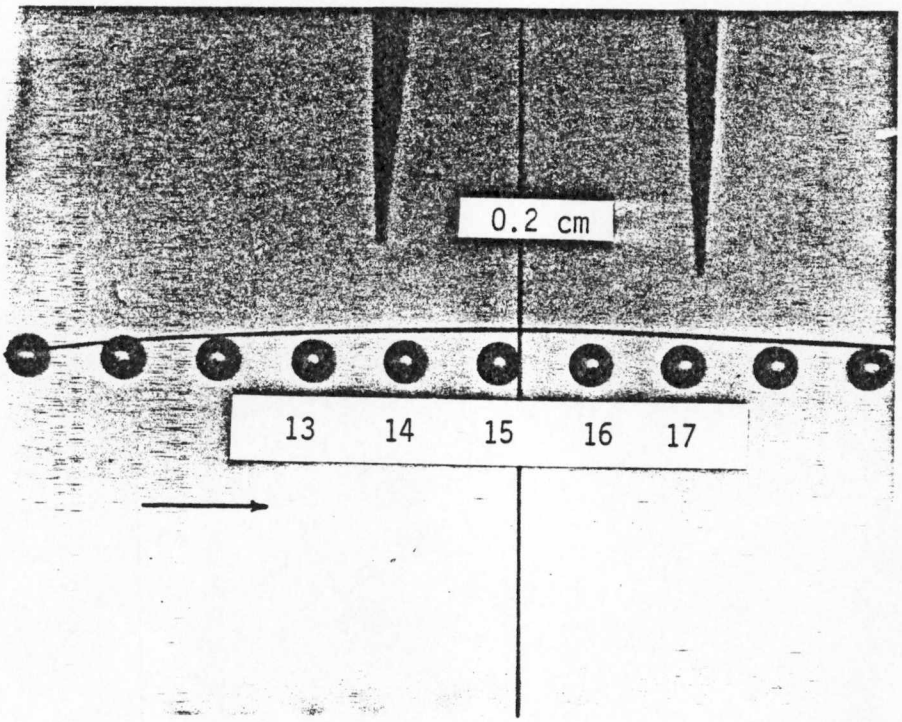


Figure 8. Temperature measurement of two different size thermocouples.

a Bead diameter is 1 mil.
b Bead diameter is 5 mil.



OLD COUNCIL TREE
BOND

Figure 9. Photograph of a representative water droplet train with magnification of about 19X.

stream with high degree of sphericity as can be seen in Figure 9. For each run, a series of twelve pictures was taken at every 0.5 cm according to the technique and procedures described in the previous chapter. In the early stage of the flying path, as shown in Figure 1 (see page 34) the droplets were subjected to some oscillation; however, it was damped out within about 1 cm. The oscillating droplets were not included in the data set.

Droplet velocity, Ud, was calculated by dividing the amount of water flowing through the nozzle over a period of 3 minutes by the initial mass of the droplet, and then the obtained droplet frequency was multiplied by the average particle spacing, X, of the run.

4.2. Experimentally Determined Vaporization Rates

4.2.1 Photographic Results

In each plate, only the droplets in the center that exhibited clear and highly spherical images were accepted for evaluation of droplet size, using a Leeds and Northrup microdensitometer. As shown in Figure 9, the numbers under the individual droplets indicate the ones selected for evaluation from the droplets in a run. Mounted on a three-way slide with the thermocouple and moved in the same path as the camera during a run, the gauge right above the droplets serves as the reference position. It also provides the magnification of each picture from the span of two sharp ends 0.2 cm apart. This setup can easily bring the gauge as close as possible to the droplet stream so both objects can be found on the same plane

with the same magnification to avoid possible distortion. With the built-in cross mark in the lens, the position of the droplet can be determined accurately from the picture. Thus, the size and the location of each droplet can be determined. According to the droplet velocity of each run, these results were plotted in terms of D^2 and time, t, as shown for two runs in Figure 10 where Run C0111 and Run D0124 are composed of 39 and 41 data points respectively. The starting point, time zero, was based on the location of the rim of the furnace tube where the hot air stream was blown out. The hot air stream temperature profile across the tube was also recorded for each run. Only the droplets exposed to the uniform temperature zone, about 1 cm from the tube rim, were used in evaluation. The complete set of D^2 vs. t plots for 33 runs are provided in Appendix B.

4.2.2 Vaporization Rate Evaluation

The vaporization rate of each run was estimated from the plot of D^2 vs. t, by means of the following relationship:

$$\dot{m} = \frac{dm}{dt} = \frac{\pi}{6} \rho_A \left(\frac{d(D^3)}{dt}\right) = \frac{\pi}{4} \rho_A D \left(\frac{d(D^2)}{dt}\right) \qquad (2\text{-}37)$$

Several investigators(13,25,30,33,59,64) have shown a linear relationship between the square of the droplet diameter and time the droplet was vaporized under steady state without appreciable influence from convection or radiation effects. This relationship was not so obvious in this investigation due to the short residence time of droplets in the hot air zone. A considerable portion of the

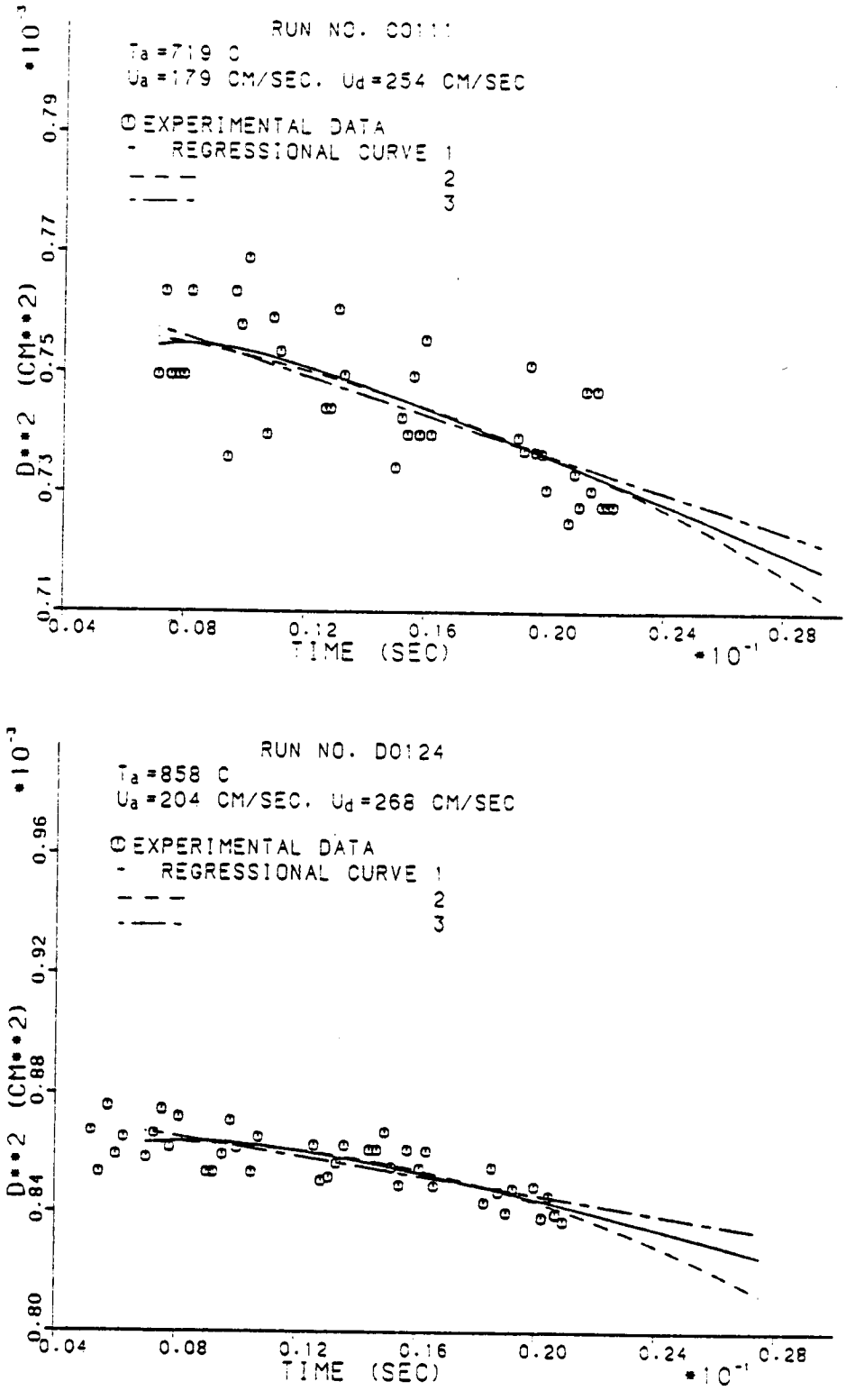


Figure 10. Typical plot of D^2 vs. t.

data in the plot was under preheating stage and unsteady state vaporization (see Figure 10). This period can be estimated by considering an unsteady state heat transfer to a droplet, and neglecting evaporation during the preheating period before reaching a steady vaporization temperature. The following equation can be derived, by use of an enthalpy balance, for a droplet with a uniform temperature distribution.

$$\frac{\pi}{6}\rho_A Do^3 Cp_A \frac{dT_d}{dt} = \pi Do^2 h(Ta-T_d) + \pi Do^2 \varepsilon \sigma F_{12}(Ta^4-T_d^4) \qquad (4\text{-}6)$$

where T_d represents droplet temperature.

Integrating this equation, it can be written:

$$t = \frac{1}{6}\rho_A Do Cp_A \int_{T_{do}}^{T_{df}} \frac{dT_d}{h(Ta-T_d)+ \varepsilon \sigma F_{12}(Ta^4-T_d^4)} \qquad (4\text{-}7)$$

By assuming $T_d^4 << Ta^4$, Eq.(4-4) can be written:

$$t = \frac{1}{6}\rho_A Do Cp_A \frac{1}{h} \ln\left(\frac{h(Ta-T_{do})+\varepsilon\sigma F_{12} Ta^4}{h(Ta-T_{df})+\varepsilon\sigma F_{12} Ta^4} \right) \qquad (4\text{-}8)$$

Then, the time for a droplet with a temperature initially at T_{do} to reach T_{df} can be estimated from the above equation. In Eq.(4-8), h, heat transfer coefficient from the hot air stream to the droplet, can be estimated from adequate heat transfer correlations such as the one proposed by Ranz and Marshall(64):

$$Nuo = 2 + 0.6\, Re^{1/2}\, Pr^{1/3} \qquad (2\text{-}40)$$

For a sample calculation, consider a water droplet initially at 20°C with a diameter of 300 μm introduced into a hot air stream at

$500^{o}C$ with Reynolds number of 10. The time to heat the droplet up to $60^{o}C$ can be estimated by using Eq.(4-8); it is about $20x10^{-3}$ sec. Under the same conditions, but with an air temperature of $800^{o}C$ and heating the droplet from $20^{o}C$ to $70^{o}C$, the result is about $10x10^{-3}$ sec. Similarly, for a smaller droplet with a diameter of 250 μm, the preheating time for vaporizing at $500^{o}C$ and $800^{o}C$ were about $16x10^{-3}$ sec and $8x10^{-3}$ sec respectively.

In this investigation, in view of the short duration of droplets exposed to the hot air stream, about 25 miliseconds, steady state vaporization can only take place in the later part of the hot zone, where the data points are too few and too scattered to obtain a statistically significant straight line. Therefore, to define a suitable equation which can represent the vaporization process, a non-linear regression analysis was adopted to correlate the data points, including those under unsteady state conditions. Under this consideration, two forms were used to fit the experimental data:

$$D^2 = a + bt + c/t + d/t^2 + e/t^3 \qquad (4-9)$$

and

$$D^2 = a + bt + ct^2 + dt^3 \qquad (4-10)$$

Linear regression was also used for comparison. It is

$$D^2 = a + bt \qquad (4-11)$$

The regression curves based on these three equations were included in D^2 versus t plots. Ideally, the curves would extend outside the range of the observed data points to represent the situation of steady state vaporization. However, when both

equations are extended beyond the observation range, Eq.(4-10) has a higher degree of curvature than Eq.(4-9). This can be seen in Figure 10. With large value of independent variable, t, Eq.(4-9) approaches linear form. Besides, comparing the correlation coefficients shown in Table 4, Eq.(4-9) gives better values in most cases than other model forms tested. Thus, Eq.(4-9) was used to obtain vaporization rates from the experimental data. The value of dD^2/dt was evaluated by taking the derivative of Eq.(4-9) with respect to t at the last data point. With the corresponding droplet diameter, Df, the vaporization rate of each run can be calculated by Eq.(2-37). These smoothed, experimentally determined vaporization rates are provided in Table 5 along with the detail information of each run. In this table, the run numbers with a "D" prefix represent the runs using degassed distilled water, while the ones with a "N" or "C" prefix indicate the runs employing the water with dissolved nitrogen or carbon dioxide gas.

4.3 Comparison with the Modified Froessling Model

4.3.1 Calculated Results

The modified Froessling model, as described in Section 2.1.2.A,

$$\dot{m}s = \dot{m}o\left(1 + \frac{\dot{m}o'}{\dot{m}o} F(Re,Pr)\right) \qquad (2\text{-}57)$$

with the consideration of the radiation effect, was used as one of the semi-empirical models to calculate droplet vaporization under the influence of forced convection. $\dot{m}o$ and $\dot{m}o'$ are the vaporization

Table 4. Correlation coefficients of three regression equations for D^2 vs. t curves.

	Run No.	Eq.(4-9)[a]	Eq.(4-10)[b]	Eq.(4-11)[c]
1	N0609	0.488	0.480	0.477
2	N0610	0.573	0.563	0.532
3	N0611	0.606	0.603	0.554
4	N0924	0.541	0.530	0.552
5	C1001	0.848	0.848	0.843
6	D0911	0.522	0.521	0.514
7	N1122	0.678	0.670	0.651
8	N1121	0.649	0.643	0.599
9	N1120	0.837	0.829	0.807
10	C1122	0.531	0.524	0.493
11	C1123	0.748	0.747	0.743
12	D0107	0.546	0.553	0.523
13	N0108	0.556	0.604	0.482
14	NA108	0.773	0.771	0.770
15	C0111	0.758	0.751	0.745
16*	CA111	0.374	0.374	0.366
17	D0113	0.641	0.642	0.638
18	N0109	0.634	0.630	0.624
19	N0121	0.481	0.480	0.468
20	C0110	0.832	0.818	0.815
21	CA110	0.657	0.641	0.612
22*	D0112	0.716	0.722	0.674
23	D0122	0.586	0.577	0.542
24	N0115	0.626	0.627	0.615
25	N0114	0.679	0.679	0.648
26	NA114	0.732	0.726	0.723
27	NA113	0.625	0.617	0.613
28	NA116	0.181	0.175	0.160
29	N0116	0.682	0.678	0.677
30	N0124	0.749	0.746	0.733
31	NA124	0.508	0.508	0.487
32	CA126	0.741	0.739	0.736
33	D0124	0.791	0.782	0.751

[a] $D^2 = a + bt + c/t + d/t^2 + e/t^3$ (4-9)

[b] $D^2 = a + bt + ct^2 + dt^3$ (4-10)

[c] $D^2 = a + bt$ (4-11)

* Omitted (excessive scatter in drop diameters)

Table 5. Experimental results of present investigation.

								cm/sec			$x10^4$ g/sec	x10 g/sec,cm^2
	Run No.	Ttc,°C	Ta,°C	Do,μm	Df,μm	X,cm	Z	Ua	Ud	Ur	mexp	Mexp
1	N0609	515	522	273	272.4	0.060	2.2	144	266	302	0.2704	0.1160
2	N0610	495	501	271	270.0	0.055	2.0	140	252	288	0.3036	0.1326
3	N0611	496	502	270	269.1	0.055	2.0	140	234	273	0.1945	0.0855
4	N0924	550	574	325	322.5	0.065	2.0	136	189	233	0.4428	0.1355
5	C1001	555	580	300	297.0	0.055	1.9	137	203	245	0.5053	0.1823
6	D0911	552	576	303	300.8	0.055	1.8	136	176	222	0.3215	0.1131
7	N1122	620	652	285	281.4	0.065	2.3	167	253	303	0.5250	0.2110
8	N1121	620	652	281	277.1	0.060	2.2	167	240	292	0.5045	0.2091
9	N1120	614	645	284	280.6	0.065	2.3	166	254	303	0.3831	0.1549
10	C1122	608	638	271	269.9	0.055	2.0	165	205	263	0.2876	0.1257
11	C1123	608	638	273	269.3	0.055	2.0	165	256	305	0.3643	0.1599
12	D0107	610	641	272	269.2	0.055	2.0	165	227	281	0.2864	0.1258
13	N0108	679	719	267	265.2	0.055	2.1	179	214	279	0.3980	0.1801
14	NA108	679	719	263	258.0	0.055	2.1	179	194	264	0.3143	0.1503
15	C0111	679	719	275	270.9	0.055	2.0	179	254	311	0.4699	0.2038
16*	CA111	679	719	271	267.8	0.055	2.1	179	270	324	0.2234	0.0991
17	D0113	680	720	264	262.0	0.055	2.1	179	243	302	0.3468	0.1608
18	N0109	727	774	271	269.0	0.055	2.0	189	252	315	0.4508	0.1983
19	N0121	727	774	277	274.0	0.060	2.2	189	240	305	0.3928	0.1665
20	C0110	721	767	273	268.6	0.055	2.0	188	255	317	0.4266	0.1882
21	CA110	721	767	272	269.4	0.055	2.0	188	249	312	0.4953	0.2172
22*	D0112	725	771	267	264.5	0.055	2.1	189	232	299	0.6682	0.3040
23	D0122	732	779	277	273.2	0.060	2.2	190	265	326	0.5467	0.2332
24	N0115	738	775	268	264.5	0.060	2.3	150	265	305	0.3753	0.1707
25	N0114	725	771	269	266.5	0.055	2.1	167	290	335	0.5766	0.2584

Table 5. (continued)

	Run No.	Ttc, °C	Ta, °C	Do, μm	Df, μm	X, cm	Z	Ua	Ud	Ur	mexp	Mexp
								cm/sec			x10^4 g/sec	x10 g/sec,cm^2
26	NA114	725	771	270	265.8	0.055	2.1	167	271	318	0.4224	0.1903
27	NA113	732	779	265	262.0	0.055	2.1	212	267	341	0.4932	0.2287
28	NA116	728	775	297	295.5	0.085	2.9	150	542	562	0.4620	0.1684
29	NO116	728	775	303	300.3	0.090	3.0	150	427	453	0.4240	0.1496
30	NO124	799	858	279	274.5	0.060	2.2	204	272	340	0.6563	0.2346
31	NA124	799	858	282	279.0	0.060	2.2	204	268	337	0.4552	0.1862
32	CA126	801	860	267	261.5	0.055	2.1	205	254	326	0.5020	0.2337
33	DO124	799	858	294	290.2	0.070	2.4	204	268	337	0.5499	0.2079

* Omitted (excessive scatter in drop diameters)

rates of droplets under stationary conditions with and without radiation respectively, and F is the ventilation factor given by an appropriately determined correlation. This model has been extensively developed and tested against available experimental data in the literature by Frazier and Chang(18). $\dot{m}o$ and $\dot{m}o'$ were based on the equations derived by Frazier and Chang(18) as shown in Eqs.(2-15), (2-16) and (2-17), and were computed with a trial value of θ_s, normalized surface temperature, to initiate the calculation until Eqs.(2-15) and (2-16) were satisfied simultaneously. This is because of the non-linearity of the equations of the model, as can be seen in Eq.(2-15) to Eq.(2-17), and because the equations require the droplet surface temperature, which is unknown at the onset. A search procedure is therefore required.

Vapor pressure at the droplet surface and other corresponding air-water vapor mixture properties in the calculation were computed according to the expressions in Appendix E.

The term q^r in Eq.(2-17) was expressed as

$$q^r = a \sigma F_{12} Tb^4 (\theta_a^4 - \theta_s^4) \qquad (4-12)$$

where θ_a is taken as the screen temperature in the heated tube.

The water droplet's absorptivity, a, was taken from Brown's data(7) as discussed in (18) and correlated into the following form:

$$a = 1.159 - 0.1167 \times Ta/Tb \qquad (4-13)$$

The value calculated for each run can be found in Table 6, in which dimensionless numbers were also evaluated.

View factor, F_{12}, was calculated by the equation proposed by

Table 6. Calculated results.

	Run No.	Ta, C	Ts, C	a	Re	Pr	Gr	$\dot{m}o'$ x10^4 g/sec	$\dot{m}o$ x10^4 g/sec	$\dot{m}s$(natural) x10^4 g/sec
1	N0609	522	63.2	0.92	12.8	0.72	0.11	0.1286	0.1326	0.1380
2	N0610	501	62.5	0.92	12.6	0.72	0.11	0.1210	0.1248	0.1299
3	N0611	502	62.6	0.92	11.8	0.72	0.11	0.1209	0.1247	0.1298
4	N0924	574	66.0	0.90	10.6	0.72	0.17	0.1723	0.1803	0.1894
5	C1001	580	66.2	0.90	10.2	0.72	0.13	0.1606	0.1681	0.1756
6	D0911	576	66.1	0.90	9.4	0.72	0.14	0.1615	0.1690	0.1767
7	N1122	652	68.0	0.87	10.6	0.72	0.10	0.1768	0.1851	0.1923
8	N1121	652	68.0	0.87	10.1	0.72	0.10	0.1741	0.1823	0.1892
9	N1120	645	67.9	0.87	10.7	0.72	0.10	0.1740	0.1822	0.1893
10	C1122	638	67.7	0.87	9.0	0.72	0.09	0.1652	0.1729	0.1793
11	C1123	638	67.7	0.87	10.4	0.72	0.09	0.1648	0.1725	0.1789
12	D0107	641	67.8	0.87	9.6	0.72	0.09	0.1655	0.1732	0.1796
13	N0108	719	69.5	0.85	8.3	0.73	0.08	0.1887	0.1990	0.2058
14	NA108	719	69.5	0.85	7.6	0.73	0.07	0.1836	0.1936	0.1999
15	C0111	719	69.5	0.85	9.4	0.73	0.08	0.1927	0.2033	0.2104
16*	CA111	719	69.5	0.85	9.7	0.73	0.08	0.1905	0.2010	0.2079
17	D0113	720	69.6	0.85	8.8	0.73	0.08	0.1868	0.1970	0.2035
18	N0109	774	71.4	0.83	8.7	0.73	0.08	0.2102	0.2234	0.2307
19	N0121	774	70.7	0.83	8.6	0.73	0.08	0.2141	0.2275	0.2353
20	C0110	767	70.5	0.83	8.9	0.73	0.08	0.2075	0.2197	0.2278
21	CA110	767	70.5	0.83	8.8	0.73	0.08	0.2081	0.2211	0.2285
22*	D0112	771	70.6	0.83	8.2	0.73	0.07	0.2059	0.2184	0.2251
23	D0122	779	71.5	0.83	9.1	0.73	0.08	0.2155	0.2290	0.2376
24	N0115	775	71.4	0.83	8.3	0.73	0.07	0.2071	0.2192	0.2271
25	N0114	771	71.4	0.83	9.2	0.73	0.07	0.2075	0.2196	0.2276

Table 6. (continued).

	Run No.	Ta, C	Ts, C	a	Re	Pr	Gr	$\dot{m}o'$ x10^4 g/sec	$\dot{m}o$ x10^4 g/sec	$\dot{m}s$(natural) x10^4 g/sec
26	NA114	771	71.4	0.83	8.8	0.73	0.07	0.2069	0.2191	0.2270
27	NA113	779	71.5	0.83	9.1	0.73	0.07	0.2067	0.2188	0.2266
28	NA116	775	71.4	0.83	17.1	0.73	0.10	0.2313	0.2467	0.2570
29	NO116	775	71.4	0.83	14.0	0.73	0.11	0.2351	0.2516	0.2614
30	NO124	858	72.8	0.80	8.6	0.73	0.07	0.2444	0.2616	0.2719
31	NA124	858	72.8	0.80	8.6	0.73	0.08	0.2484	0.2669	0.2761
32	CA126	860	72.9	0.80	7.8	0.73	0.06	0.2337	0.2496	0.2575
33	DO124	858	72.8	0.80	9.0	0.73	0.09	0.2584	0.2776	0.2882

* Omitted (excessive scatter in drop diameters)

Feingold and Gupta(16) in order to estimate the radiant heat transfer from the furnace tube to a droplet. Figure 11 depicts a sphere moving across the center line of a disk at some distance, a, above it. F_{12} can be derived and written in the following form for the case of b<c:

$$F_{12} = \int_{c-b}^{b+c} \frac{\cos^{-1}((x^2+b^2-c^2)/2bx)}{\pi} \frac{ax}{2} (a^2 + x^2)^{-3/2} \, dx$$

$$+ \frac{1}{2} - \frac{a}{2(a^2+(c-b))^{1/2}} \qquad (4\text{-}14)$$

Based on this equation, F_{12} was calculated simulating a droplet moving from the center to the edge of the nozzle at a distance of 0.25 inch and 0.5 inch above the disk. The results are shown in Figure 12. In the experiments, efforts were made to keep the droplet train flying over the furnace tube at 0.25 inch above the disk. An integrated value of F_{12} was thus calculated based on that curve from the center extended to 1 inch away, where the data were considered to be reliable and were under evaluation. The integrated average value of view factor, F_{12}, was estimated to be 0.395. In the calculation, the value of 0.4 was used. Finally, the vaporization rate with forced convection, $\dot{m}s$, was computed using the resulting value of $\dot{m}o$ and $\dot{m}o'$ in Eq.(2-57) where F(Re,Pr) was evaluated from four heat transfer correlations published by different investigators. These correlations, along with their corresponding ventilation factor forms, are as follows:

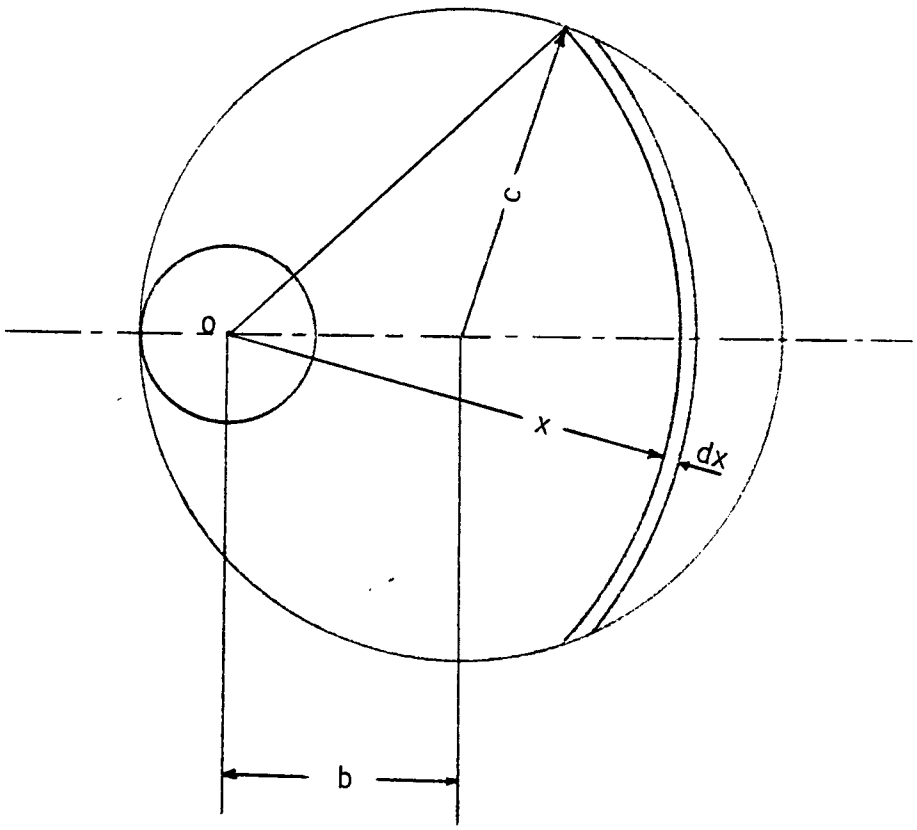


Figure 11. Diagram of view factor derivation.

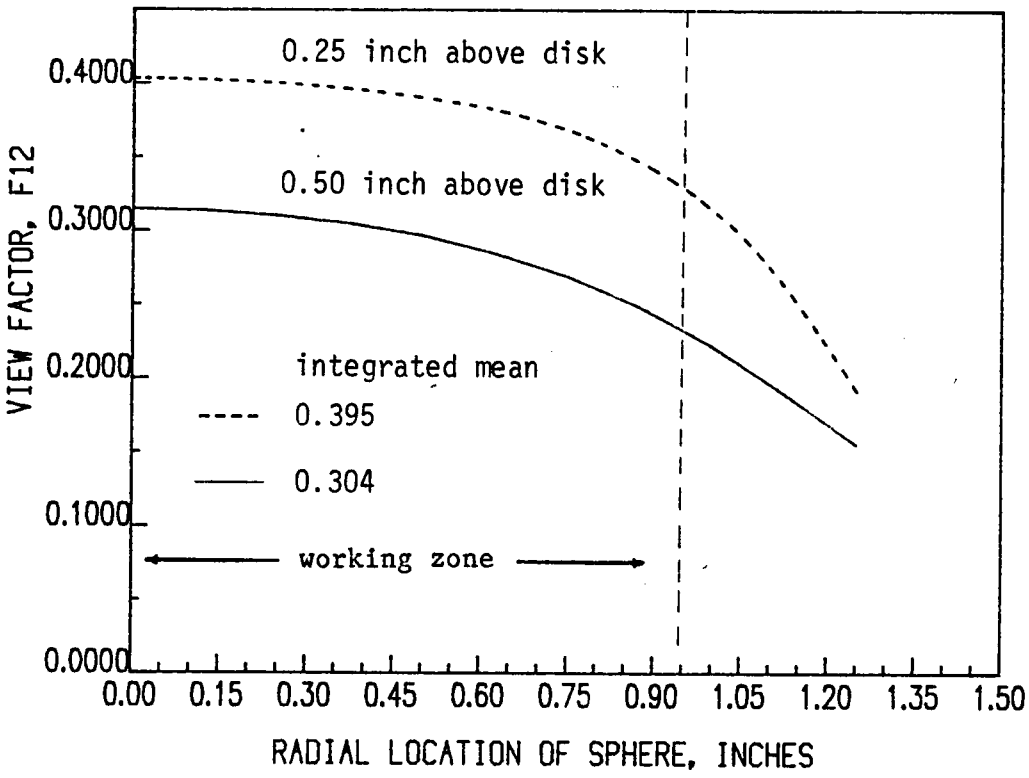


Figure 12. Calculated view factor from a sphere to a noncoaxial disk with a radius of 1.25 inches. Diameter of the sphere is 300 μm.

Froessling(20):

$$Nuo = 2(1+0.276\ Re^{1/2}\ Pr^{1/3})$$

$$F(Re,Pr) = 0.276\ Re^{1/2}\ Pr^{1/3} \qquad (4\text{-}15)$$

Ranz and Marshall(64):

$$Nuo = 2(1+0.3\ Re^{1/2}\ Pr^{1/3})$$

$$F(Re,Pr) = 0.3\ Re^{1/2}\ Pr^{1/3} \qquad (4\text{-}16)$$

Rowe, Claxton and Lewis(68):

$$Nuo = 2(1+0.345\ Re^{1/2}\ Pr^{1/3})$$

$$F(Re,Pr) = 0.345\ Re^{1/2}\ Pr^{1/3} \qquad (4\text{-}17)$$

Lee and Ryley(47):

$$Nuo = 2(1+0.37\ Re^{1/2}\ Pr^{1/3})$$

$$F(Re,Pr) = 0.37\ Re^{1/2}\ Pr^{1/3} \qquad (4\text{-}18)$$

From numerous publications (see Table 2, Page 37), the above four correlations were selected that present in the same form and represent the low and high predicted values of Nu among the investigators.

The calculated values of $\dot{m}o$, $\dot{m}o'$ and $\dot{m}_s$ with the corresponding results for 33 experimental runs were listed in Table 6. An estimate of the extent of enhancement of vaporization by free convection was also calculated by substituting F(Gr,Pr) for F(Re,Pr) from Eq.(2-57). However, this effect was not included in the evaluation of vaporization rate in this study. It just shows the possible contribution of free convection. The results for Ms using the above four correlations are summarized in Table 7.

To simulate this model, a computer program was developed, using

Table 7. Summary of vaporization rates from Froessling model predictions.

		Vaporization Flux, x10 g/sec,cm^2			
	Run No.	Ms(Froessling)	Ms(R&M)	Ms(R,C&L)	Ms(L&R)
1	N0609	0.1057	0.1100	0.1188	0.1232
2	N0610	0.1009	0.1049	0.1125	0.1167
3	N0611	0.1001	0.1040	0.1114	0.1155
4	N0924	0.0977	0.1014	0.1092	0.1131
5	C1001	0.1065	0.1105	0.1188	0.1230
6	D0911	0.1027	0.1064	0.1144	0.1183
7	N1122	0.1317	0.1367	0.1472	0.1524
8	N1121	0.1323	0.1372	0.1476	0.1528
9	N1120	0.1306	0.1356	0.1460	0.1512
10	C1122	0.1292	0.1339	0.1438	0.1486
11	C1123	0.1335	0.1385	0.1491	0.1544
12	D0107	0.1317	0.1366	0.1468	0.1519
13	N0108	0.1510	0.1563	0.1676	0.1731
14	NA108	0.1527	0.1579	0.1691	0.1745
15	C0111	0.1518	0.1573	0.1694	0.1751
16*	CA111	0.1545	0.1602	0.1722	0.1781
17	D0113	0.1552	0.1607	0.1725	0.1783
18	N0109	0.1661	0.1720	0.1849	0.1910
19	N0121	0.1626	0.1684	0.1814	0.1874
20	C0110	0.1645	0.1708	0.1832	0.1894
21	CA110	0.1640	0.1698	0.1825	0.1886
22*	D0112	0.1657	0.1718	0.1842	0.1902
23	D0122	0.1665	0.1728	0.1859	0.1922
24	N0115	0.1671	0.1733	0.1857	0.1918
25	N0114	0.1685	0.1750	0.1879	0.1943
26	NA114	0.1672	0.1735	0.1861	0.1923
27	NA113	0.1733	0.1799	0.1932	0.1997
28	NA116	0.1765	0.1843	0.2002	0.2080
29	N0116	0.1658	0.1725	0.1871	0.1941
30	N0124	0.1856	0.1925	0.2072	0.2140
31	NA124	0.1832	0.1899	0.2042	0.2109
32	CA126	0.1916	0.1984	0.2131	0.2199
33	D0124	0.1776	0.1843	0.1985	0.2050

* Omitted (excessive scatter in drop diameters)

an iterative trial and error procedure, given the size of the droplet and the conditions under which it vaporizes. A block diagram is presented in Figure 13. A copy of the computer program, with necessary constants used in the calculations, is provided as Appendix C.

In Figures 14 to 17, experimental results are also compared with model predictions using different ventilation factors. In view of the scatter of the data, a statistical analysis using one of the SAS (Statistical Analysis System) procedures(21), GLM, was employed in realizing the deviation of model results from experimental results. GLM is a regression procedure which analyzes general linear models developed by SAS Institute Inc. In each figure, the best fit line and upper and lower limits at a 95% confidence interval were plotted in solid lines. The dash line represents a perfect agreement line with a slope of 1. Except for Figure 17, the rest of the three figures show that experimental vaporization rates were significantly higher than the results predicted by the theoretical model at the 95% confidence interval even though the deviations were small. The slopes of the best fit line are 0.82 ± 0.05, 0.85 ± 0.05, 0.91 ± 0.06 and 0.95 ± 0.06 for the figures that compare experimental results with those calculated by using the four correlations as shown in Eqs.(4-15), (4-16), (4-17) and (4-18) respectively. The results also indicate that dissolved gases in the pressure ranges used in this investigation (up to 1.3 atm) had a negligible effect on vaporization rates.

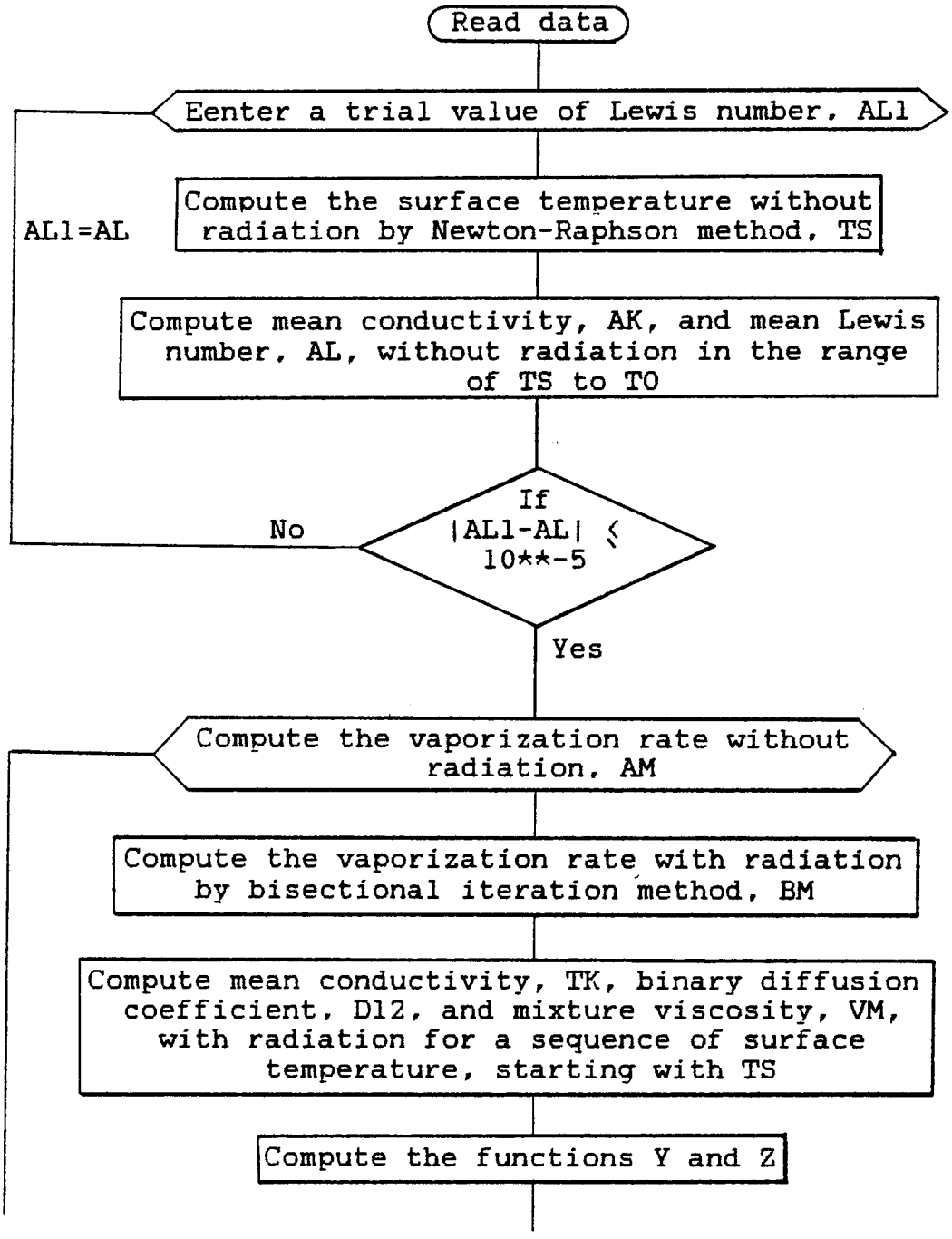


Figure 13. Flow sheet of computer program for Froessling model calculation.

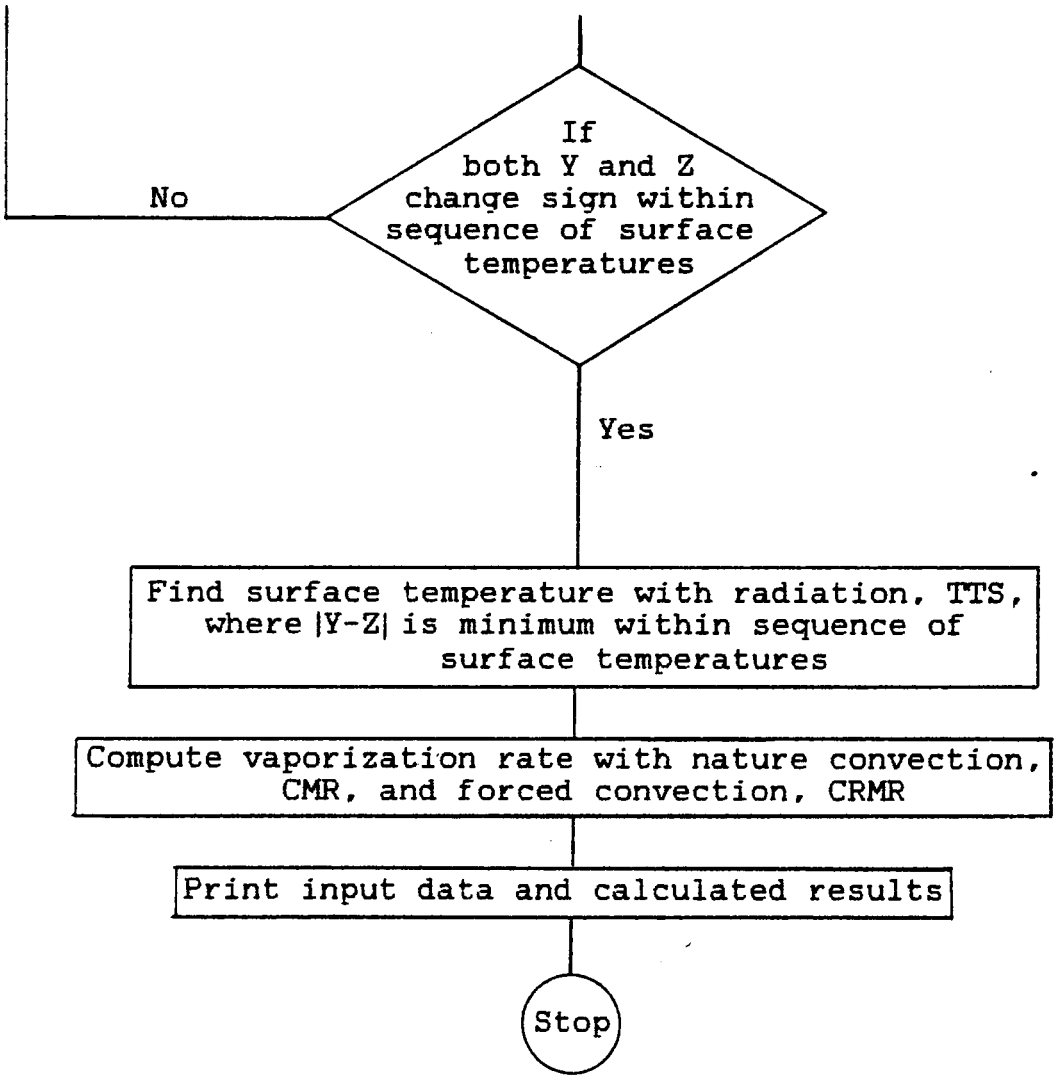


Figure 13. (Continued).

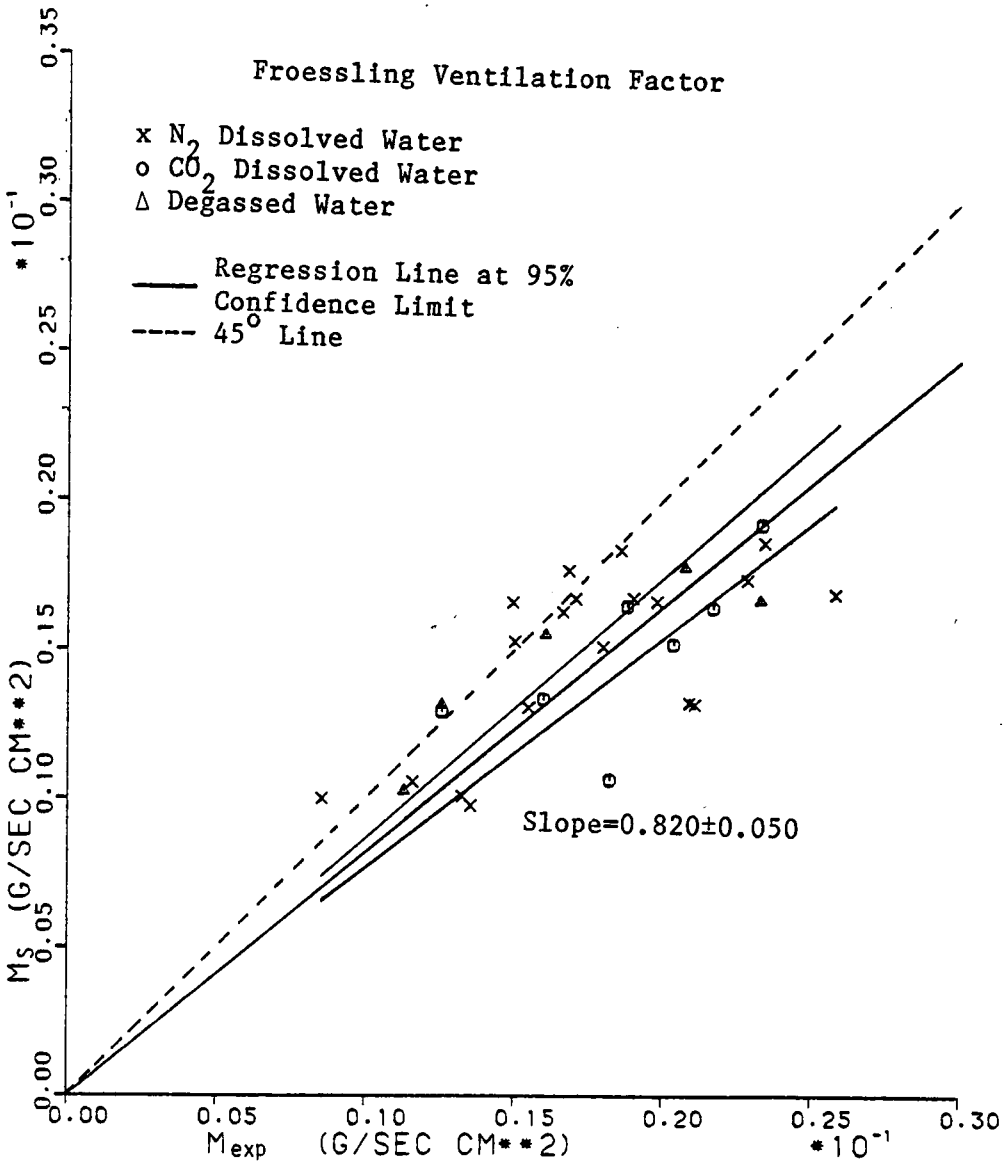


Figure 14. Comparison of experimental results with the modified Froessling vaporization model using the Froessling ventilation factor (Eq.(4-15)).

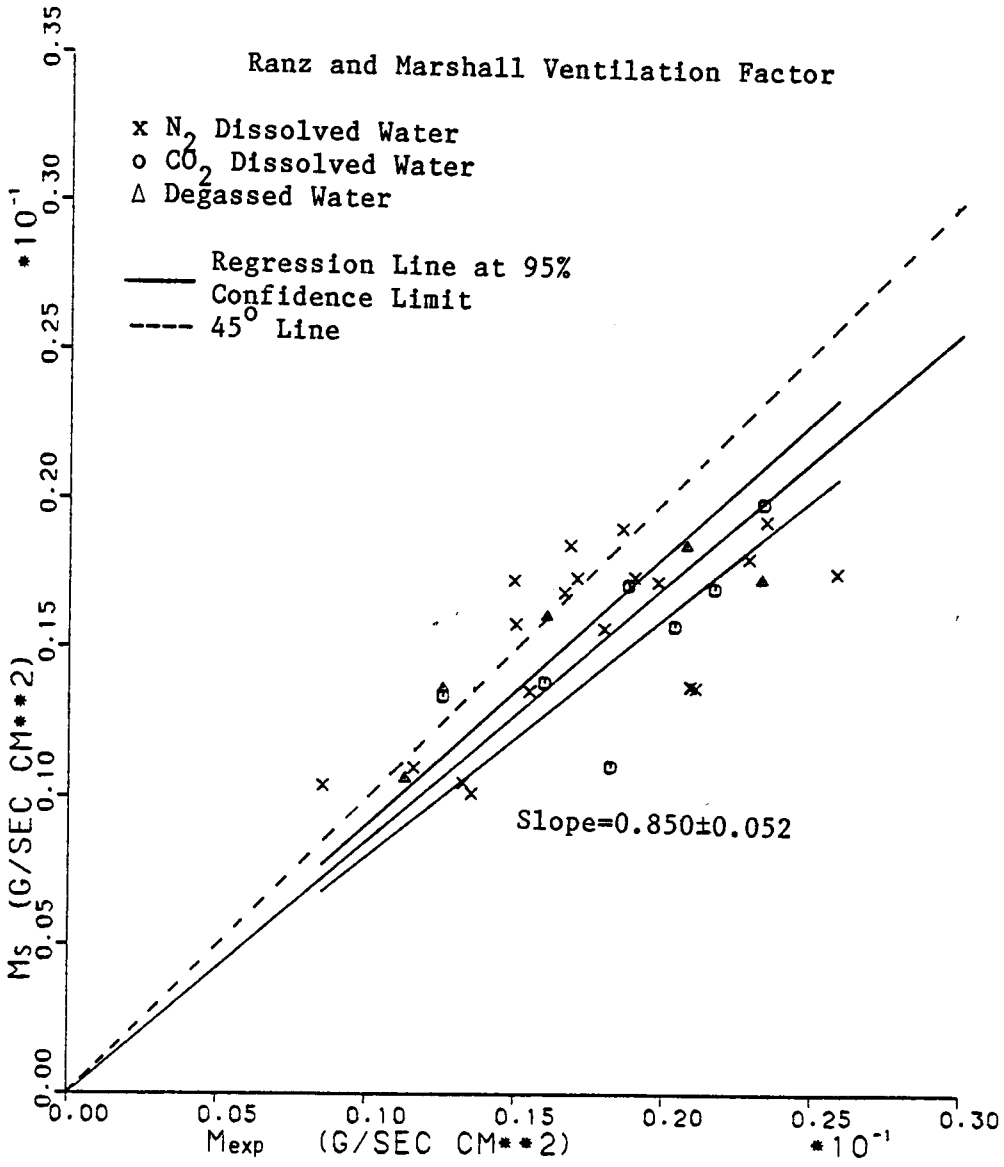


Figure 15. Comparison of experimental results with the modified Froessling vaporization model using the Ranz and Marshall ventilation factor (Eq.(4-16)).

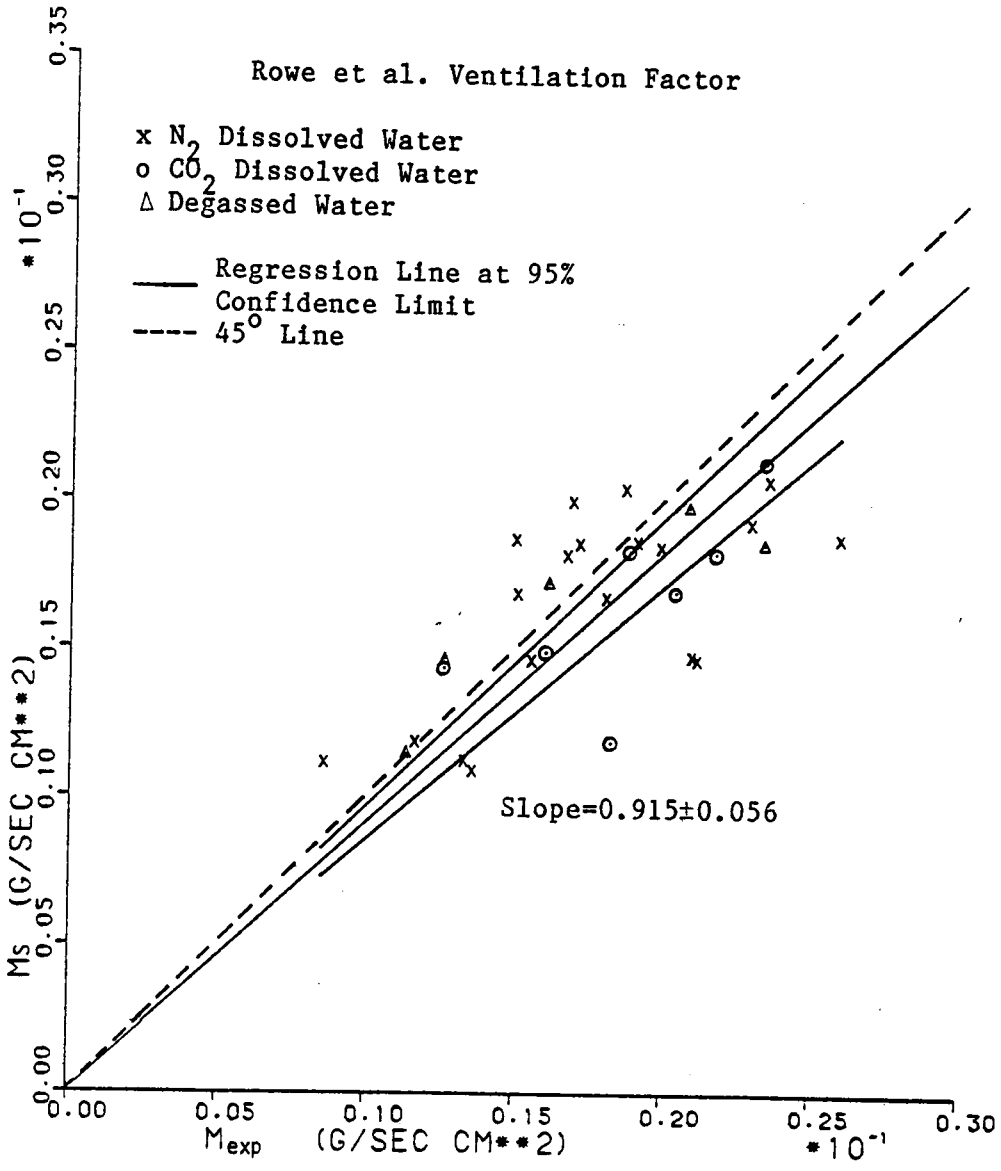


Figure 16. Comparison of experimental results with the modified Froessling vaporization model using the Rowe et al. ventilation factor (Eq.(4-17)).

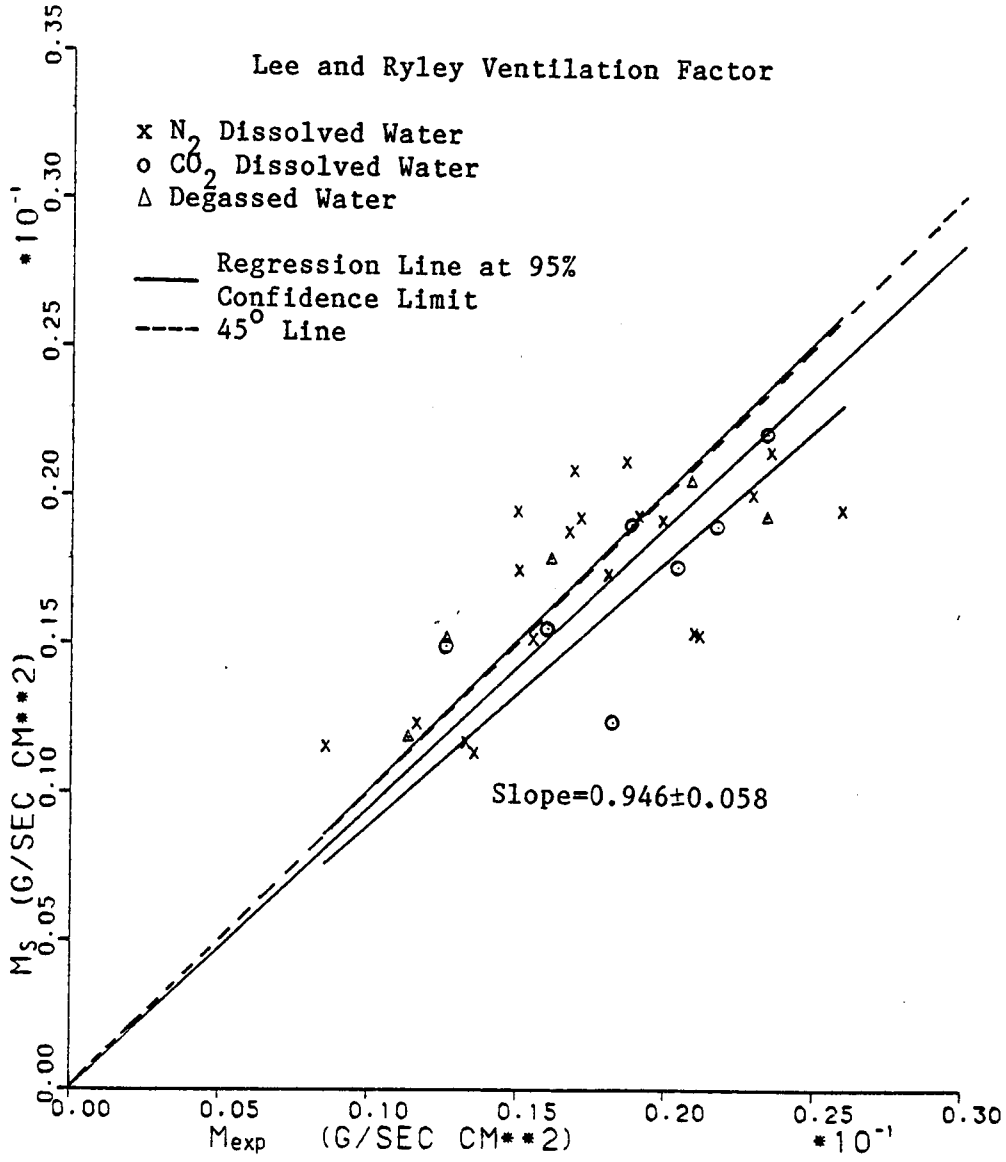


Figure 17. Comparison of experimental results with the modified Froessling vaporization model using the Lee and Ryley ventilation factor (Eq.(4-18)).

Figure 18 includes the sequence number of the experiments for convenience in referring to the information cited in the tables.

Table 8 provides the errors between experimental vaporization rates and the rates calculated according to the model predictions using four ventilation factors. This table shows that the best agreement with the experimental data is given by use of the Lee and Ryley ventilation correlation in the modified Froessling model, the mean error being only -5.5%. The poorest agreement occurs by use of the Froessling correlation, which is based on relatively low temperature data, where the average error is -18%. All four ventilation factors used in this model under predict the experimental results on the average, although the prediction are generally within the data scatter.

4.4 Comparison with the Large Flux Model

This model was developed by several investigators(1,11,48,58) and summarized by Bird et al.(6) to correct the simple film model with a factor for the net flow through an interface during mass transfer. As discussed in Section 2.1.2.B, the results of the mean fluxes of heat and mass into the gas phase are

$$qs^c = \frac{N_{As}\ Cp_A(Ts - Ta)}{\exp((N_{As}\ Cp_A)/h_x) - 1} \qquad (4\text{-}19)$$

$$N_{As} = k_x \ln\left(1 + \frac{X_{As} - X_{A\infty}}{1 - X_{As}}\right) \qquad (4\text{-}20)$$

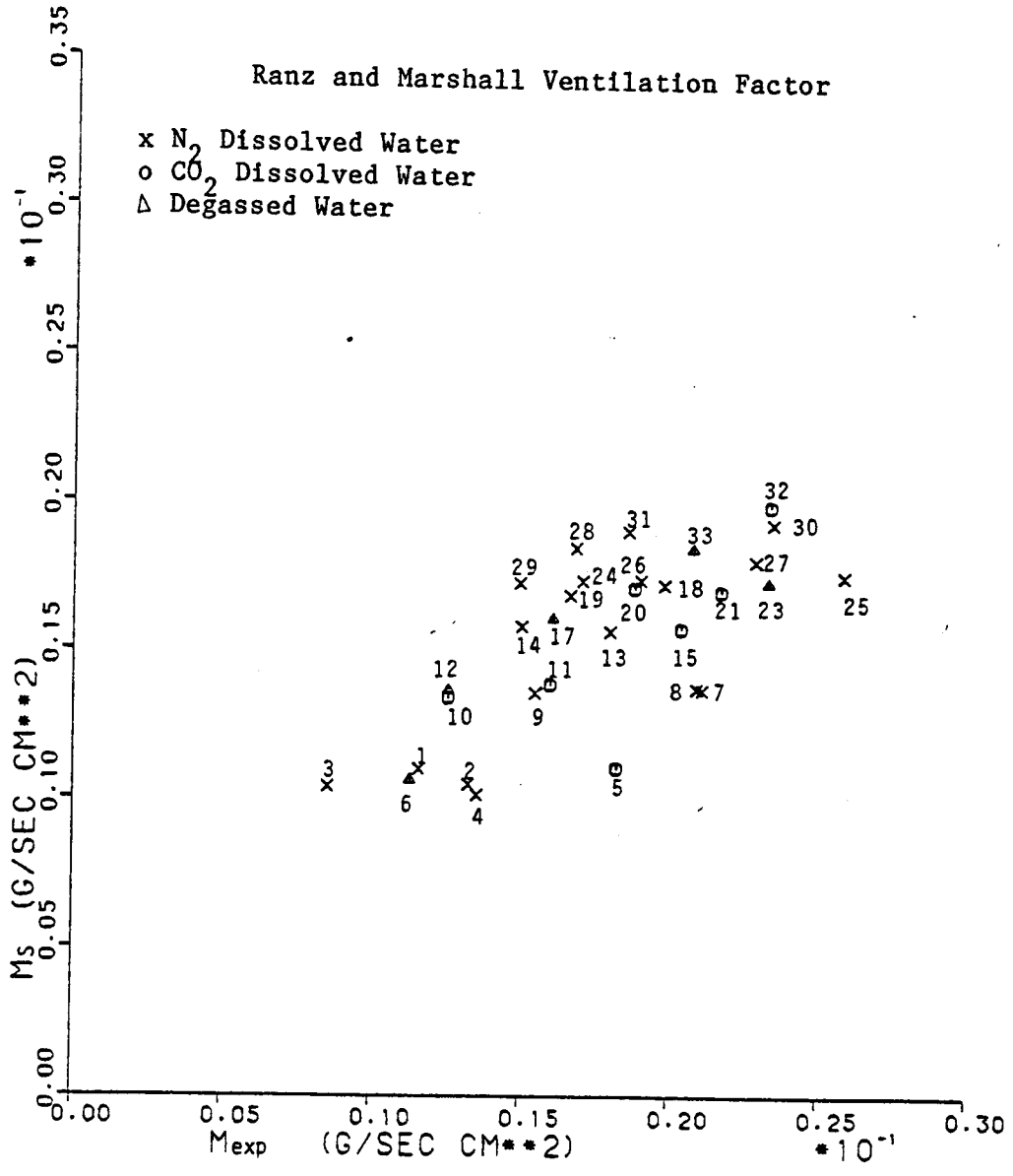


Figure 18. Experimental sequence number of the data points for model calculations vs. experimental results.

Table 8. Errors between experimental vaporization rates and rates calculated according to the modified Froessling model.

Ventilation Correlation	Mean Per cent Error[a]
Froessling	-18.0
Ranz and Marshall	-15.0
Rowe, Claxton and Lewis	- 8.5
Lee and Ryley	- 5.5

a By regression analysis, with per cent error=(Ms-Mexp)/Ms

where the transfer coefficients k_x and h_x were obtained by using the Ranz-Marshall correlation as shown in Eq.(2-23) and Eq.(2-24).

The interfacial energy balance for steady state is then written as follows:

$$N_{As}\,\lambda_A + qs^c + qs^r = 0 \qquad (4\text{-}21)$$

where qs^r is defined by Eq.(4-12).

In calculation, the fluxes and interfacial states are regarded as averages over the surface of the droplet. The composition of water vapor at the interface is evaluated at isothermal droplet temperature, Ts, by the equation

$$X_{As} = \frac{P_A}{Pt} = \frac{Pc}{Pt}\exp(\tau(\theta_s)) \qquad (2\text{-}18)$$

which assumes the gas phase is ideal, and where the function $\tau(\theta_s)$ is given by Keenan and Keyes(38). This equation is the same as used in the Froessling model calculations of Section 4.2. The pressure P_A was calculated from Eq.(E-1) in Appendix E. Fluid properties were calculated at the arithmetic mean fluid state of the surrounding air and droplet surface. By a trial value of surface temperature, Ts, the result of Eq.(4-20) can be computed. A satisfactory convergence could be reached after a few iterations. A copy of the computer program written for this model is provided in Appendix D. The flow sheet of the computer program is presented in Figure 19.

The vaporization rates computed from this model are listed in Table 9. Predicted results are plotted against experimental results

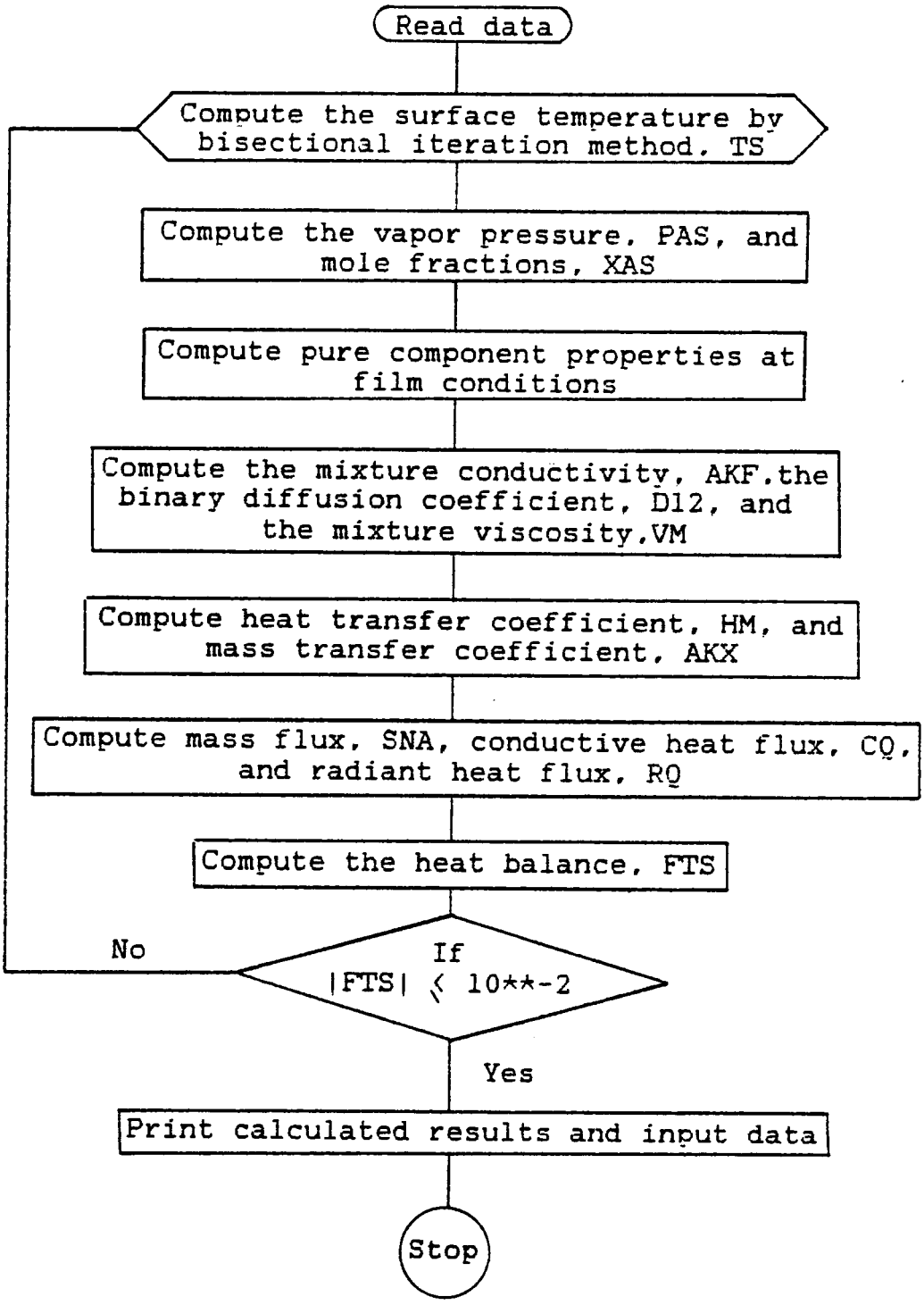


Figure 19. Flow sheet of computer program for Large Flux model calculation.

Table 9. Summary of vaporization rates from Large Flux model predictions.

		Vaporization Flux, x10 g/sec,cm^2			
	Run No.	ML(Froessling)	ML(R&M)	ML(R,C&L)	ML(L&R)
1	N0609	0.1140	0.1191	0.1281	0.1332
2	N0610	0.1083	0.1132	0.1215	0.1264
3	N0611	0.1075	0.1119	0.1204	0.1251
4	N0924	0.1060	0.1103	0.1185	0.1227
5	C1001	0.1151	0.1197	0.1285	0.1334
6	D0911	0.1110	0.1153	0.1234	0.1280
7	N1122	0.1443	0.1503	0.1612	0.1674
8	N1121	0.1448	0.1507	0.1615	0.1674
9	N1120	0.1429	0.1487	0.1597	0.1659
10	C1122	0.1407	0.1461	0.1563	0.1621
11	C1123	0.1456	0.1514	0.1626	0.1689
12	D0107	0.1436	0.1492	0.1598	0.1658
13	N0108	0.1656	0.1719	0.1837	0.1903
14	NA108	0.1670	0.1731	0.1850	0.1915
15	C0111	0.1670	0.1737	0.1858	0.1928
16*	CA111	0.1701	0.1768	0.1894	0.1966
17	D0113	0.1702	0.1770	0.1893	0.1963
18	N0109	0.1833	0.1905	0.2037	0.2112
19	N0121	0.1795	0.1864	0.1994	0.2067
20	C0110	0.1817	0.1889	0.2021	0.2096
21	CA110	0.1807	0.1878	0.2009	0.2083
22*	D0112	0.1828	0.1897	0.2029	0.2100
23	D0122	0.1841	0.1914	0.2049	0.2125
24	N0115	0.1844	0.1914	0.2049	0.2120
25	N0114	0.1863	0.1937	0.2076	0.2151
26	NA114	0.1845	0.1918	0.2054	0.2127
27	NA113	0.1918	0.1994	0.2135	0.2214
28	NA116	0.1975	0.2066	0.2236	0.2332
29	N0116	0.1840	0.1927	0.2078	0.2164
30	N0124	0.2067	0.2148	0.2297	0.2378
31	NA124	0.2037	0.2117	0.2264	0.2348
32	CA126	0.2130	0.2209	0.2359	0.2444
33	D0124	0.1982	0.2057	0.2202	0.2284

* Omitted (excessive scatter in drop diameters)

in Figures 20 to 22, in which the corresponding slope of the best fit lines determined at a 95% confindence interval are 0.94 ± 0.06, 1.006 ± 0.063 and 1.04 ± 0.06. The errors between the experimental results and the calculated results using different ventilation factors are listed in Table 10. These results show that the Large Flux model gives best agreement with the data when equipped with the Rowe, Claxton, and Lewis ventilation factor correlation, the mean error being only +0.6%, although all three ventilation factors considered yield results that are well within the data scatter.

Finally, on comparing the results for the Froessling model, Table 8 (Page 83) with those of Table 10 for the Large Flux model, it is concluded that the latter model generally gives closer agreement with the vaporization data in the temperature range of $550^{\circ}C$-$860^{\circ}C$. Further the ventilation factor of Rowe, Claxton and Lewis is more satisfactory in this temperature range than the others considered, although scatter in the data precludes an interpretation of the data in terms of the Rowe, Claxton, and Lewis factor alone.

4.5 Prediction of Vaporization Rates at Elevated Pressures

The results in Sections 4.3 and 4.4 indicate that calculated results from each of the models considered can, within experimental error, provide agreement with the experimental data over a wide temperature range. A further test of the vaporization models can be made by comparing calculated and experimental results at elevated pressures. Hall and Diederichsen(30) provide vaporization data on

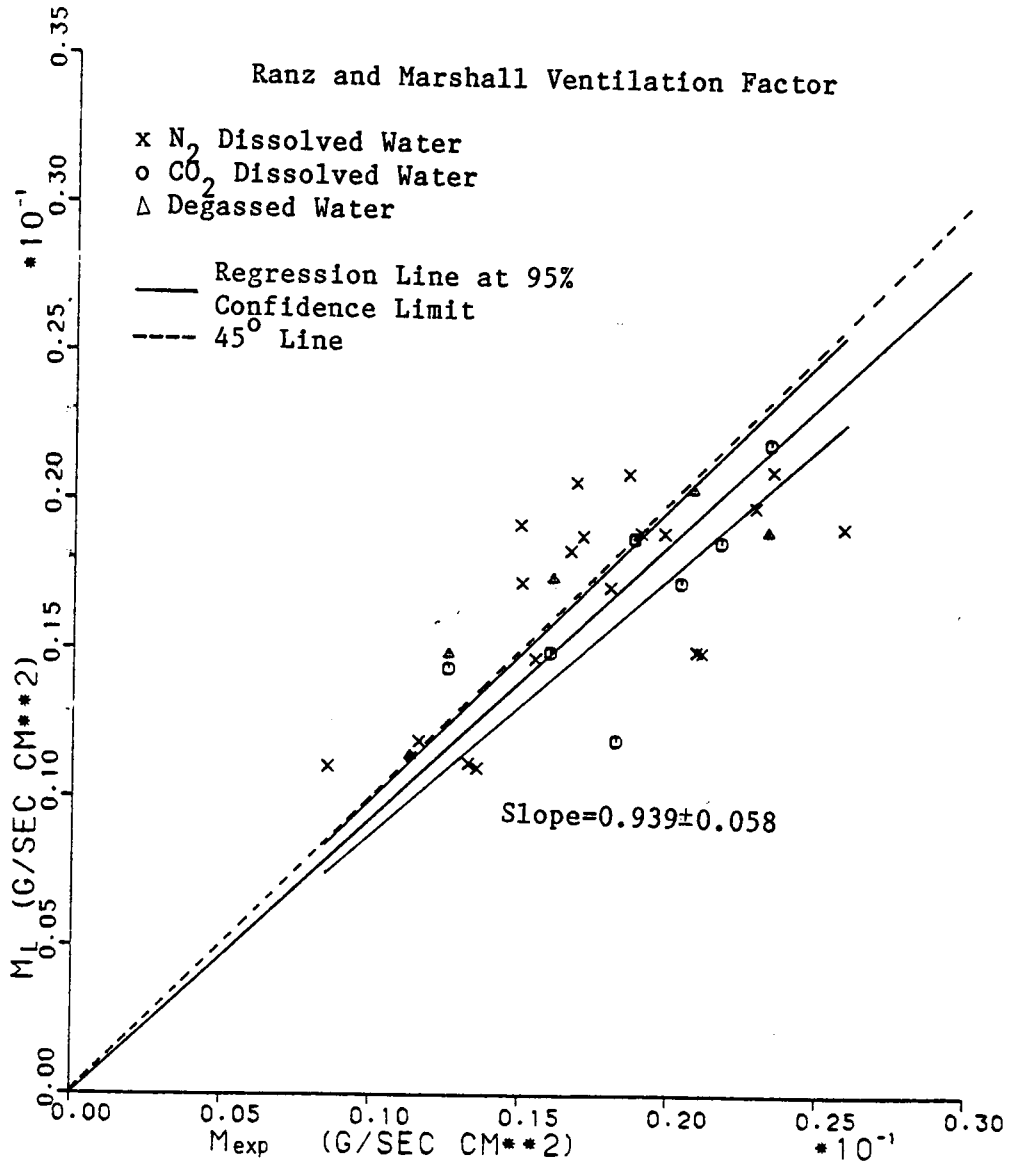


Figure 20. Comparison of experimental results with the Large Flux vaporization model using the Ranz and Marshall ventilation factor (Eq.(4-16)).

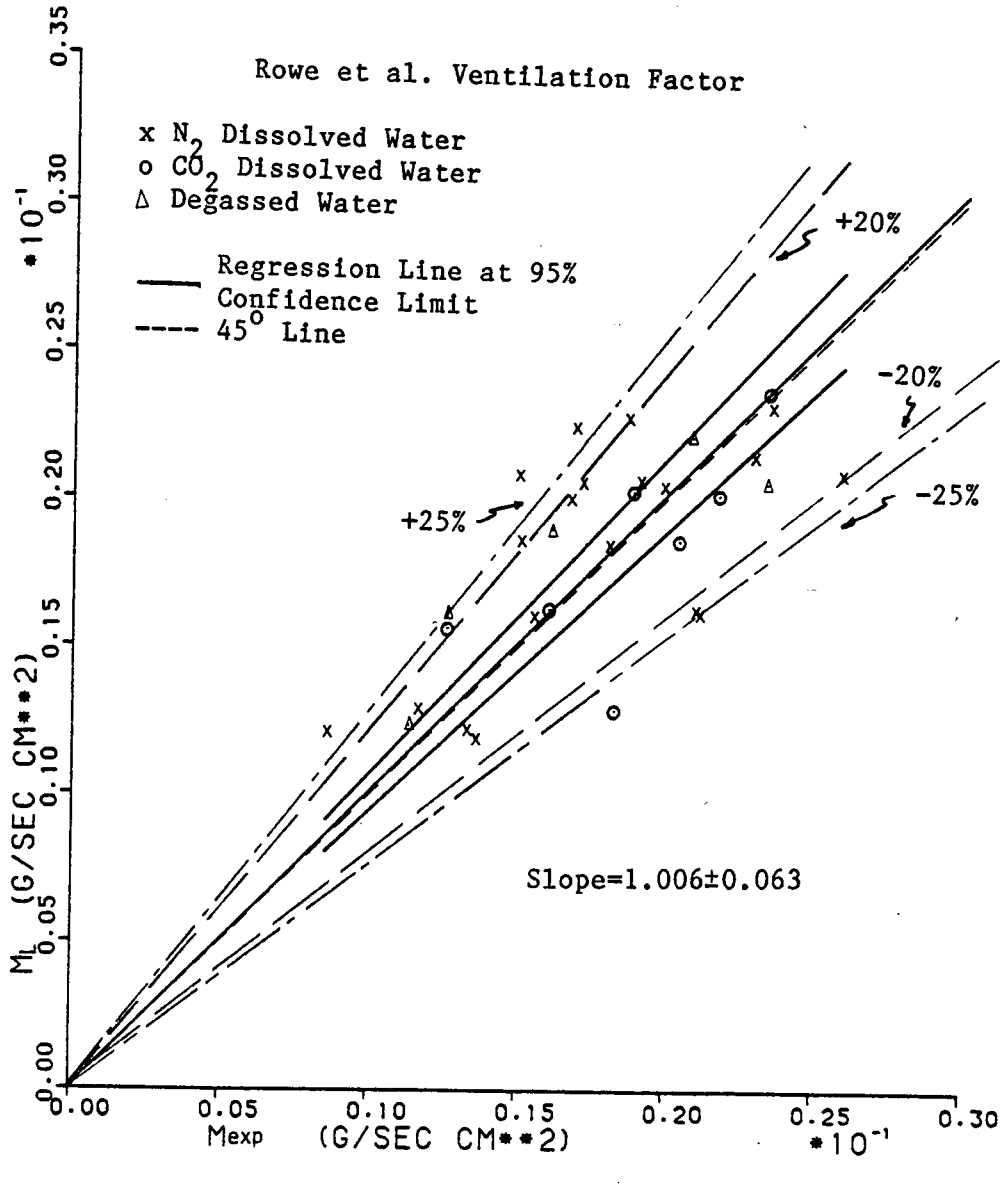


Figure 21. Comparison of experimental results with the Large Flux vaporization model using the Rowe et al. ventilation factor (Eq.(4-17)).

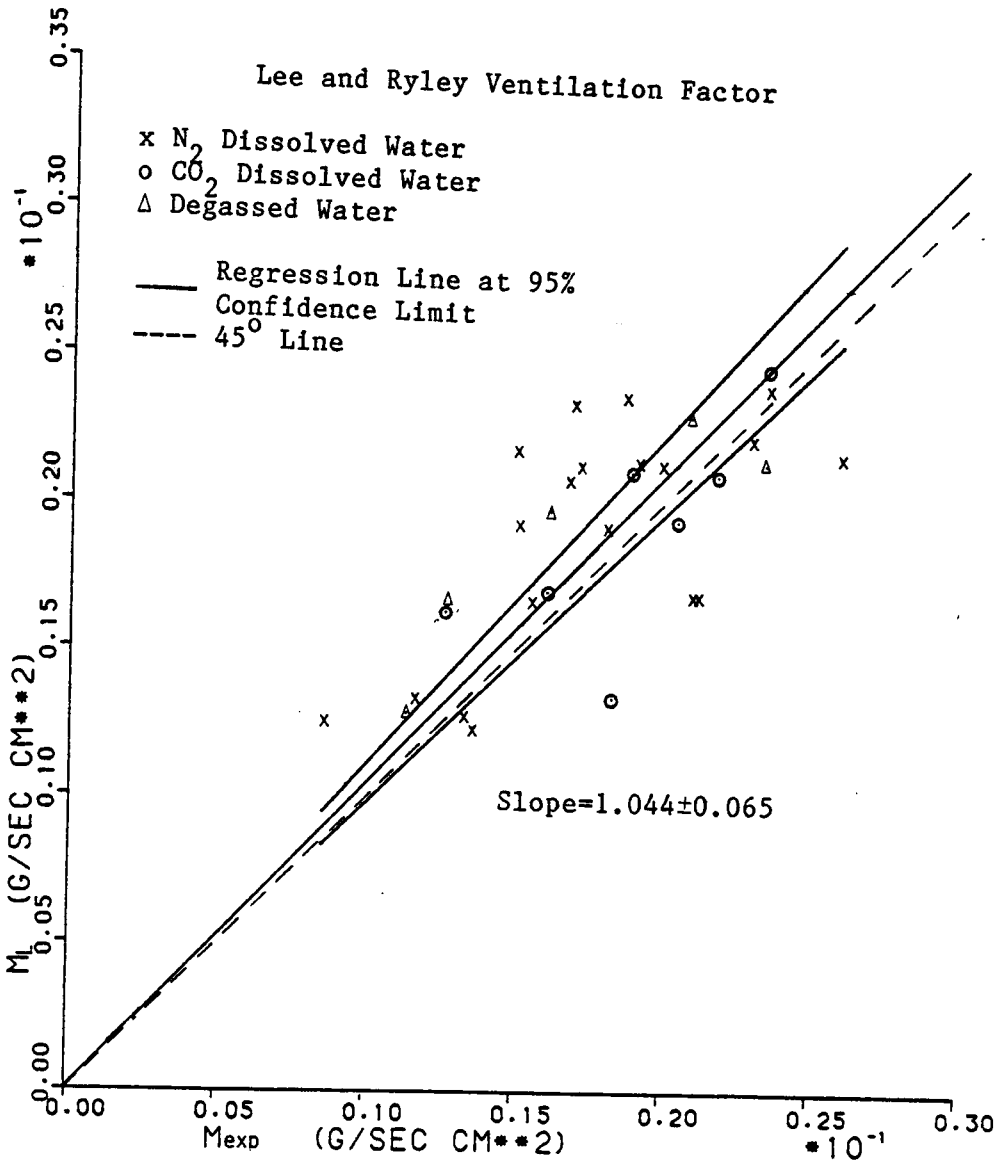


Figure 22. Comparison of experimental results with the Large Flux vaporization model using the Lee and Ryley ventilation factor (Eq.(4-18)).

Table 10. Errors between experimental vaporization rates and rates calculated according to the Large Flux model.

Ventilation Correlation	Mean Per cent Error[a]
Ranz and Marshall	- 6.1
Rowe, Claxton and Lewis	+ 0.6
Lee and Ryley	+ 4.4

a By regression analysis, with per cent error=(ML-Mexp)/ML

suspended water droplets at one, ten, and twenty atmospheres. These experiments were carried out in a pressurized chamber heated with a coal gas flame. Temperature data were not provided in this report. In view of this uncertainty, several temperatures were considered in the model calculations in order to established a feasible range for the vaporization trials. The temperatures found to give the best agreement with the data were 1500°K, 1750°K and 1750°K for one, ten and twenty atmospheres respectively. These values are in the range of the flame temperature for coal gas burning in air(49). Flame temperatures increasing with pressure are consistent with the results of Gutoff(29) and of Brown et al.(8), who showed the increase in flame temperature is a logarithmic function of pressure.

The model chosen for test against the data on vaporization under pressure is that of Froessling, as a computer program has previously been written for those calculations. The computer program is similar to that listed in Appendix C for the Froessling model, except that droplet size changes are calculated by an outer DO LOOP as a function of time until the droplet is completely vaporized. The computing procedure is shown in block diagram form in Figure 23. Property expressions used in these calculations can be found in Appendix E.

Figures 24, 25 and 26 show the experimental data points and the prediction curves for pressures of one, ten and twenty atmospheres respectively. Although the temperatures used here are somewhat uncertain, the degree of fit to the data points is very encouraging.

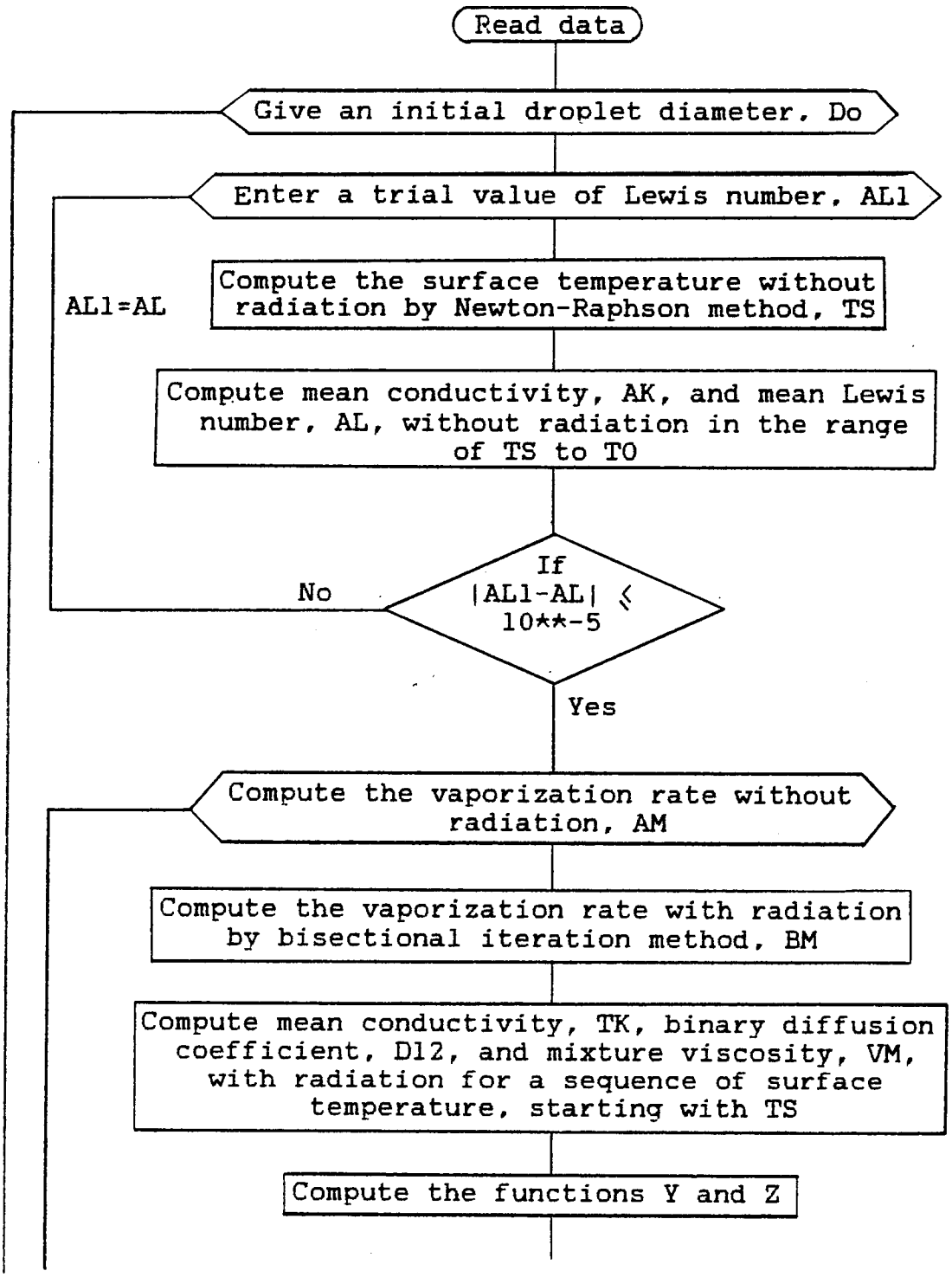


Figure 23. Flow sheet of computer program for calculating droplet dimension changes as a function of time using Froessling model.

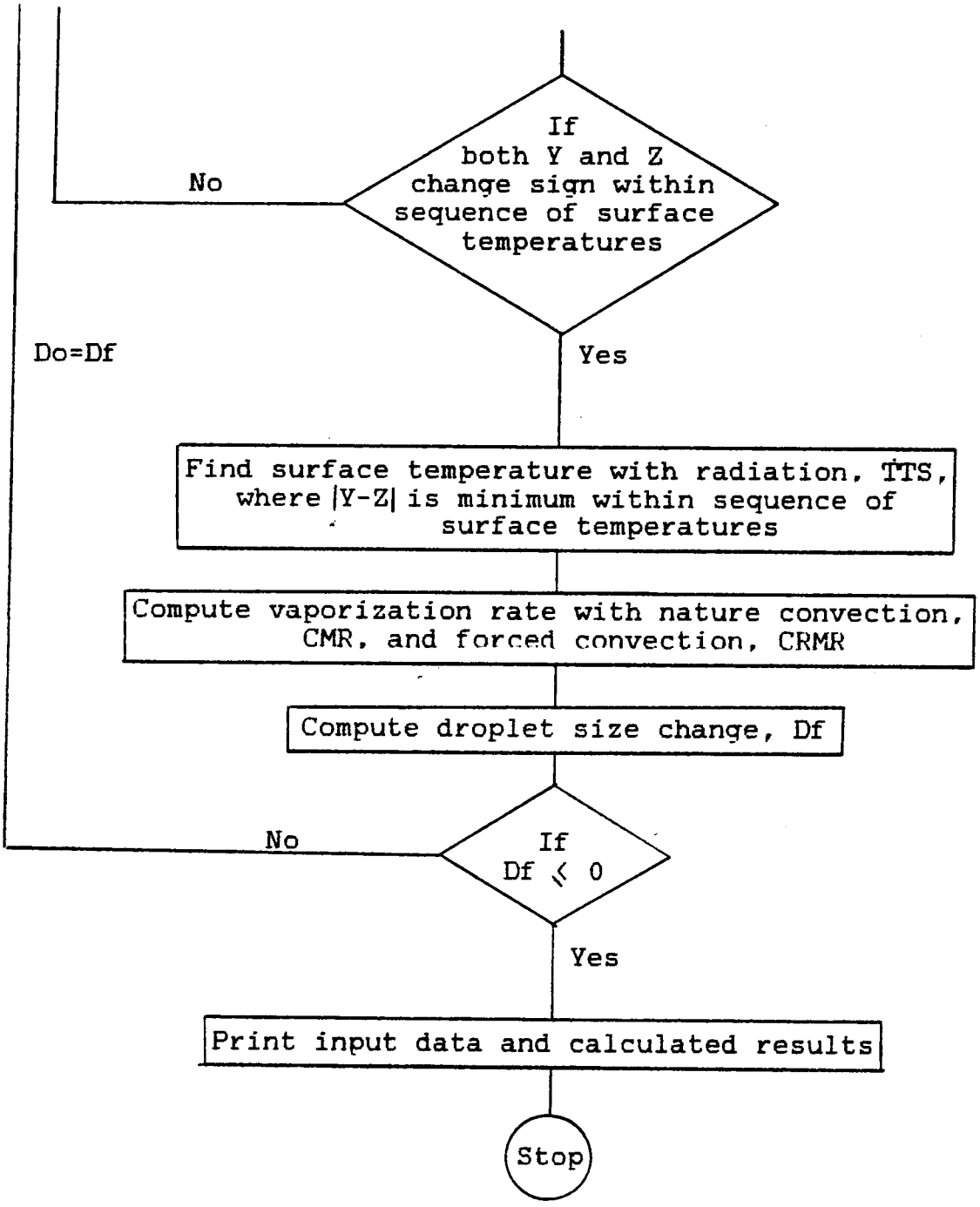


Figure 23. (Continued).

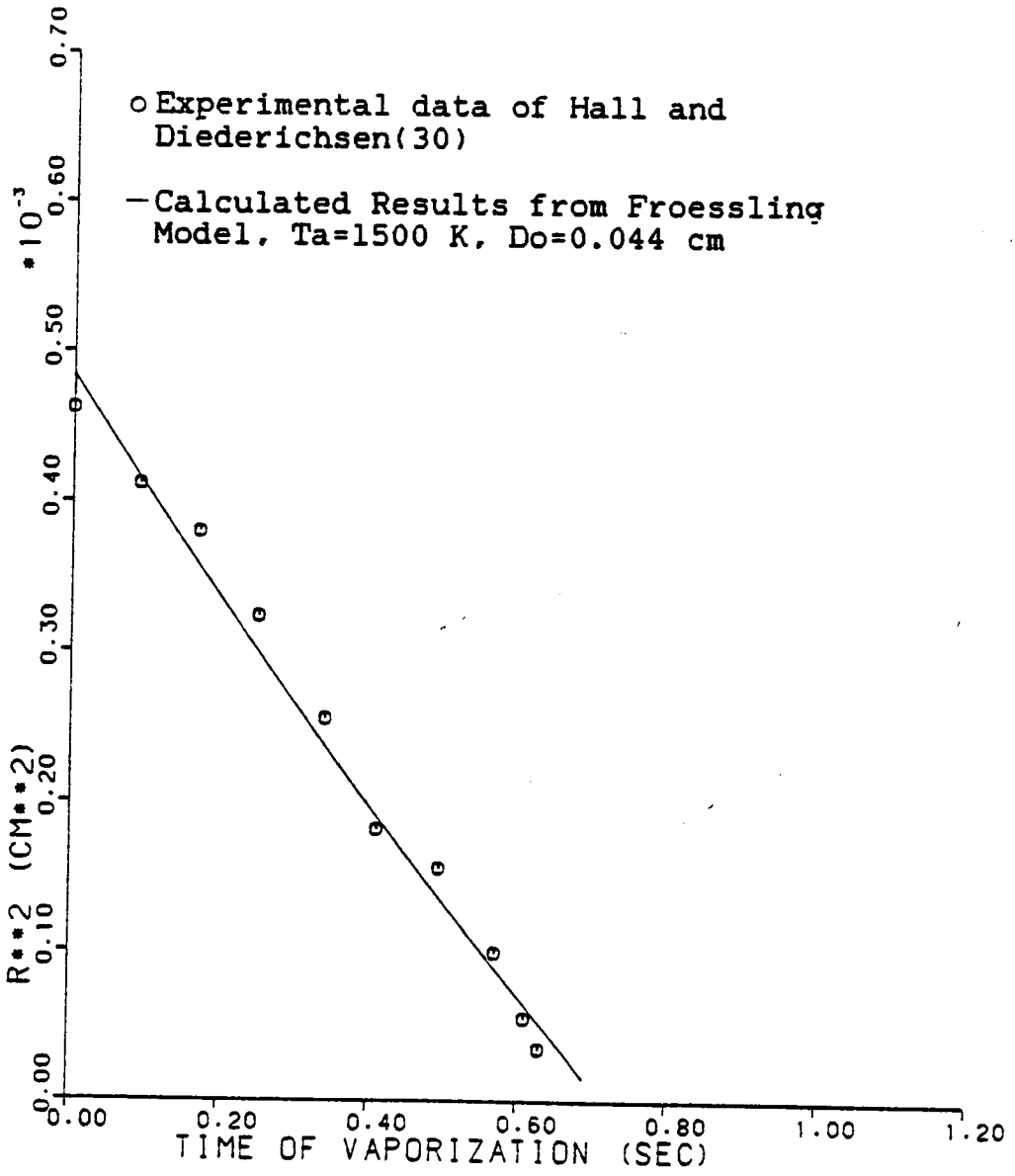


Figure 24. Comparison of experimental and calculated vaporization histories of a water droplet at one atmosphere.

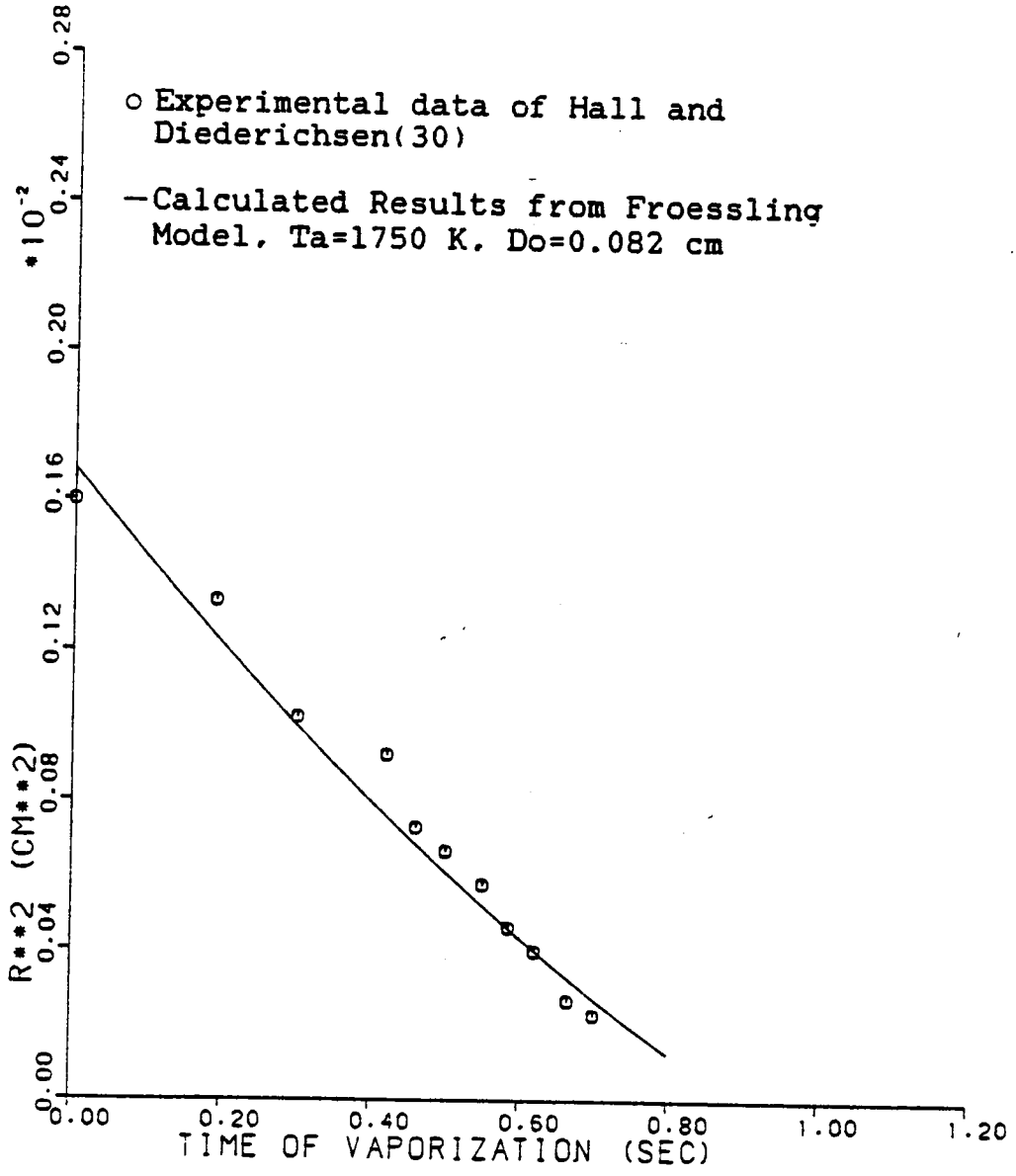


Figure 25. Comparison of experimental and calculated vaporization histories of a water droplet at ten atmospheres.

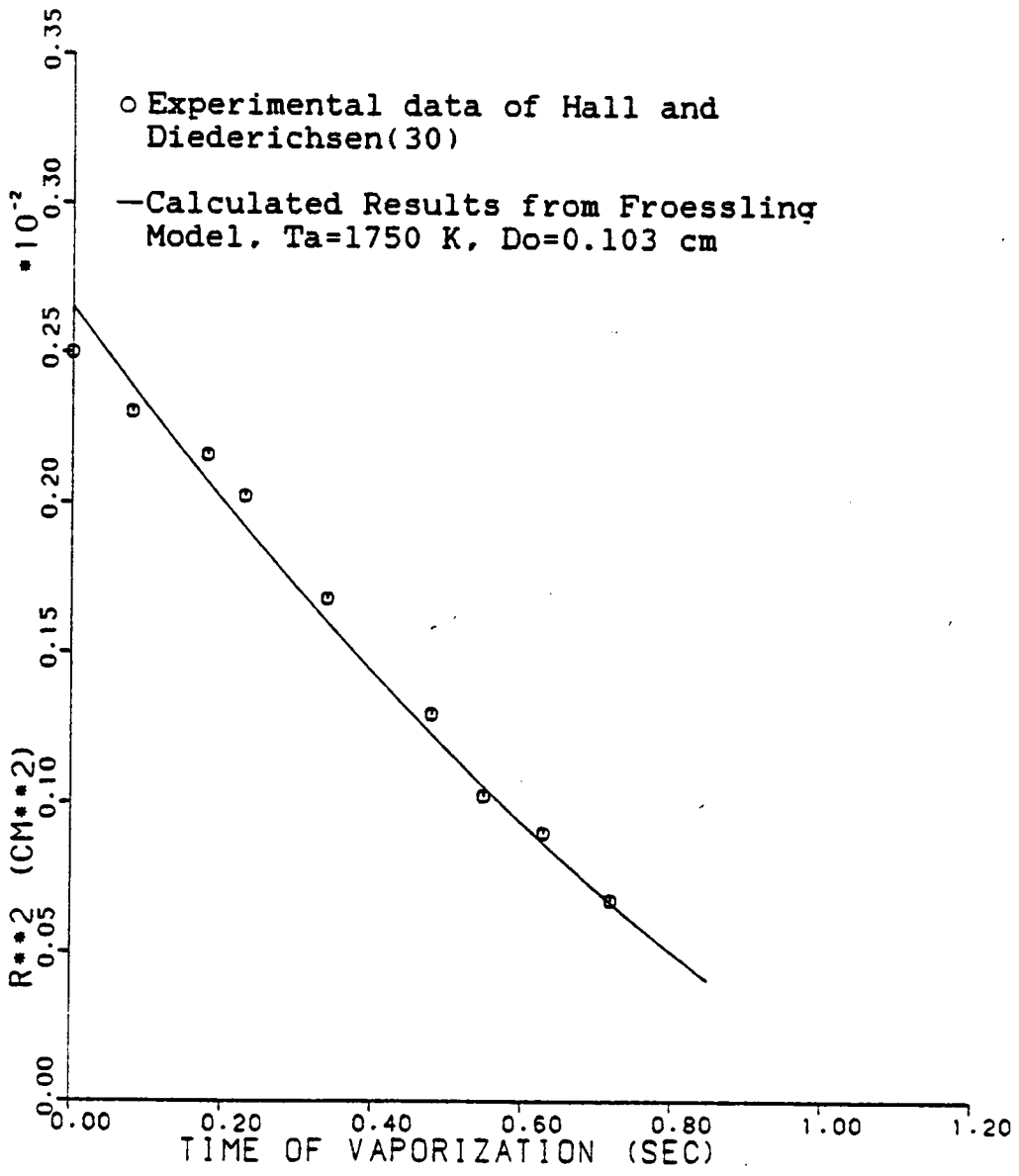


Figure 26. Comparison of experimental and calculated vaporization histories of a water droplet at twenty atmospheres.

The nonlinearity of D^2 vs. t seems to be explained by the effect of free convection. This effect has been reported on previously by Frazier(17).

CHAPTER 5

DISCUSSION OF RESULTS

5.1 Comparison of the Froessling and Large Flux Model Predictions, with Different Ventilation Factors

The primary objective of this work is to provide a set of reliable droplet vaporization data for testing vaporization models at high temperature surroundings. Two vaporization models described in the previous chapters are subjected to some essential differences in computation. However, both models require searching for the surface temperature to satisfy the energy and material balance equations simultaneously. In the Large Flux model, the average film temperature and average compositions of film are used to evaluate physical and transport properties. On the other hand, integrated mean values of the properties over the gas film are used in the Froessling model. The other major difference between these two models is that in the Large Flux model, the surface temperature of the droplet changes as the vaporization rate changes; but in the Froessling model, the surface temperature is calculated based on vaporizing in a stagnant medium and the convection effect on the surface temperature change is not taken into account. This is the advantage of using the Large Flux model.

5.2 Droplet-Droplet Interaction

The bulk of previous vaporization experimental work has been on single suspended droplets. The question arises as to how close do droplets have to be before they interfere with one another. Sangiovanni and Kesten(69,70) addressed this question in the context of the effect of droplet spacing on ignition delay times. They found that ignition delay was not decreased appreciably until the relative droplet spacings were reduced to about four to five diameters, depending on liquid volatility and other factors such as surrounding temperature, droplet velocity and convection conditions. Figure 27 shows these effects. In the present vaporization investigation, the relative droplet spacings are about two to three diameters as listed in Table 5 (Page 64). However, in contrast to the present investigation, Sangiovanni and Kesten's experimental setup was such that the droplets moved axially with the gas stream, so each droplet was located directly in the wake of the preceeding droplet. Figure 28 depicts the angle of droplets wakes relative to the direction of travel of the train for a typical experiment on the present study. This configuration may explain in part the fact that ignition delay in their setup decreased at larger relative spacings than that which appears to be required to appreciably influence vaporization rates in the present experiments. The reasonably good agreement between the calculated results obtained under the assumption of negligible droplet-droplet interaction suggests that

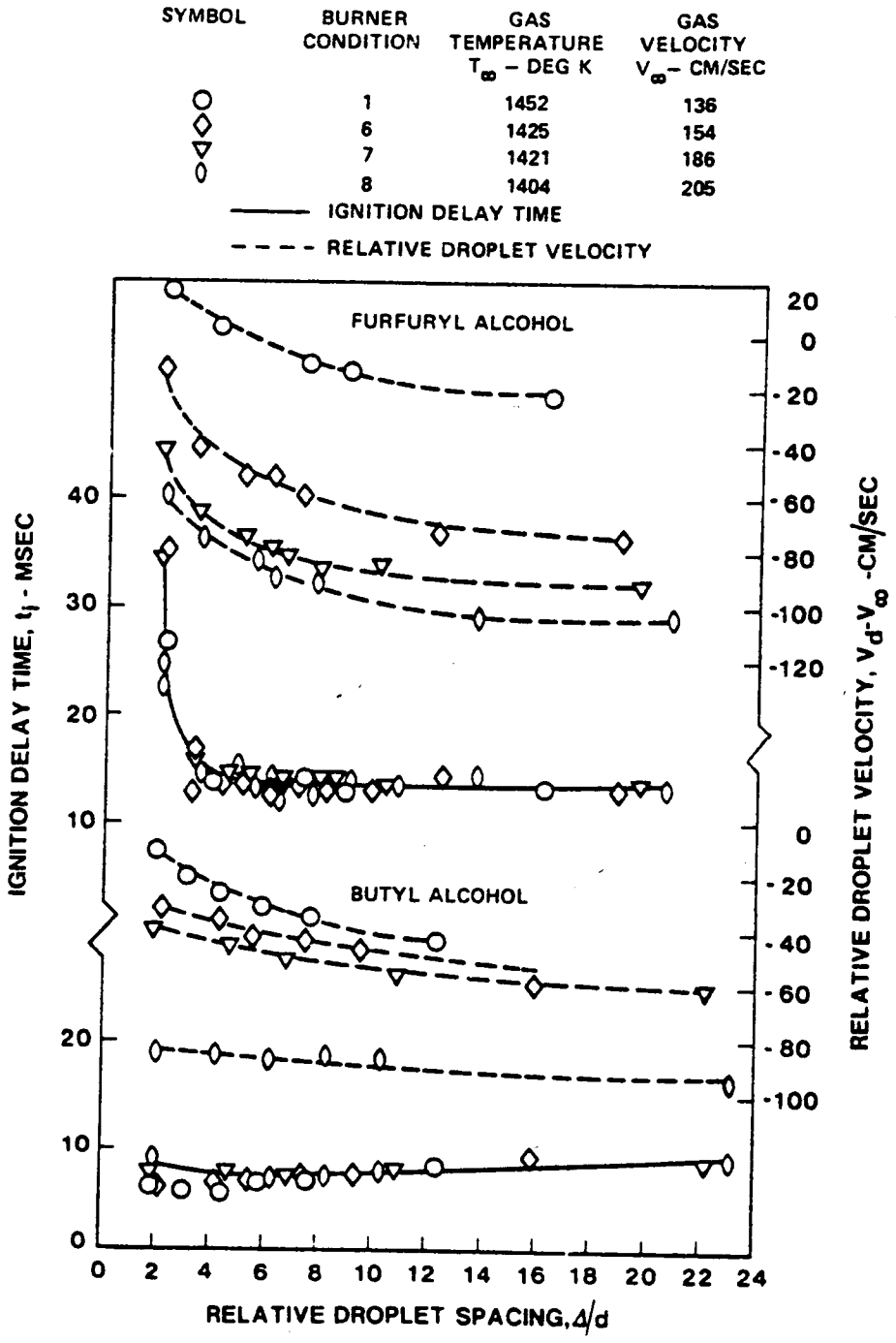


Figure 27. Variation of ignition delay time with droplet spacing (from Sangiovanni and Kesten(69)).

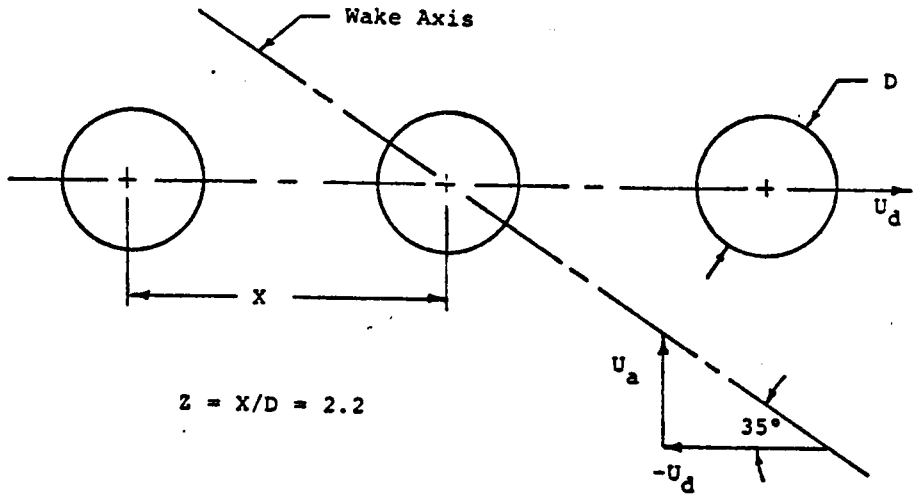


Figure 28. Section of a droplet train, showing location of the wake axis relative to the direction of the droplet motion (Run No.8).

such an effect is not large under the conditions of this experiment, that is, with the hot air in cross flow to the droplet train motion.

5.3 Droplet Oscillation

By using the technique of generating droplets in this investigation, droplet oscillation is inevitable. Figure 1 (Page 34) is a picture taken at the early stage of the droplet stream just ejected from the nozzle when the oscillations were still obvious. However, the droplets used in the analysis are the ones where no visual oscillations were observed. With this concern, all the experiments were carried out within a limited range of droplet sizes and velocities. Figure 9 (Page 56) is a typical photograph of a droplet train which exhibits high degree of droplet sphericity. Vaporization rates were evaluated from photomicrographs exhibiting this degree of droplet sphericity. The influence of oscillation on vaporization rates was thus negligible in this study.

5.4 Effect of Outgassing

A subsidiary objective of this investigation is to test the effect of dissolved gasses on vaporization rates. No significant differences in vaporization rates were found in the entire range of experimental conditions, between the degassed water and gas-dissolved water (CO_2, O_2 and N_2 , at pressures up to 1.3 atm). Stable droplet streams could always be generated by the sonic driver operated within the frequency of 3500 HZ to 3600 HZ. No evidence of further atomization due to outgassing was observed. The unstable

droplet train was formed when the frequency of sonic driver was beyond the stable range for both degassed and gas-dissolved water droplets. This has been discussed by Wissema and Davies(80) in their development of the formation of uniformly sized drops by vibration-atomization. Although no significant effect of dissolved gases on heat and mass transfer was revealed under the current experimental conditions, the possibility of such effects is not excluded for the liquids with higher gas solubilities and in high pressure situations. One previous study(34) has shown the possibility of internal boiling due to the dissolved gases in droplets during the evaporation process. Further studies to conduct such experiments under high pressure conditions are suggested.

CHAPTER 6

SUMMARY AND CONCLUSIONS

A novel experimental apparatus was constructed and used to study the vaporization rates of trains of uniformly-sized water droplets moving through the central, laminar core of a hot air jet whose temperature was controlled at specified values in the range of $500^{o}C$-$860^{o}C$. Quantitative vaporization studies on moving droplets in this temperature range are not known. The droplets were produced by induced breakup of a water jet streaming from a fine capillary tube. A sonic driver, operating at frequencies in the range of 3500 to 3600 HZ, was used to induce breakup of the liquid jet. The droplets studied are about 260 to 300 μm in diameter and are spaced within two to three diameters of one another. The droplet train moves in cross-flow through the hot air jet. Evaporation rates were calculated from measurements of droplet diameters taken from photomicrographs of the droplet train. A total of thirty-three experimental runs were made throughout the temperature range. The number of droplets evaluated in each run are in the range of 17 to 41 (see Appendix F). In most cases, there are about 30 data points in a run. The Reynolds number of the droplets ranges from 7 to 17.

The principal objective of this investigation was to obtain sufficient, quantitative data for testing two, simple models of the vaporization process. The models considered are a modified form of the Froessling model and the Large Flux model. Each of these models

requires an experimental correlation for the heat or mass transfer coefficient for its use of the form:

$$Nu = 2(1 + K\ Re^{1/2}\ Pr^{1/3})$$

$$Sh = 2(1 + K\ Re^{1/2}\ Sc^{1/3})$$

These correlations, taken from the literature, are based primarily on low to moderately high temperature experimental data taken from observation of small droplets suspended from fine fibers in air streams, although a limited amount of data were employed from freely falling droplets in hot furnaces. In addition to the question of the better model for use at high temperatures is the question of the appropriate value of K, the ventillation coefficient, for use in the above heat or mass transfer correlations. Various investigators have suggested values of 0.276 (Froessling), 0.3 (Ranz and Marshall), 0.345 (Rowe, Claxton and Lewis), and 0.37 (Lee and Ryley).

Computer programs were developed to facilitate the iterative calculations required for determing the droplet vaporization rate according to each of the two models, each model containing alternately each of the above literature values of the constant K. The following conclusions are based on a statistical comparison of the model results with the experimentally determined vaporization rates, for the thirty-three runs.

1. The modified Froessling model predictions agree with the experimental results with average deviations of -18% to -5%, depending on the value used for the coefficient on the ventilation factor. The poorest agreement (-18%) was obtained by use of

Froessling's coefficient of 0.276, while the best agreement (-5%) was provided by use of Lee and Ryley's value of 0.37 for this coefficient.

2. The Large Flux model predictions agree with the experimental results with average deviations of -6% to +4%, depending on the value for the coefficient of the ventilation factor.

3. The best agreement with the experimental results was obtained using the Large Flux model containing the value of the ventilation coefficient recommended by Rowe, Claxton, and Lewis, 0.345. For this case the average deviation between the predictions and the experimental results is -0.6%.

4. Even though the average deviations between model predictions and experimental results were relatively small in many of the cases considered, the relatively wide scatter in the experimental data prevents a definitive choice for the model and ventilation factor coefficient at this time. For example, about 75% of the data points fall within 20% of the mean, and about 88% of the data fall within 25% of the mean. This situation is due to imprecision in determining the drop diameters, and consequently, the experimentally determined vaporization rates.

5. The vaporization models tested were developed for isolated droplets in an elevated temperature gas. However, the droplets in these experiments were within about two to three diameters of one another. In spite of this relatively close proximity, the extent of the agreement between the model predictions and data is relatively

good on the average in most cases. This result suggests that droplet-droplet interactions are not appreciable under these conditions. The cross flow arrangement between the air jet and the droplet train in these experiments produces an angle of inclination of about 35° between the droplet wake axis and the axis of the droplet motion. The droplets are thus not contained entirely in the wake of their preceeding neighbor.

6. Based on a limited number of experiments with oxygen, nitrogen, and carbon dioxide, dissolved gases under pressures up to about 1.3 atmospheres do not produce an observable effect on the water droplet vaporization rates.

7. The modified Froessling model was tested against elevated pressure droplet vaporization data from the literature, in the pressure range of one to twenty atmospheres. Using estimated values of the gas temperatures, quantitative agreement was obtained between both the absolute data values and the general curvature in the data. This result gives additional support to the validity of this simple model. A similar calculation was not made for the Large Flux model.

CHAPTER 7

RECOMMENDATIONS

The results of this investigation have shown that simple vaporization model equations are capable of predicting droplet vaporization rates even at relatively large fluxes. However, there are certain areas where additional data and analytical work would be useful.

In the present work, the data scatter prevented a definitive choice between vaporization models and the corresponding ventilation coefficient. Recommendations for further work directed toward clarification of this question are as follows:

1. Should future work be performed in an experimental setup of the type used here, provision should be made for longer residence times in the hot air stream. The better approach to achieving this result is by increasing the furnace tube size to at least one or two inches in diameter, or more, beyond the two and one-half inches size used here.

2. The Reynolds number range of the data can most readily be extended, from the experimental standpoint, by working with droplets in a size range that is larger than that used here (about 300 μm). However this will necessitate the use of a large furnace tube to minimize the effect of droplet oscillations and to provide ample heat up time for the droplets.

3. Use of liquids more volatile than water is also a way of

extending the data with respect to the range in certain of the non-dimensional groups, such as the Schmidt and Prandtl numbers and the Spalding number.

4. The effect of dissolved gases on droplet vaporization is suggested to be studied in a high pressure chamber where considerable amount of gas dissolved in the liquid is possible instead of using the present type of setup.

Finally, an area in which there are virtually no data in the literature is that of the effect of droplet oscillations on the vaporization rate. Droplets are naturally oscillating when they are formed by breakup of a liquid jet. If a way can be found to maintain the principal oscillation frequency, such as by passing the droplet stream through an oscillating electric field, it may be possible to achieve a steady state in which the oscillation amplitude is constant during the period of time of a vaporization experiment.

LIST OF REFERENCES

LIST OF REFERENCES

1. Ackermann, G., Forschungsheft, 382, 1 (1937).

2. Agoston, G. A., Wise, H., and Rosser, W. A., Sixth Int. Symp. on Combustion, 708 (1957).

3. Agoston, A., Wood, B. J., and Wise, H., Jet Propulsion, 28, 181 (1958).

4. Beard, K. V., and Pruppacher, H. R., J. Atmos. Sci., 28, 1455 (1971).

5. Bhogte, S. M., M.S. Thesis, The University of Tennessee, Knoxville (1972).

6. Bird, R. B., Stewart, W. E., and Lightfoot, E. N., "Transport Phenomena," John Wiley & Sons, New York (1960).

7. Brown, S. L., Phys. Rev., 21, 2, 103 (1923).

8. Brown, R. L., Everest, D. A., Lewis, J. D., and Williams, A., J. Inst. Fuel, 41, 433 (1968).

9. Brzustowski, T. A., Can. J. Chem. Engng., 43, 30 (1965).

10. Chang, H. W., M.S. Thesis, The University of Tennessee, Knoxville (1970).

11. Colburn, A. P., and Drew, T. B., Trans. A.I.Ch.E., 33, 197 (1937).

12. Crosby, E. J., and Stewart, W. E., Ind. Eng. Chem. Fundam., 9, 3, 515 (1970).

13. Downing, C. G., A.I.Ch.E.J., 12, 4, 760 (1966).

14. Eckert, E. R. G., and Drake, R. M., Jr., "Heat and Mass Transfer," McGraw-Hill, New York (1959).

15. Eisenklam, P., Arunachalam, S. A., and Weston, J. A., Eleventh Int. Symp. on Combustion, 715 (1967).

16. Feingold, A., and Gupta, K. G., J. Heat Transfer, 92, 69 (1970).

17. Frazier, G. C., Can. J. Chem. Engng., 55, 678 (1977).

18. Frazier, G. C., and Chang, H. W., Can. J. Chem. Engng., 55, 736 (1977).

19. Frazier, G. C., and Hellier, W. W., I & EC Fund., 8, 4, 807 (1969).

20. Froessling, N., Gerlands Beitr. Geophys., 52, 170 (1938).

21. Freund, R. J., and Littell, R. C., SAS for Linear Models, SAS Institute INC. (1981).

22. Galloway, T. R., and Sage, B. H., Int. J. Heat Mass Transfer, 7, 283 (1964).

23. Garner, F. H., and Grafton, R. W., Proc. Roy. Soc., A224, 64 (1954).

24. Garner, F. H., and Lane, J. J., Trans. Inst. Chem. Engrs., 37, 154 (1959).

25. Godsave, G. A. E., Fourth Int. Symp. on Combustion, 818 (1953).

26. Goldsmith, M., and Penner, S. S., Jet Propulsion, 24, 245 (1954).

27. Goldsmith, M., Jet Propulsion, 26, 172 (1956).

28. Griffith, R. M., Chem. Engng. Sci., 12, 198 (1960).

29. Gutoff, E. B., Advances in Petroleum Chemistry and Refining, Interscience, 8, 237 (1964).

30. Hall, A. R., and Diederichsen, J., Fourth Int. Symp. on Combustion, 837 (1953).

31. Harpole, G. M., J. Heat Transfer Trans. A.S.M.E., 103, 1, 86 (1981).

32. Hersch, M., NASA TND-2881 (1965).

33. Hoffman, T. W., and Gauvin, W. H., Can. J. Chem. Engng., 38, 129 (1960).

34. Hoffman, T. W., and Ross, L. L., Int. J. Heat Mass Transfer, 15, 599 (1972).

35. Houghton, H. G., J. Appl. Phys., 4, 419 (1933).

36. Ingebo, R. D., NACA TN 2368 (1951).

18. Frazier, G. C., and Chang, H. W., Can. J. Chem. Engng., 55, 736 (1977).

19. Frazier, G. C., and Hellier, W. W., I & EC Fund., 8, 4, 807 (1969).

20. Froessling, N., Gerlands Beitr. Geophys., 52, 170 (1938).

21. Freund, R. J., and Littell, R. C., SAS for Linear Models, SAS Institute INC. (1981).

22. Galloway, T. R., and Sage, B. H., Int. J. Heat Mass Transfer, 7, 283 (1964).

23. Garner, F. H., and Grafton, R. W., Proc. Roy. Soc., A224, 64 (1954).

24. Garner, F. H., and Lane, J. J., Trans. Inst. Chem. Engrs., 37, 154 (1959).

25. Godsave, G. A. E., Fourth Int. Symp. on Combustion, 818 (1953).

26. Goldsmith, M., and Penner, S. S., Jet Propulsion, 24, 245 (1954).

27. Goldsmith, M., Jet Propulsion, 26, 172 (1956).

28. Griffith, R. M., Chem. Engng. Sci., 12, 198 (1960).

29. Gutoff, E. B., Advances in Petroleum Chemistry and Refining, Interscience, 8, 237 (1964).

30. Hall, A. R., and Diederichsen, J., Fourth Int. Symp. on Combustion, 837 (1953).

31. Harpole, G. M., J. Heat Transfer Trans. A.S.M.E., 103, 1, 86 (1981).

32. Hersch, M., NASA TND-2881 (1965).

33. Hoffman, T. W., and Gauvin, W. H., Can. J. Chem. Engng., 38, 129 (1960).

34. Hoffman, T. W., and Ross, L. L., Int. J. Heat Mass Transfer, 15, 599 (1972).

35. Houghton, H. G., J. Appl. Phys., 4, 419 (1933).

36. Ingebo, R. D., NACA TN 2368 (1951).

37. Ingebo, R. D., NACA TN 2850 (1953).

38. Keenan, J. H., and Keyes, F. G., "Thermodynamic Properties of Steam," Wiley, New York (1936).

39. Keey, R. B., and Glen, J. B., Can. J. Chem. Engng., 42, 227 (1964).

40. Kent, J. C., Appl. Sci. Res., 28, 315 (1973).

41. Kinzer, G. D., and Gunn, R. J., J. Meteror., 8, 71 (1951).

42. Kobayasi, K., Fifth Int. Symp. on Combustion, 141 (1955).

43. Kobayasi, K., Trans. J.S.M.E., 20, 100, 826, 831 (1954).

44. Langmuir, I., Phys. Rev., 12, 368 (1918).

45. Law, C. K., Prog. Energy Combust. Sci., 8, 171 (1982).

46. Lazar, R. S., and Faeth, G. M., Thirteen Int. Symp. on Combustion, 801 (1970).

47. Lee, K., and Ryley, D. J., J. of Heat Transfer, 90, 4, 445 (1968).

48. Lewis, W. K., and Chang, K. C., Trans. A.I.Ch.E., 21, 127 (1928).

49. Lewis, B., and von Elbe, G., "Combustion, Flame, and Explosions of Gases," 2nd Ed., Academic (1961).

50. Lindsay, A. L., and Bromley, L. A., Ind. Eng. Chem. 42, 8, 1508 (1950).

51. Mahoney, J. J., Proc. Royal Soc. London, A, 238, 412 (1956).

52. Manning, W. P., and Gauvin, W. H., A.I.Ch.E.J., 6, 184 (1960).

53. Manrique, J. A., and Borman, G. L., Int. J. Heat Mass Transfer, 12, 1081 (1969).

54. Mason, C. L., M.S. Thesis, The University of Tennessee, Knoxville (1975).

55. Mason, E. A., and Monchick, L., J. Chem. Phys. 36, 2746 (1962).

56. Matlosz, R. L., Leipziger, S., and Torda, T. P., Int. J. Heat Mass Transfer, 15, 831 (1972).

57. Maxwell, J. C., Collected Scientific Papers, Cambridge, 11, 625 (1890).

58. Mickley, H. S., Ross, R. C., Squyers, A. L., and Stewart, W.E., NACA TN 3208 (1954).

59. Nishiwaki, N., Fifth Int. Symp. on Combustion, 148 (1955).

60. Pasternak, I. S., and Gauvin, W. H., A.I.Ch.E.J., 7, 254 (1961).

61. Perry, J. H., and Chilton, C. H., "Chemical Engineers' Handbook," 4th Ed., McGraw-Hill, New York (1963).

62. Pritchard, C. L., and Biswas, S. K., British Chem. Eng., 12, 6, 879 (1967).

63. Ranz, W. E., Trans. A.S.M.E., 78, 909 (1956).

64. Ranz, W. E., and Marshall, W. R., Jr., Chem. Eng. Prog., 48, 141 (1952).

65. Richardson, P. D., Chem. Eng. Sci., 18, 149 (1963).

66. Ross, L. L., and Hoffman, T. W., Proceedings of Third International Heat Transfer Conference, V, 50 (1966).

67. Rosner, D. E., A.I.A.A.J., 5, 163 (1967).

68. Rowe, P. N., Claxton, K. T., and Lewis, J. B., Trans. Inst. Chem. Engrs., 43, 14 (1965).

69. Sangiovanni, J. J., and Kesten, A. S., Sixteenth Int. Symp. on Combustion, 577 (1976).

70. Sangiovanni, J. J., and Kesten, A. S., Combustion Science and Technology, 16, 59 (1977).

71. Schubauer, G. B., Spangenberg, W. G., and Klebanoff, P. S., NACA TN 2001 (1950).

72. Spalding, D. B., Fourth Int. Symp. on Combustion, 847 (1953).

73. Spalding, D. B., A.R.S.J., 29, 825 (1959).

74. Walker, R. E., and Westenberg, A. A., J. Chem. Phys. 29, 1139 (1958).

75. Whitaker, S., A.I.Ch.E.J., 18, 361 (1972).

76. White, R. R., and Churchill, S. W., A.I.Ch.E.J., 5, 354 (1959).

77. Wieber, P. R., A.I.A.A.J., 1, 2764 (1963).

78. Williams, A., "Combustion and Flame," 21, 1 (1973).

79. Wise, H., Lorell, J., and Wood, B. J., Fifth Int. Symp. on Combustion, 132 (1955).

80. Wissema, J. G., and Davies, G. A., Can. J. Chem. Engng., 47, 530 (1969).

81. Yao, S. C., and Schrock, V. E., J. Heat Transfer, Trans. A.S.M.E., 120 (1976).

82. Yuen, M. C., and Chen, L. W., Int. J. Heat Mass Transfer, 21, 537 (1978).

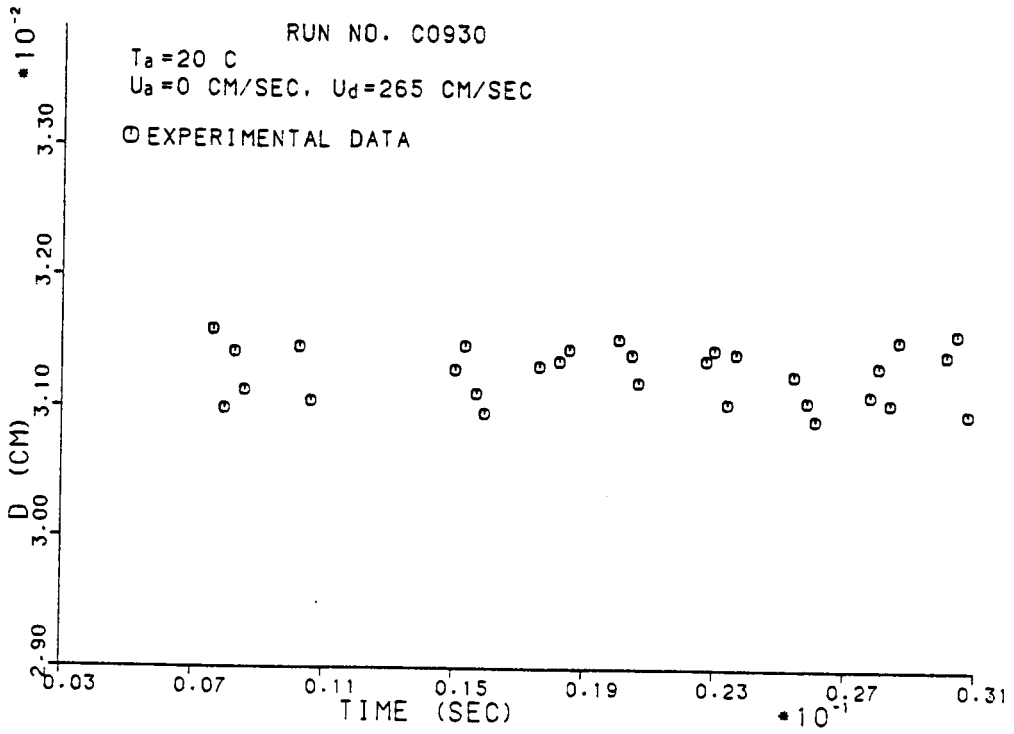
83. Yuge, T., J. Heat Transfer, Trans. A.S.M.E., 82, 214 (1960).

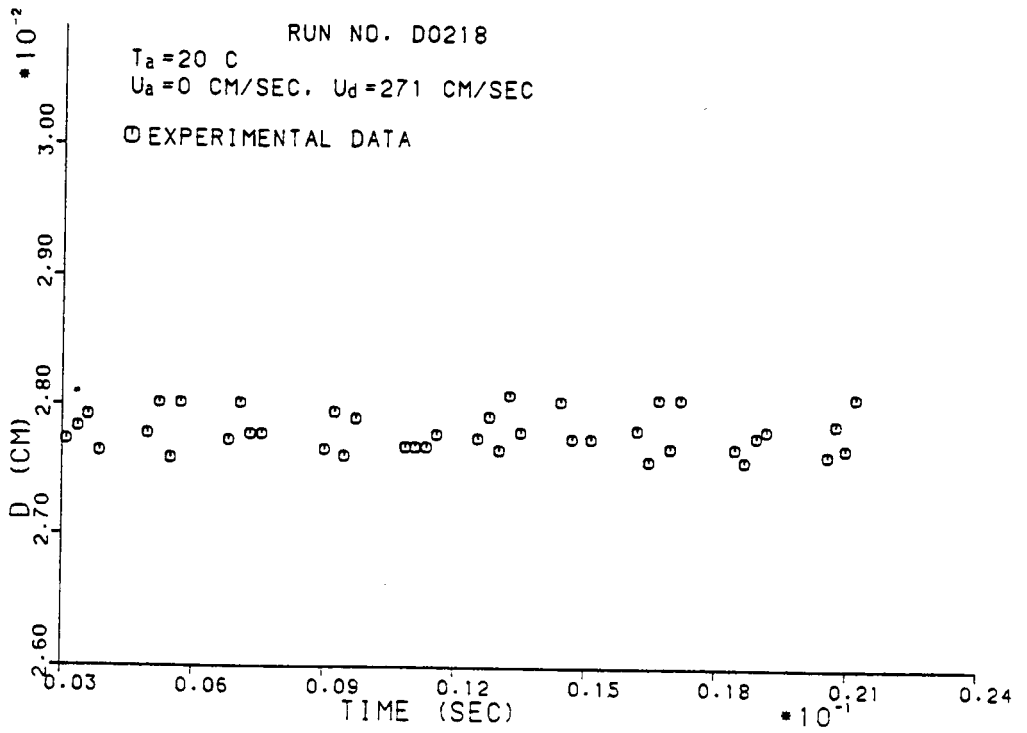
APPENDIXES

APPENDIX A

DROPLET SIZE HISTORIES IN STILL AIR AND AT ROOM TEMPERATURE

These two plots represent the size histories of droplets generated and injected through the nozzle at room temperature in still air, to measure the uniformity and the degree of scatter by using the technique employed in this study.


RUN NO. C0930
Ta =20 C
Ua =0 CM/SEC. Ud =265 CM/SEC
EXPERIMENTAL DATA
D (CM)
*10⁻²
2.90
3.00
3.10
3.20
3.30
0.03
0.07
0.11
0.15
0.19
0.23
0.27
0.31
TIME (SEC)
*10⁻¹


RUN NO. D0218
Ta =20 C
Ua =0 CM/SEC. Ud =271 CM/SEC
EXPERIMENTAL DATA
D (CM)
*10⁻²
2.60
2.70
2.80
2.90
3.00
0.03
0.06
0.09
0.12
0.15
0.18
0.21
0.24
TIME (SEC)
*10⁻¹

APPENDIX B

THE PLOTS OF D^2 VS. t OF THE COMPLETE SET

In the following pages, a complete set of D^2 vs. t plots are collected in the same order as the experiments listed in Table 5.

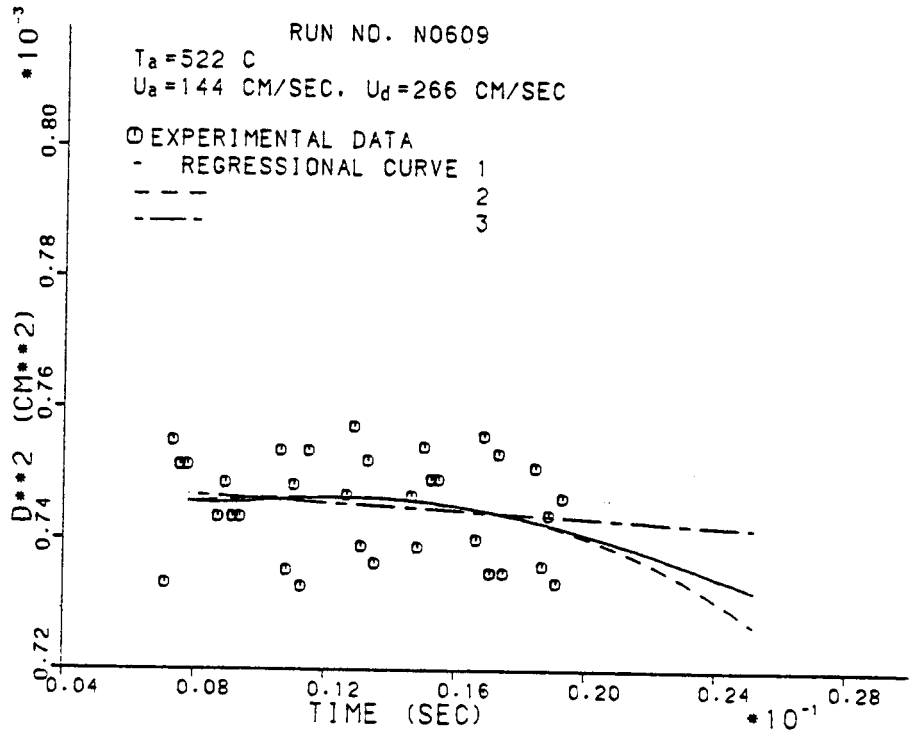
Three regression curves 1, 2, and 3 are drawn corresponding to the regression equations (B-1), (B-2), (B-3) below.

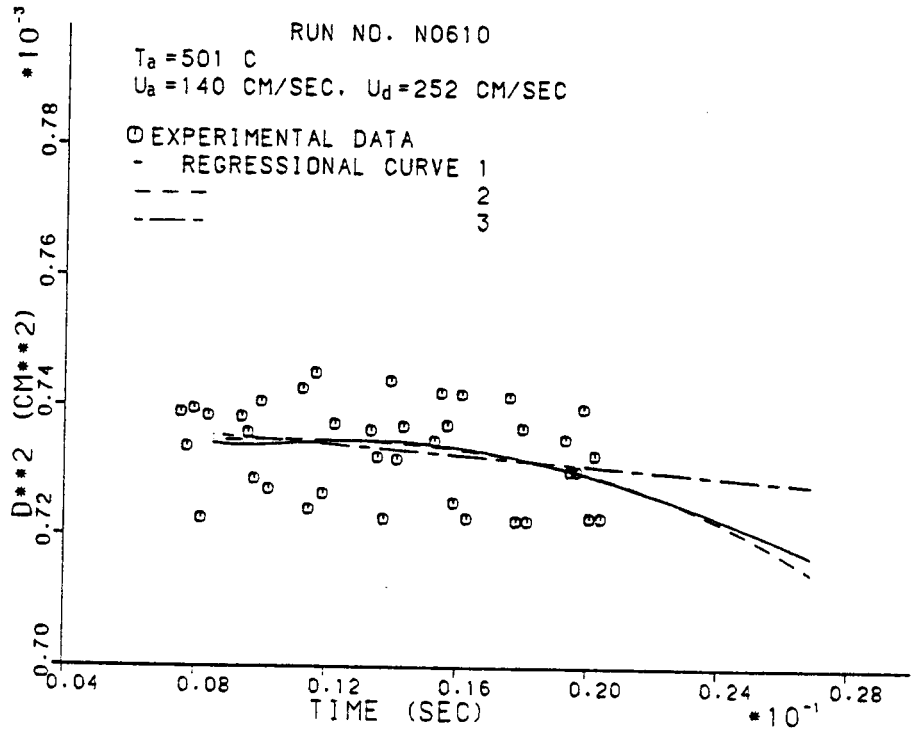
$$D^2 = a + bt + c/t + d/t^2 + e/t^3 \qquad \text{(B-1)}$$

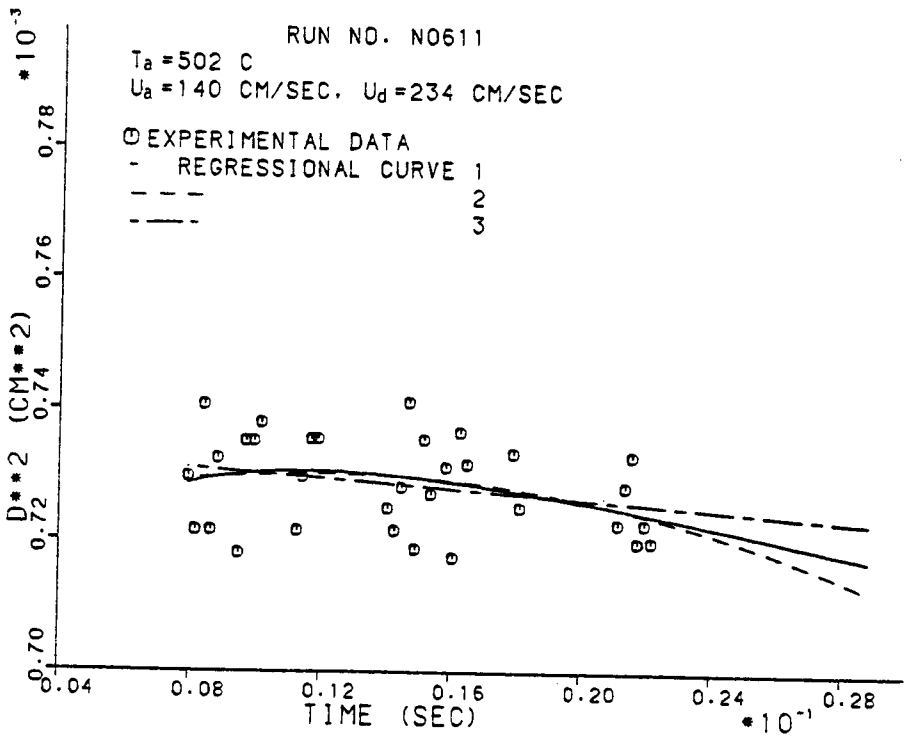
$$D^2 = a + bt + ct^2 + dt^3 \qquad \text{(B-2)}$$

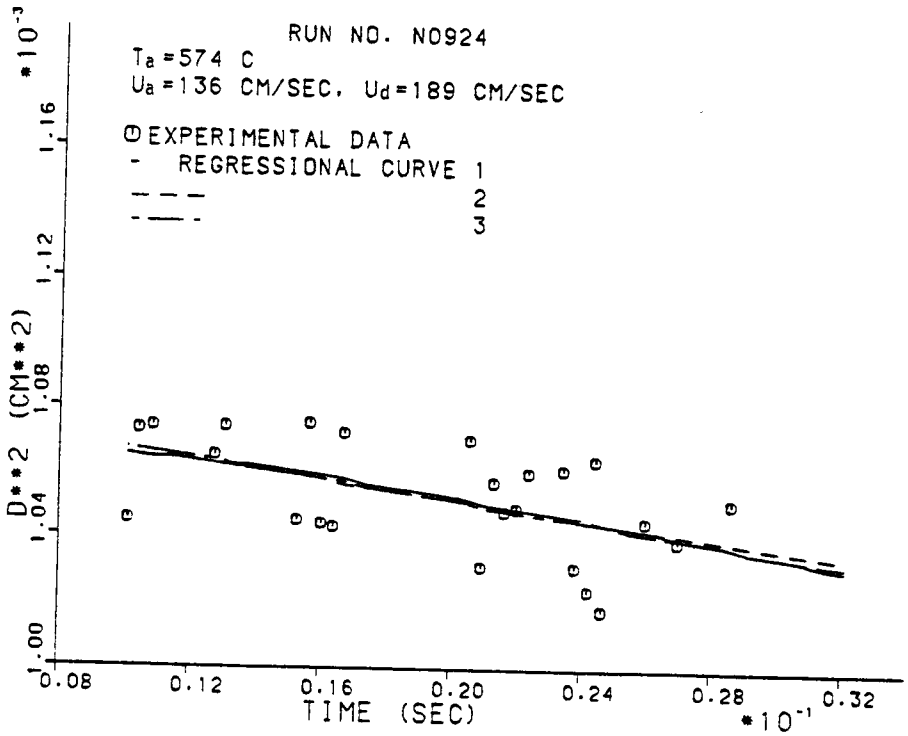
$$D^2 = a + bt \qquad \text{(B-3)}$$

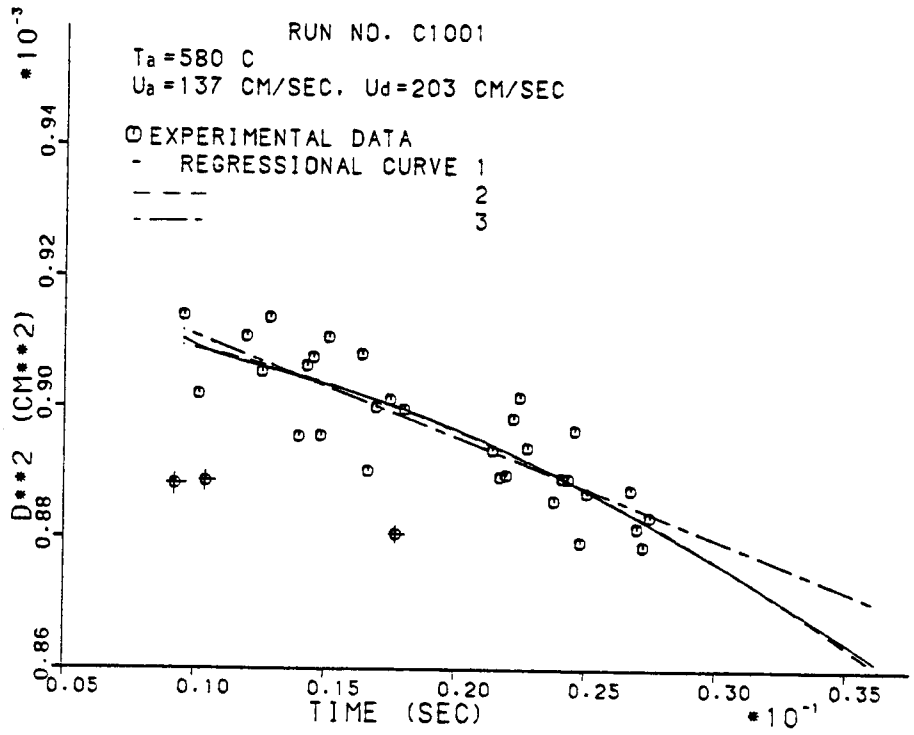
The data points with "⊕" have been excluded in regression analysis.

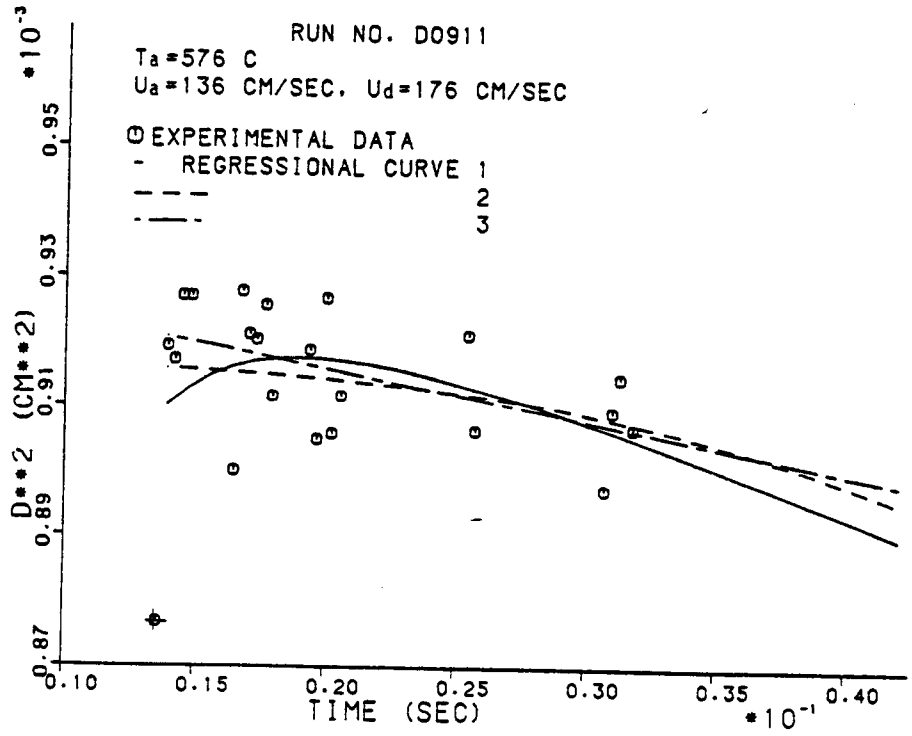

RUN NO. N0609
Ta =522 C
Ua =144 CM/SEC. Ud =266 CM/SEC
EXPERIMENTAL DATA
REGRESSIONAL CURVE 1
2
3
D**2 (CM**2)
*10⁻³
0.72
0.74
0.76
0.78
0.80
0.04
0.08
0.12
0.16
0.20
0.24
0.28
TIME (SEC)
*10⁻¹

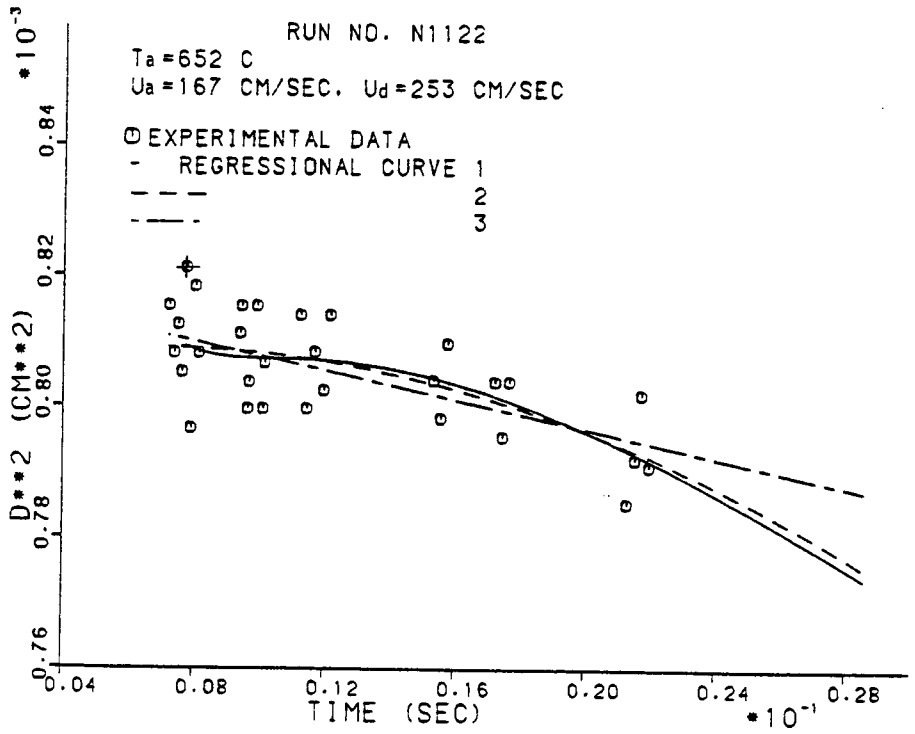

RUN NO. N0610
Ta =501 C
Ua =140 CM/SEC. Ud =252 CM/SEC
EXPERIMENTAL DATA
REGRESSIONAL CURVE 1
2
3
D**2 (CM**2)
*10⁻³
0.70
0.72
0.74
0.76
0.78
0.04
0.08
0.12
0.16
0.20
0.24
0.28
TIME (SEC)
*10⁻¹

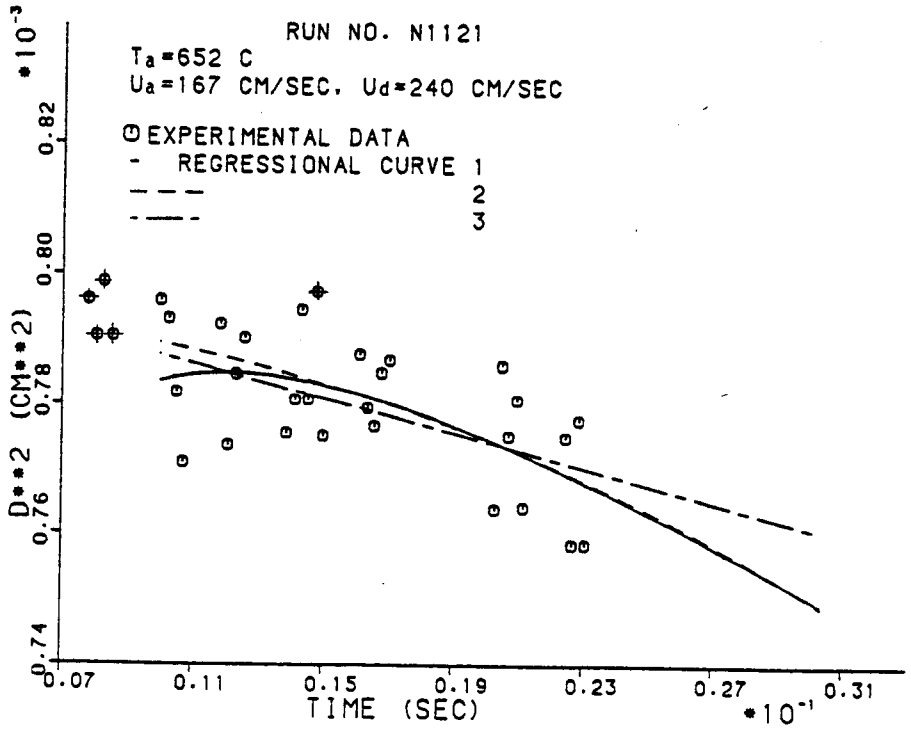

RUN NO. N0611
Ta =502 C
Ua =140 CM/SEC. Ud =234 CM/SEC
EXPERIMENTAL DATA
REGRESSIONAL CURVE 1
2
3
D**2 (CM**2)
*10⁻³
0.70
0.72
0.74
0.76
0.78
0.04
0.08
0.12
0.16
0.20
0.24
0.28
TIME (SEC)
*10⁻¹

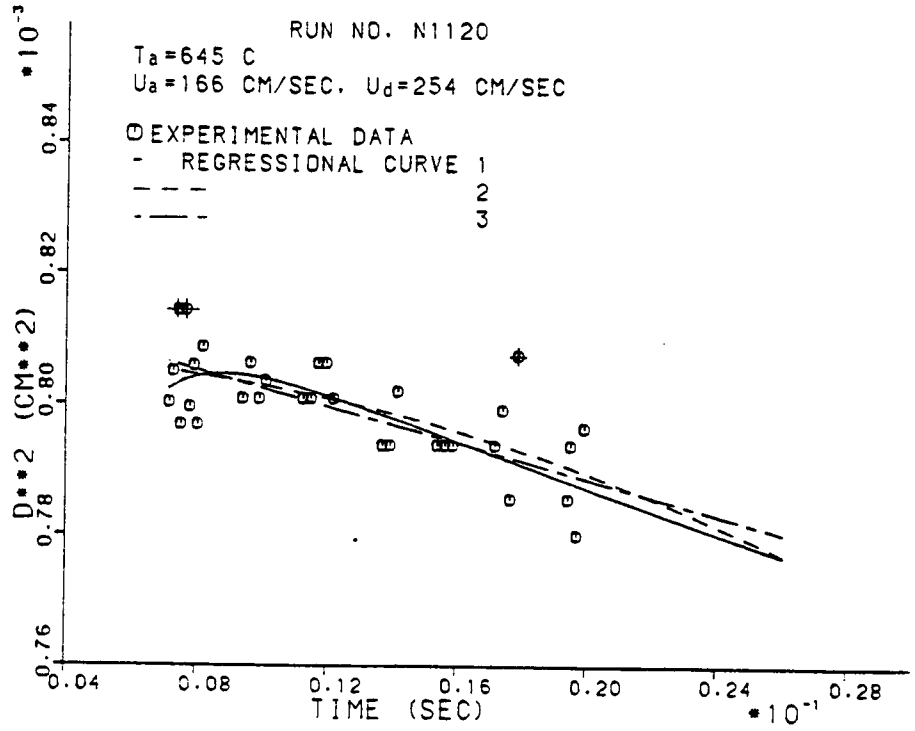

RUN NO. N0924
Ta =574 C
Ua =136 CM/SEC. Ud =189 CM/SEC
EXPERIMENTAL DATA
REGRESSIONAL CURVE 1
2
3
D**2 (CM**2)
*10⁻³
1.00
1.04
1.08
1.12
1.16
0.08
0.12
0.16
0.20
0.24
0.28
0.32
TIME (SEC)
*10⁻¹

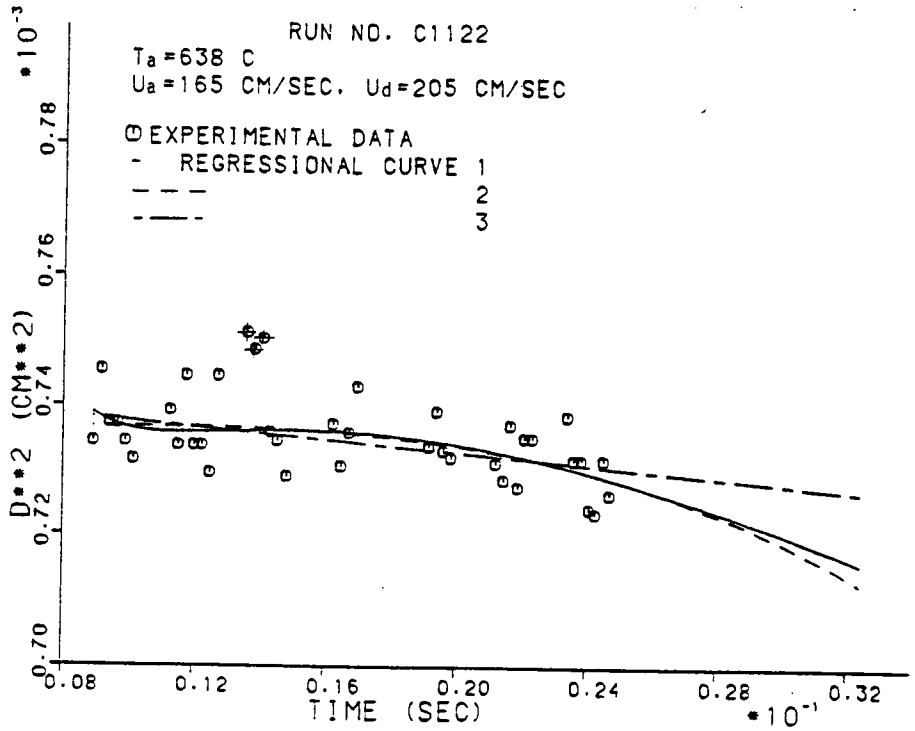

RUN NO. C1001
Ta=580 C
Ua=137 CM/SEC. Ud=203 CM/SEC
EXPERIMENTAL DATA
REGRESSIONAL CURVE 1
2
3
D**2 (CM**2)
*10**-3
0.86
0.88
0.90
0.92
0.94
0.05
0.10
0.15
0.20
0.25
0.30
0.35
TIME (SEC)
*10**-1

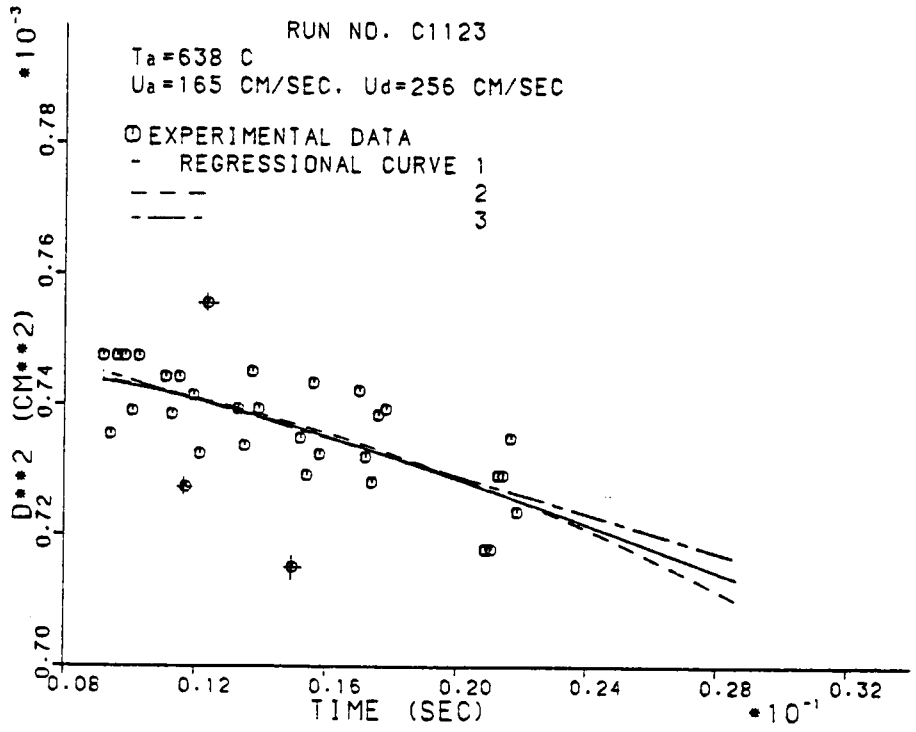

RUN NO. D0911
Ta=576 C
Ua=136 CM/SEC. Ud=176 CM/SEC
EXPERIMENTAL DATA
REGRESSIONAL CURVE 1
2
3
D**2 (CM**2)
*10**-3
0.87
0.89
0.91
0.93
0.95
0.10
0.15
0.20
0.25
0.30
0.35
0.40
TIME (SEC)
*10**-1

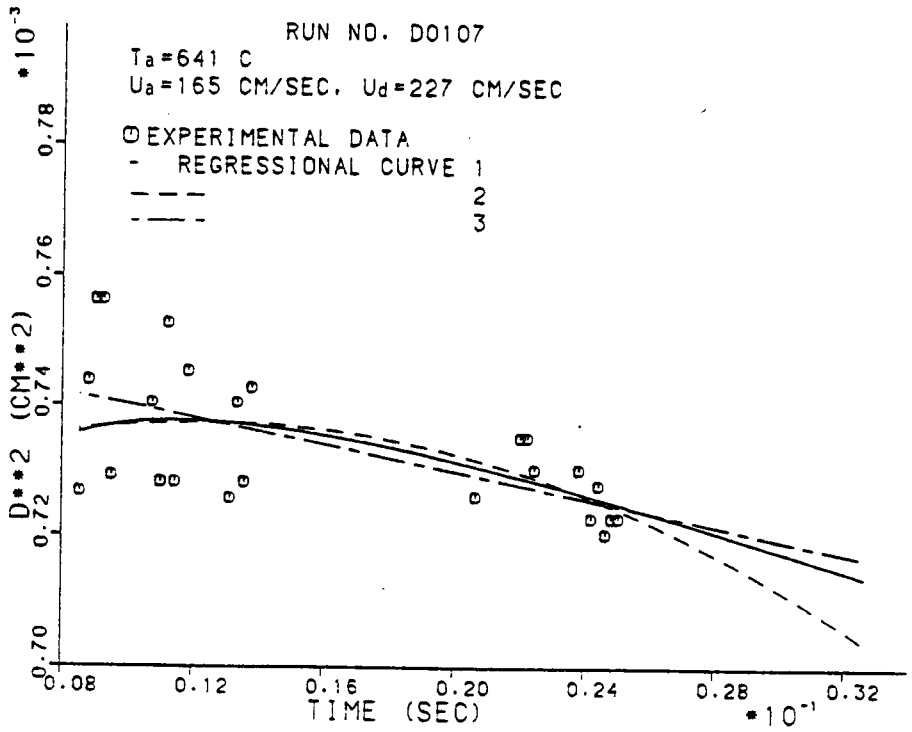

RUN NO. N1122
Ta=652 C
Ua=167 CM/SEC. Ud=253 CM/SEC
EXPERIMENTAL DATA
REGRESSIONAL CURVE 1
2
3
D**2 (CM**2)
*10⁻³
0.76
0.78
0.80
0.82
0.84
0.04
0.08
0.12
0.16
0.20
0.24
0.28
TIME (SEC)
*10⁻¹

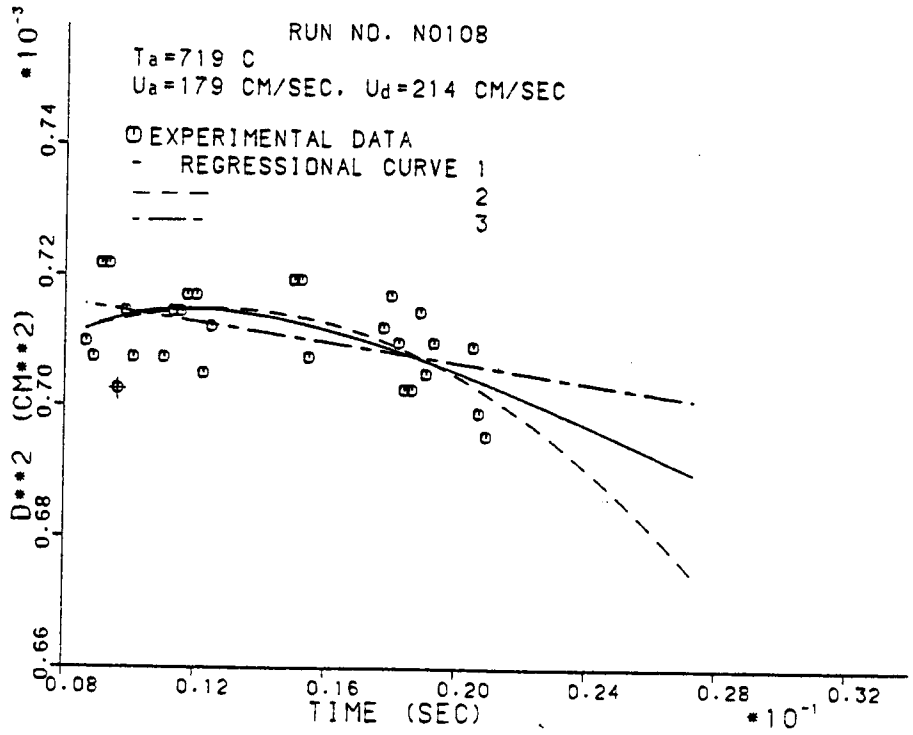

RUN NO. N1121
Ta=652 C
Ua=167 CM/SEC. Ud=240 CM/SEC
EXPERIMENTAL DATA
REGRESSIONAL CURVE 1
2
3
D**2 (CM**2)
*10⁻³
0.74
0.76
0.78
0.80
0.82
0.07
0.11
0.15
0.19
0.23
0.27
0.31
TIME (SEC)
*10⁻¹

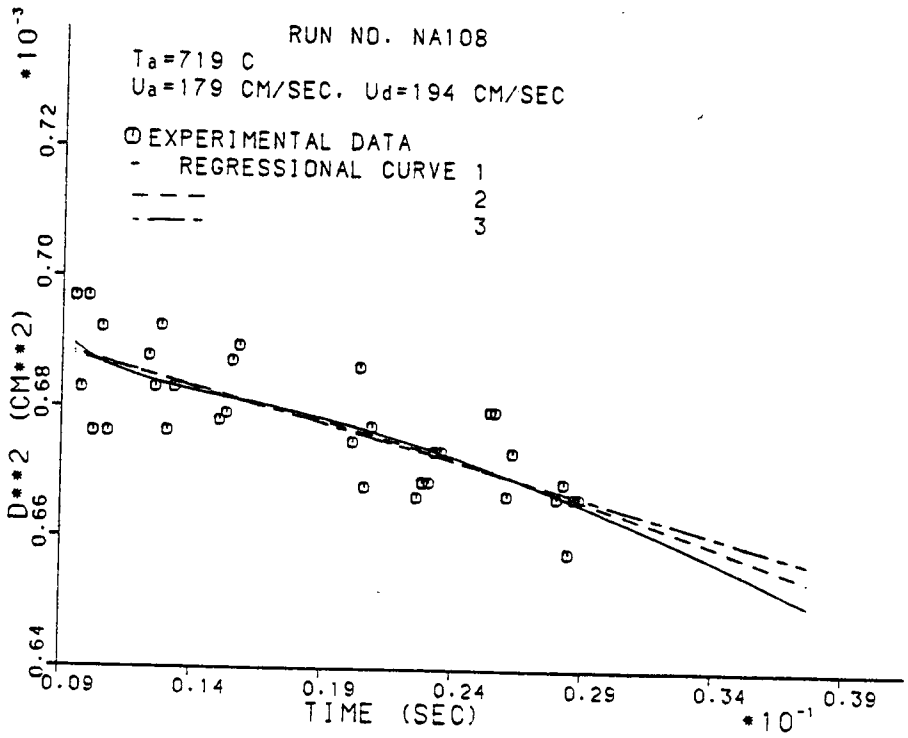

RUN NO. N1120
Ta=645 C
Ua=166 CM/SEC. Ud=254 CM/SEC
EXPERIMENTAL DATA
REGRESSIONAL CURVE 1
2
3
D**2 (CM**2)
*10**-3
0.76
0.78
0.80
0.82
0.84
0.04
0.08
0.12
0.16
0.20
0.24
0.28
TIME (SEC)
*10**-1

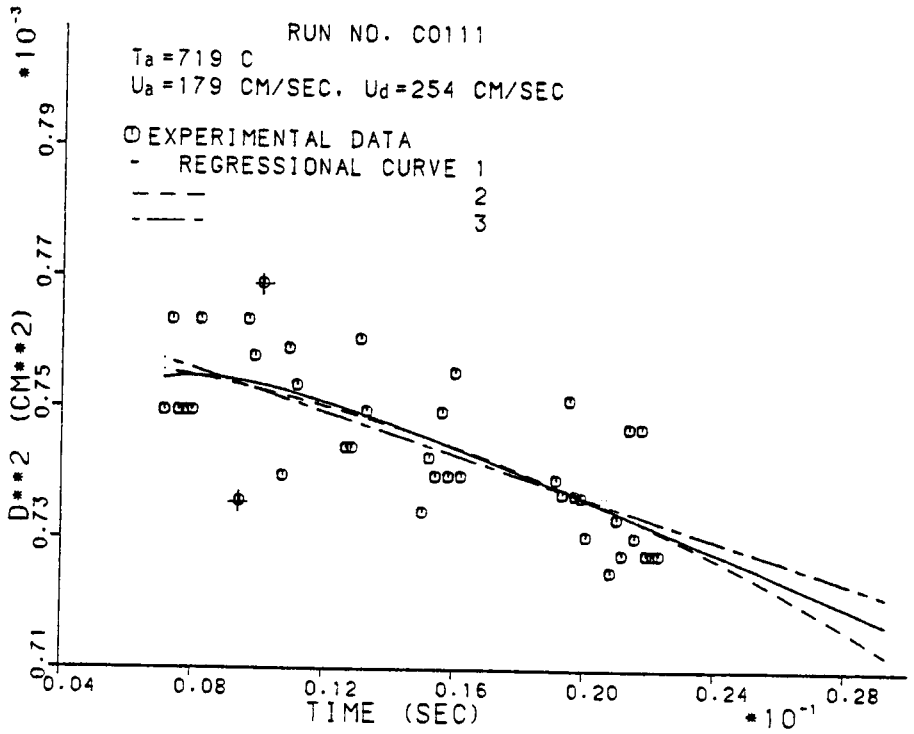

RUN NO. C1122
Ta=638 C
Ua=165 CM/SEC. Ud=205 CM/SEC
EXPERIMENTAL DATA
REGRESSIONAL CURVE 1
2
3
D**2 (CM**2)
*10**-3
0.70
0.72
0.74
0.76
0.78
0.08
0.12
0.16
0.20
0.24
0.28
0.32
TIME (SEC)
*10**-1

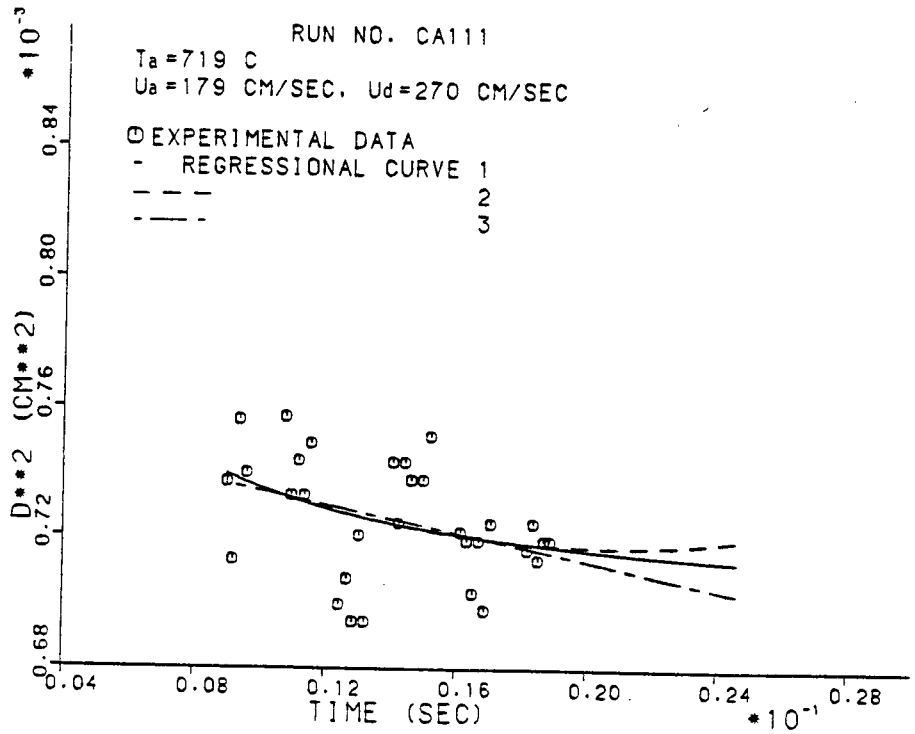

RUN NO. C1123
Ta=638 C
Ua=165 CM/SEC. Ud=256 CM/SEC
EXPERIMENTAL DATA
REGRESSIONAL CURVE 1
2
3
D**2 (CM**2)
*10**-3
0.70
0.72
0.74
0.76
0.78
0.08
0.12
0.16
0.20
0.24
0.28
0.32
TIME (SEC)
*10**-1

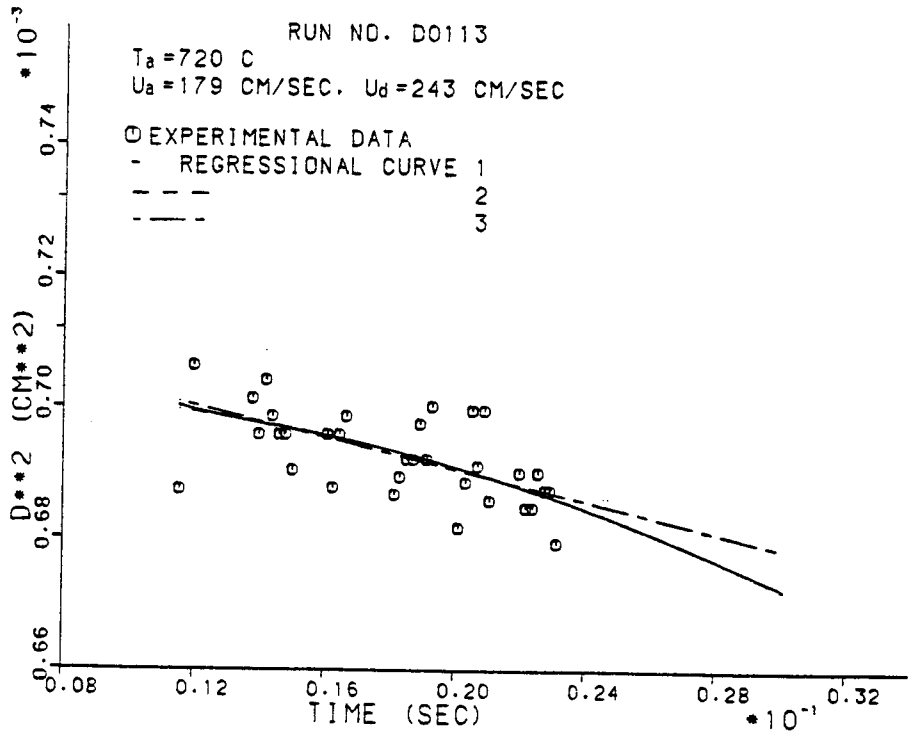

RUN NO. D0107
Ta=641 C
Ua=165 CM/SEC. Ud=227 CM/SEC
EXPERIMENTAL DATA
REGRESSIONAL CURVE 1
2
3
D**2 (CM**2)
*10**-3
0.70
0.72
0.74
0.76
0.78
0.08
0.12
0.16
0.20
0.24
0.28
0.32
TIME (SEC)
*10**-1

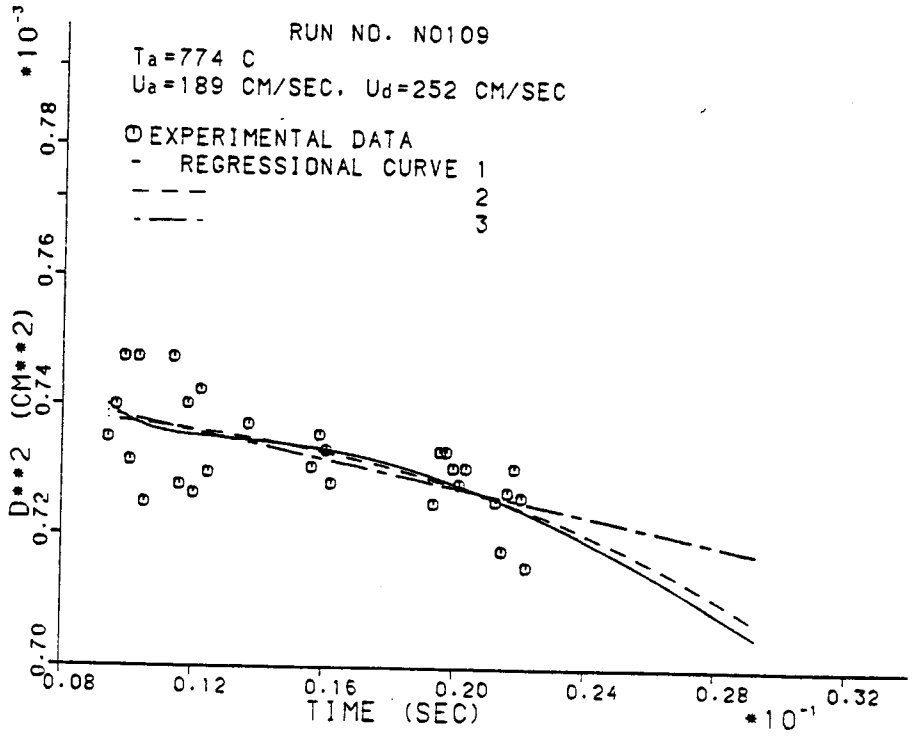

RUN NO. NO108
Ta=719 C
Ua=179 CM/SEC. Ud=214 CM/SEC
EXPERIMENTAL DATA
REGRESSIONAL CURVE 1
2
3
D**2 (CM**2)
*10⁻³
0.66
0.68
0.70
0.72
0.74
0.08
0.12
0.16
0.20
0.24
0.28
0.32
TIME (SEC)
*10⁻¹

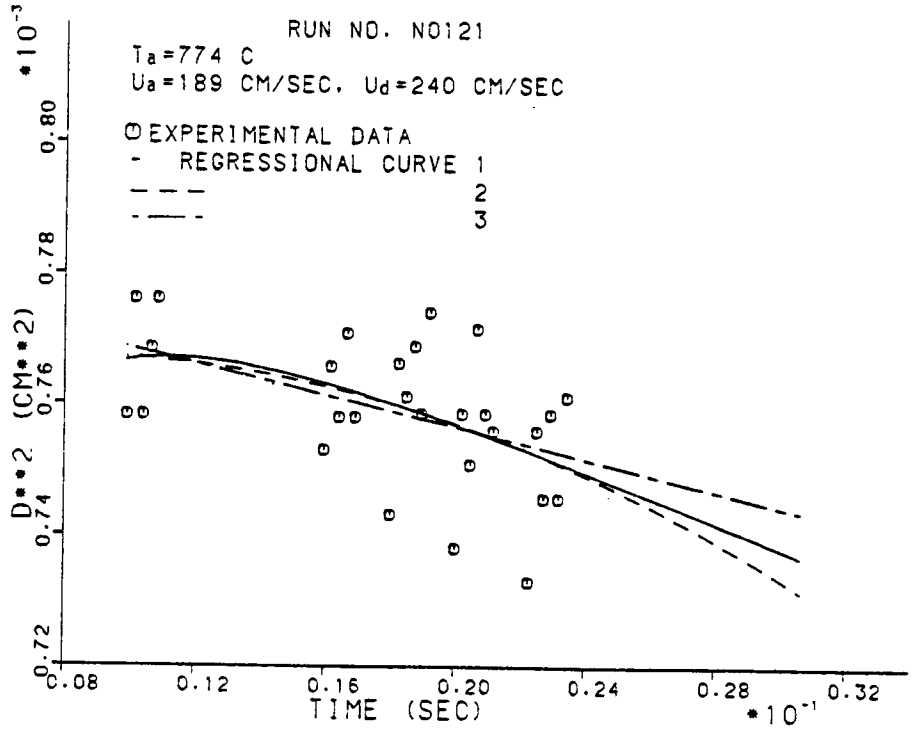

RUN NO. NA108
Ta=719 C
Ua=179 CM/SEC. Ud=194 CM/SEC
EXPERIMENTAL DATA
REGRESSIONAL CURVE 1
2
3
D**2 (CM**2)
*10⁻³
0.64
0.66
0.68
0.70
0.72
0.09
0.14
0.19
0.24
0.29
0.34
0.39
TIME (SEC)
*10⁻¹

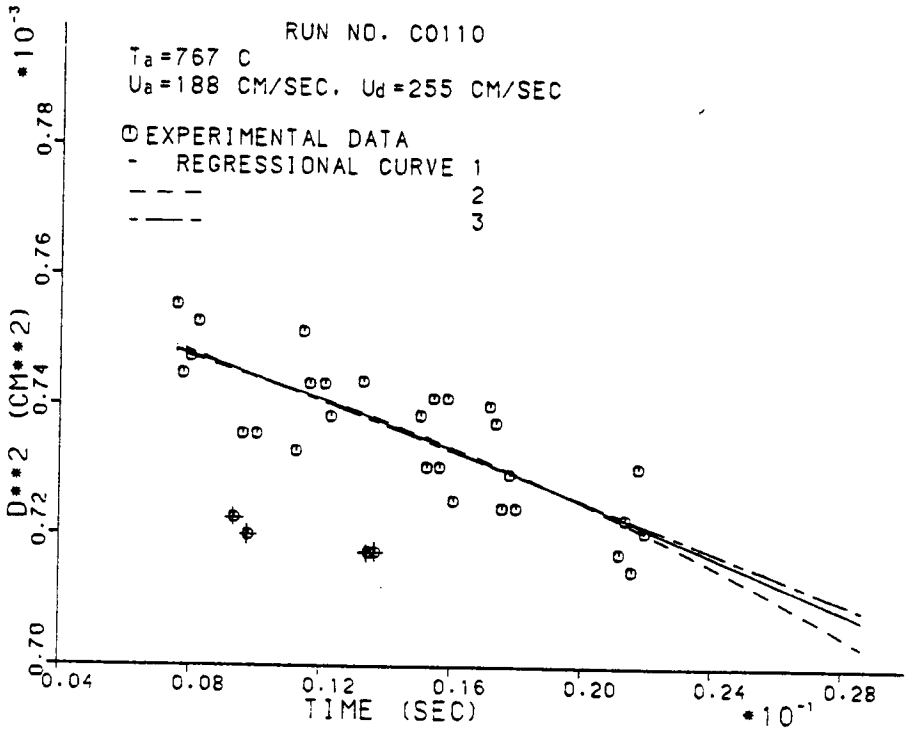

RUN NO. CO111
Ta=719 C
Ua=179 CM/SEC. Ud=254 CM/SEC
EXPERIMENTAL DATA
REGRESSIONAL CURVE 1
2
3
D**2 (CM**2)
*10**-3
0.71
0.73
0.75
0.77
0.79
0.04
0.08
0.12
0.16
0.20
0.24
0.28
TIME (SEC)
*10**-1

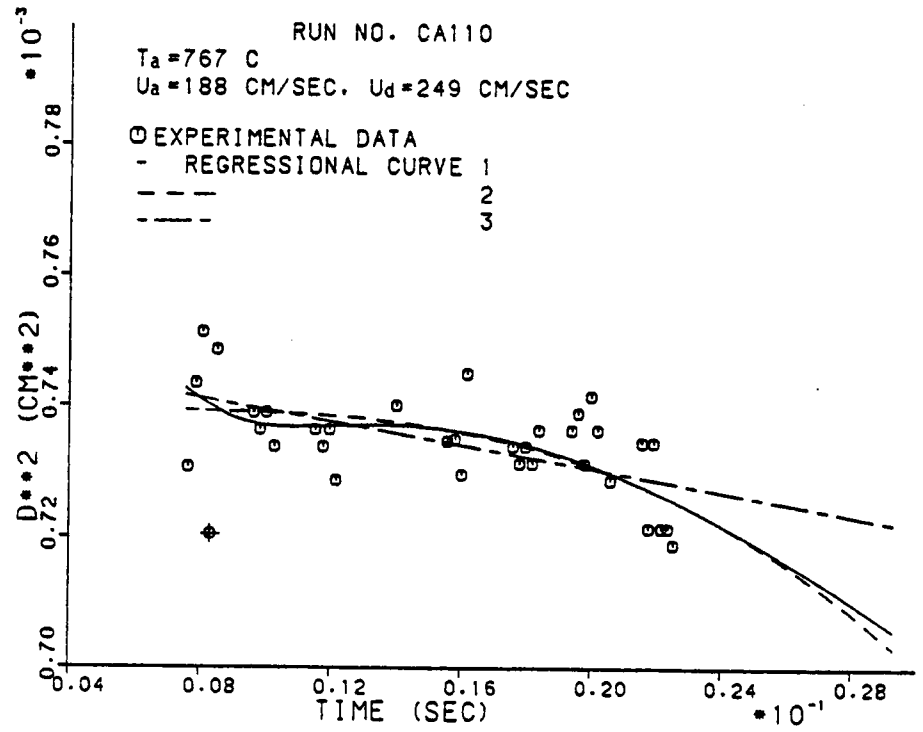

RUN NO. CA111
Ta=719 C
Ua=179 CM/SEC. Ud=270 CM/SEC
EXPERIMENTAL DATA
REGRESSIONAL CURVE 1
2
3
D**2 (CM**2)
*10**-3
0.68
0.72
0.76
0.80
0.84
0.04
0.08
0.12
0.16
0.20
0.24
0.28
TIME (SEC)
*10**-1

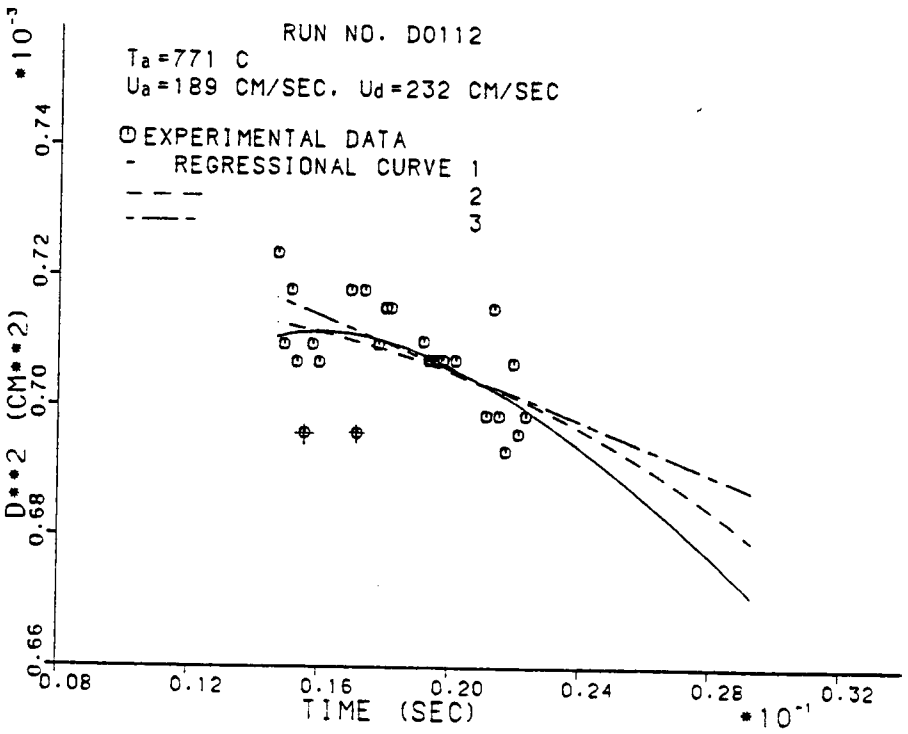

RUN NO. DO113
Ta=720 C
Ua=179 CM/SEC. Ud=243 CM/SEC
EXPERIMENTAL DATA
REGRESSIONAL CURVE 1
2
3
D**2 (CM**2)
*10⁻³
0.66
0.68
0.70
0.72
0.74
0.08
0.12
0.16
0.20
0.24
0.28
0.32
TIME (SEC)
*10⁻¹

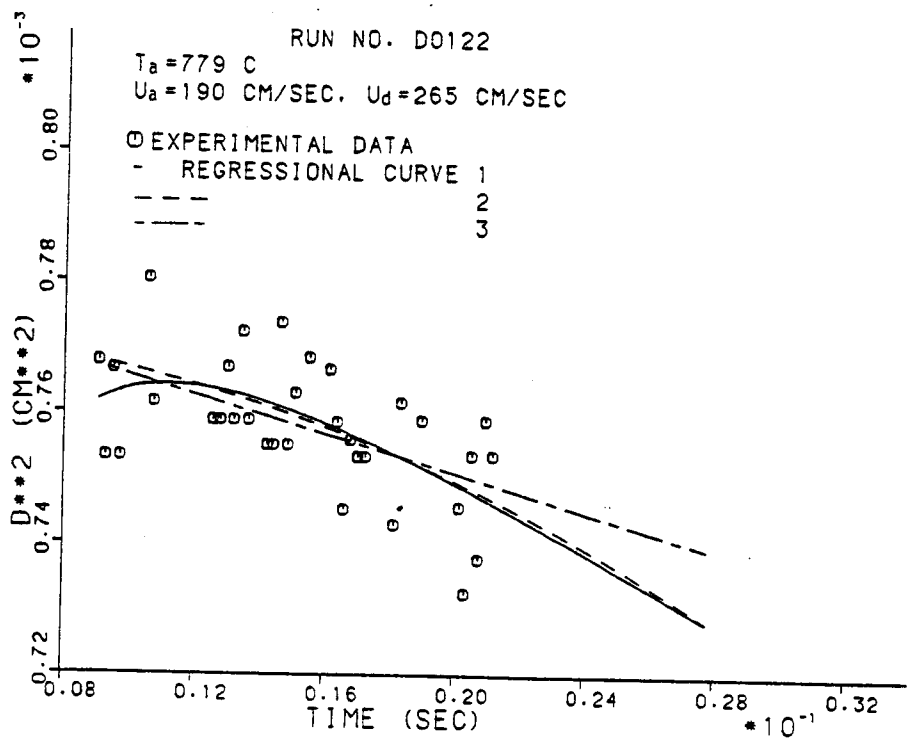

RUN NO. NO109
Ta=774 C
Ua=189 CM/SEC. Ud=252 CM/SEC
EXPERIMENTAL DATA
REGRESSIONAL CURVE 1
2
3
D**2 (CM**2)
*10⁻³
0.70
0.72
0.74
0.76
0.78
0.08
0.12
0.16
0.20
0.24
0.28
0.32
TIME (SEC)
*10⁻¹

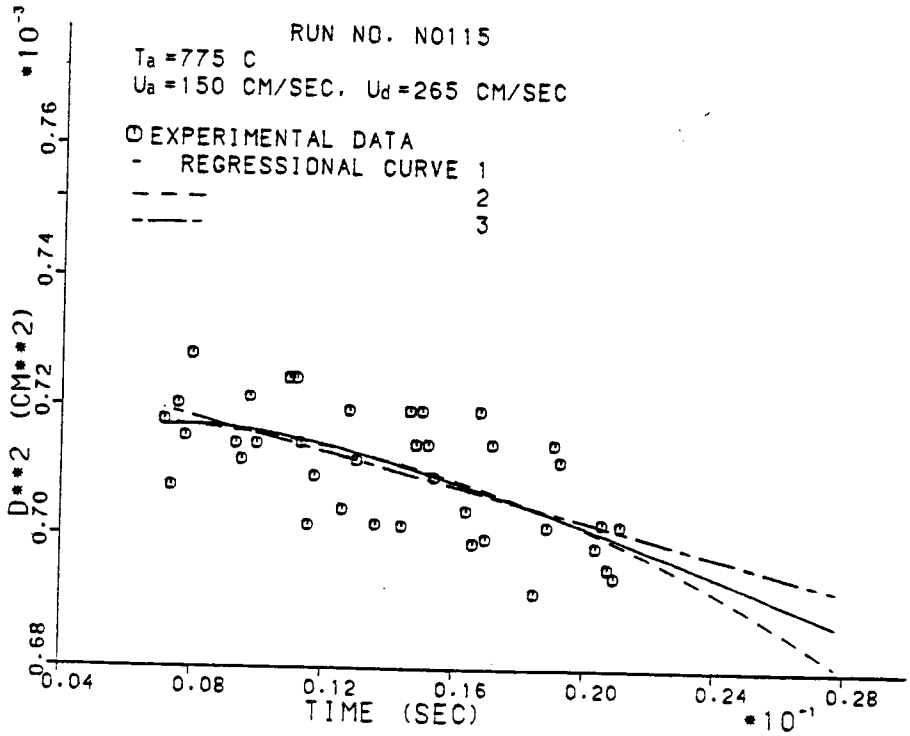

RUN NO. N0121
Ta=774 C
Ua=189 CM/SEC. Ud=240 CM/SEC
EXPERIMENTAL DATA
REGRESSIONAL CURVE 1
2
3
D**2 (CM**2)
*10⁻³
0.72
0.74
0.76
0.78
0.80
0.08
0.12
0.16
0.20
0.24
0.28
0.32
TIME (SEC)
*10⁻¹

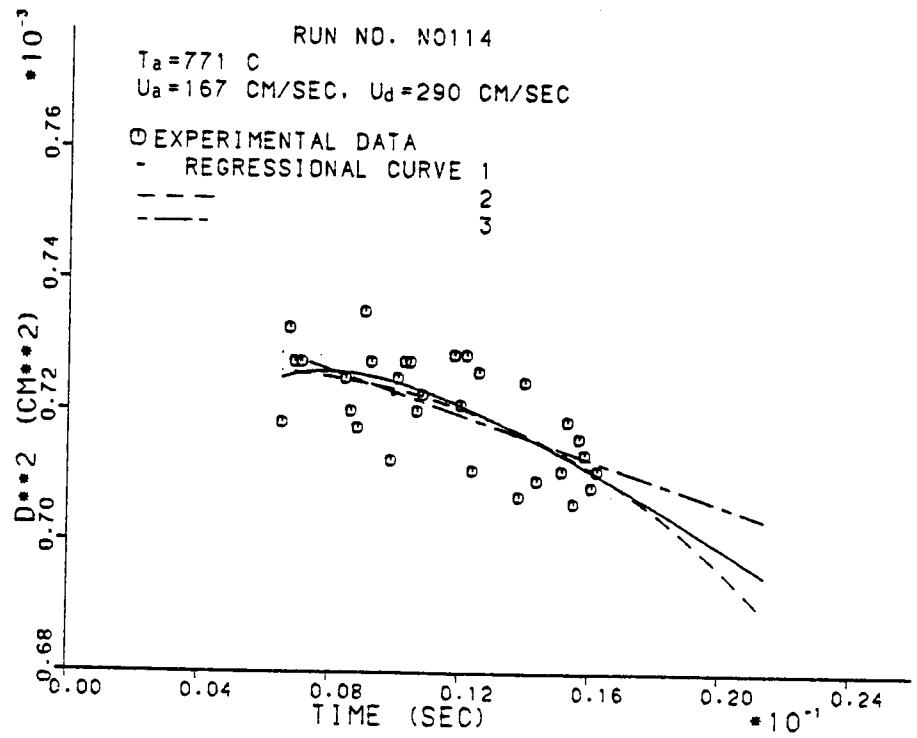

RUN NO. C0110
Ta=767 C
Ua=188 CM/SEC. Ud=255 CM/SEC
EXPERIMENTAL DATA
REGRESSIONAL CURVE 1
2
3
D**2 (CM**2)
*10⁻³
0.70
0.72
0.74
0.76
0.78
0.04
0.08
0.12
0.16
0.20
0.24
0.28
TIME (SEC)
*10⁻¹

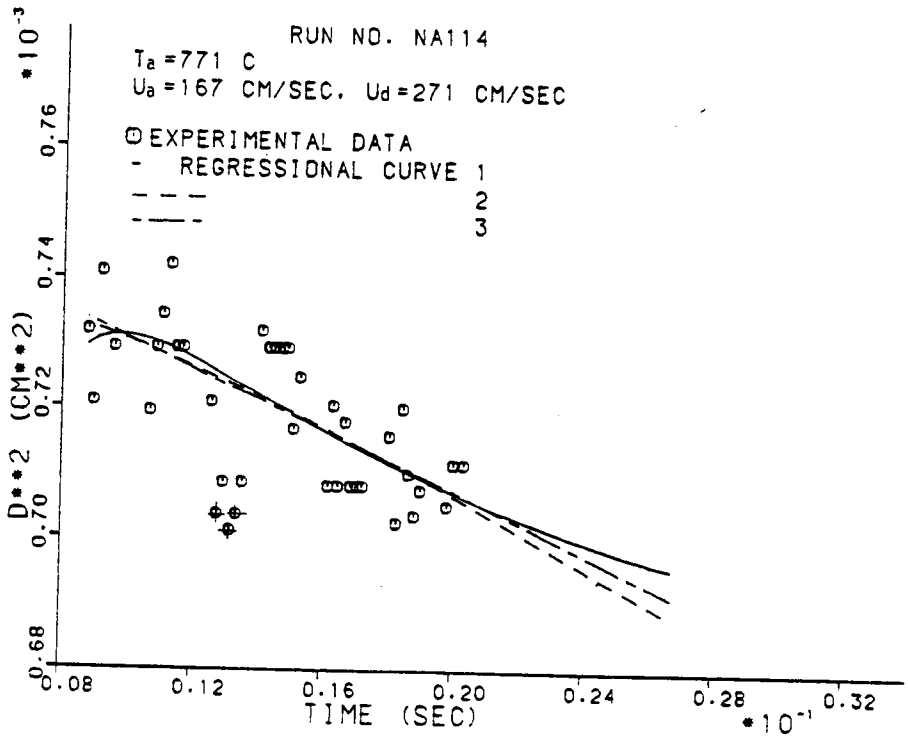

RUN NO. CA110
Ta=767 C
Ua=188 CM/SEC. Ud=249 CM/SEC
EXPERIMENTAL DATA
REGRESSIONAL CURVE 1
2
3
D**2 (CM**2)
*10**-3
0.70
0.72
0.74
0.76
0.78
0.04
0.08
0.12
0.16
0.20
0.24
0.28
TIME (SEC)
*10**-1

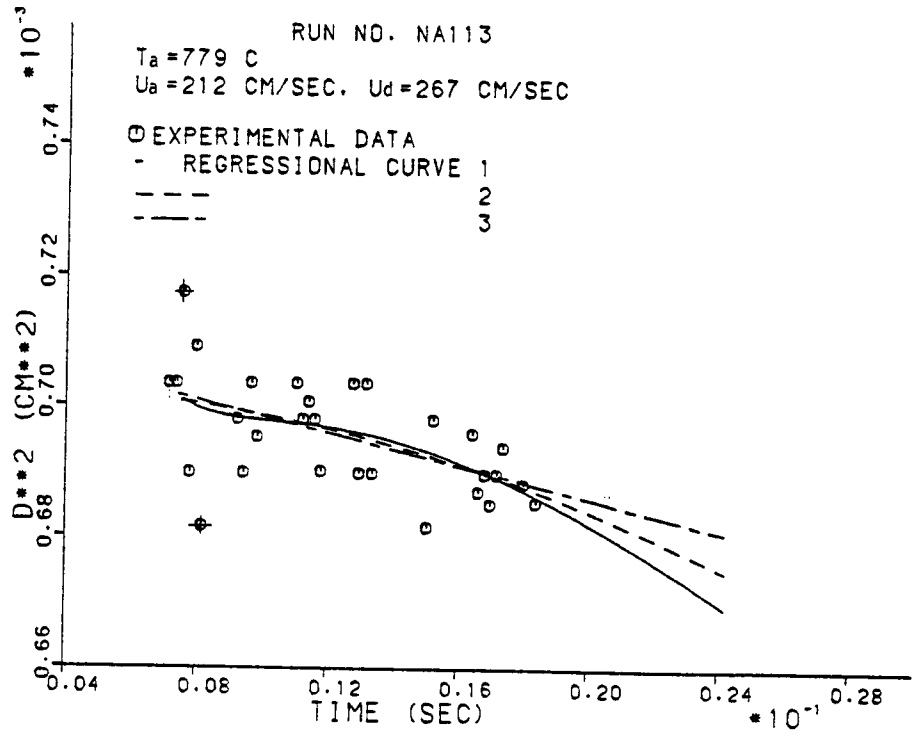

RUN NO. DO112
Ta=771 C
Ua=189 CM/SEC. Ud=232 CM/SEC
EXPERIMENTAL DATA
REGRESSIONAL CURVE 1
2
3
D**2 (CM**2)
*10**-3
0.66
0.68
0.70
0.72
0.74
0.08
0.12
0.16
0.20
0.24
0.28
0.32
TIME (SEC)
*10**-1

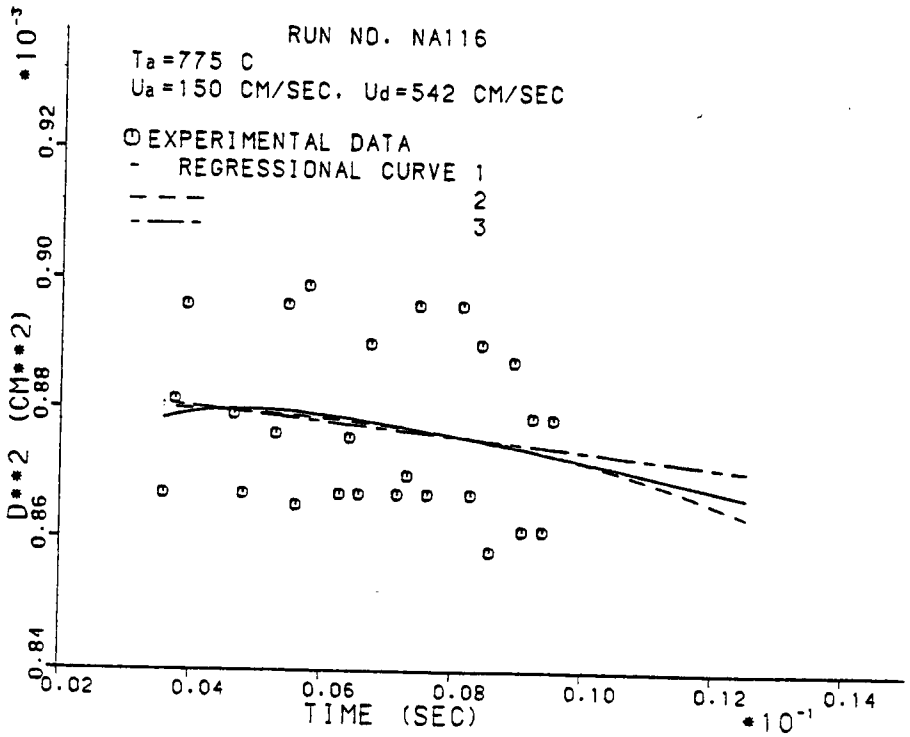

RUN NO. D0122
Ta =779 C
Ua =190 CM/SEC. Ud =265 CM/SEC
EXPERIMENTAL DATA
REGRESSIONAL CURVE 1
2
3
D**2 (CM**2)
*10⁻³
0.72
0.74
0.76
0.78
0.80
0.08
0.12
0.16
0.20
0.24
0.28
0.32
TIME (SEC)
*10⁻¹

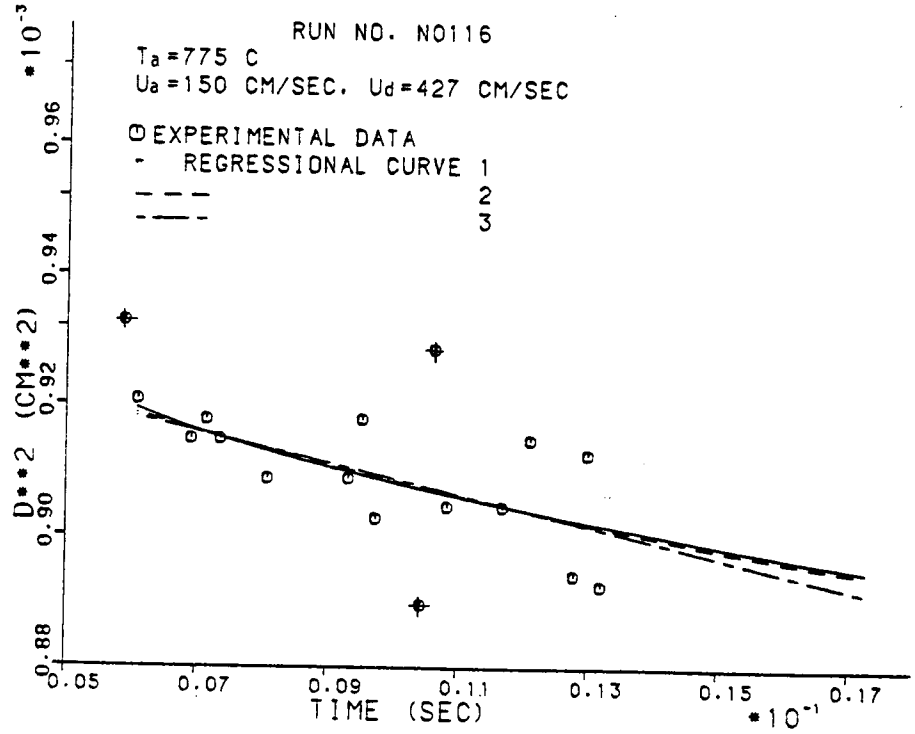

RUN NO. N0115
Ta =775 C
Ua =150 CM/SEC. Ud =265 CM/SEC
EXPERIMENTAL DATA
REGRESSIONAL CURVE 1
2
3
D**2 (CM**2)
*10⁻³
0.68
0.70
0.72
0.74
0.76
0.04
0.08
0.12
0.16
0.20
0.24
0.28
TIME (SEC)
*10⁻¹

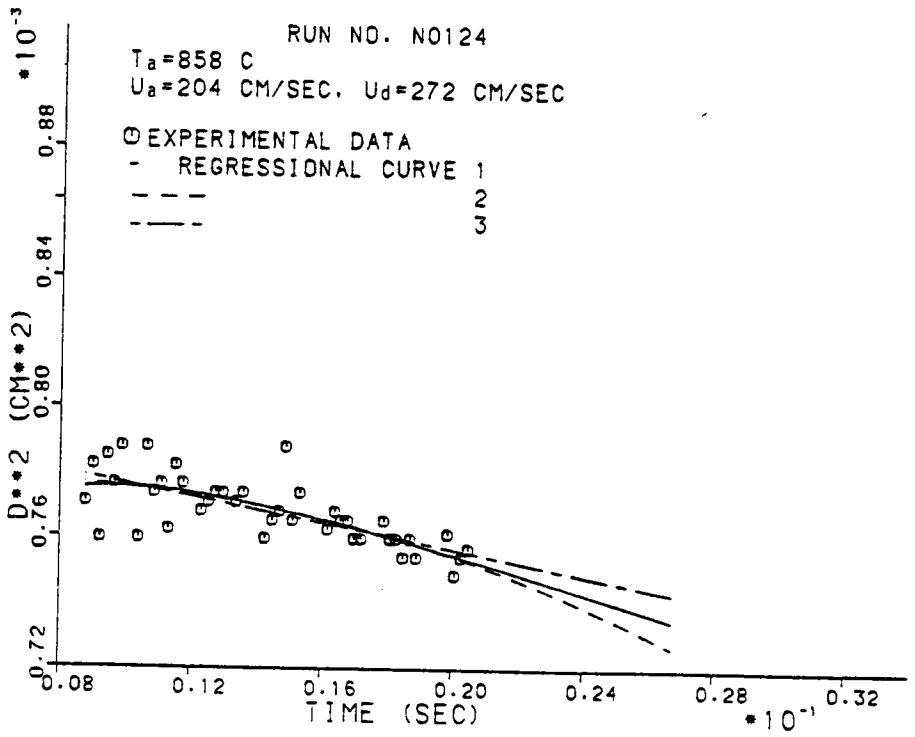

RUN NO. NO114
Ta=771 C
Ua=167 CM/SEC. Ud=290 CM/SEC
EXPERIMENTAL DATA
REGRESSIONAL CURVE 1
2
3
D**2 (CM**2)
*10⁻³
0.68
0.70
0.72
0.74
0.76
0.00
0.04
0.08
0.12
0.16
0.20
0.24
TIME (SEC)
*10⁻¹

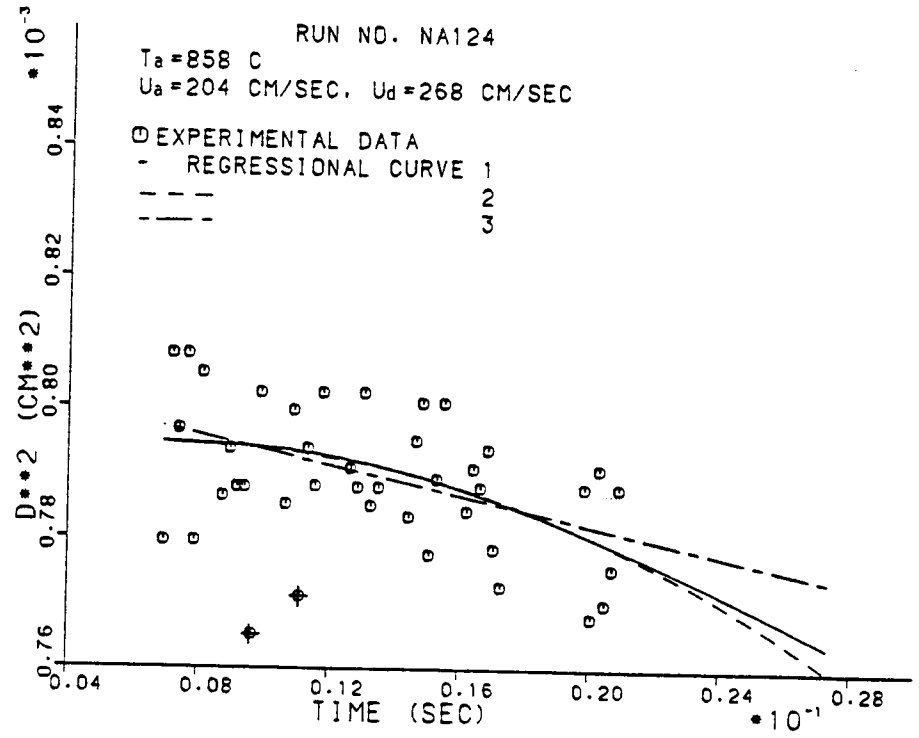

RUN NO. NA114
Ta=771 C
Ua=167 CM/SEC. Ud=271 CM/SEC
EXPERIMENTAL DATA
REGRESSIONAL CURVE 1
2
3
D**2 (CM**2)
*10⁻³
0.68
0.70
0.72
0.74
0.76
0.08
0.12
0.16
0.20
0.24
0.28
0.32
TIME (SEC)
*10⁻¹

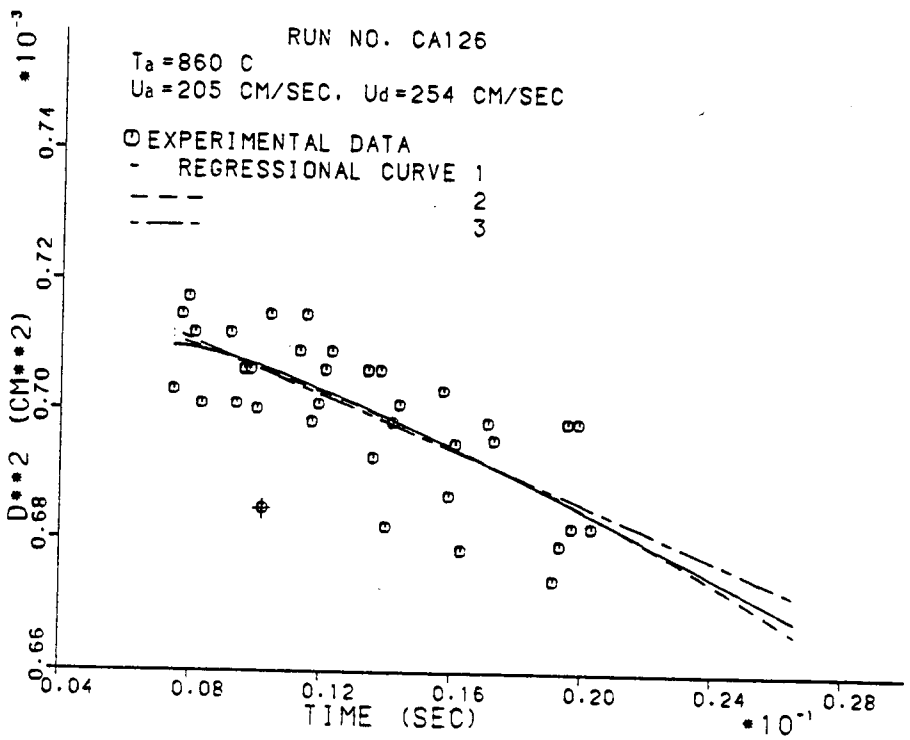

RUN NO. NA113
Ta=779 C
Ua=212 CM/SEC. Ud=267 CM/SEC
EXPERIMENTAL DATA
REGRESSIONAL CURVE 1
2
3
D**2 (CM**2)
*10⁻³
0.66
0.68
0.70
0.72
0.74
0.04
0.08
0.12
0.16
0.20
0.24
0.28
TIME (SEC)
*10⁻¹

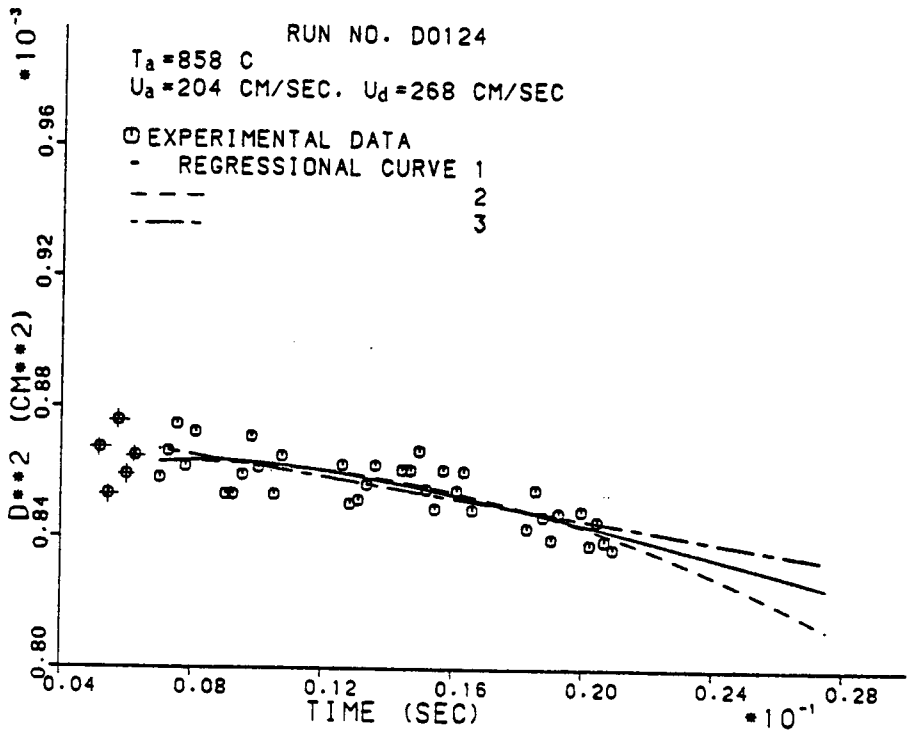

RUN NO. NA116
Ta=775 C
Ua=150 CM/SEC. Ud=542 CM/SEC
EXPERIMENTAL DATA
REGRESSIONAL CURVE 1
2
3
D**2 (CM**2)
*10⁻³
0.84
0.86
0.88
0.90
0.92
0.02
0.04
0.06
0.08
0.10
0.12
0.14
TIME (SEC)
*10⁻¹


RUN NO. NO116
Ta=775 C
Ua=150 CM/SEC. Ud=427 CM/SEC
EXPERIMENTAL DATA
REGRESSIONAL CURVE 1
2
3
D**2 (CM**2)
*10⁻³
0.88
0.90
0.92
0.94
0.96
0.05
0.07
0.09
0.11
0.13
0.15
0.17
TIME (SEC)
*10⁻¹


RUN NO. NO124
Ta=858 C
Ua=204 CM/SEC. Ud=272 CM/SEC
EXPERIMENTAL DATA
REGRESSIONAL CURVE 1
2
3
D**2 (CM**2)
*10⁻³
0.72
0.76
0.80
0.84
0.88
0.08
0.12
0.16
0.20
0.24
0.28
0.32
TIME (SEC)
*10⁻¹


RUN NO. NA124
Ta=858 C
Ua=204 CM/SEC. Ud=268 CM/SEC
① EXPERIMENTAL DATA
- REGRESSIONAL CURVE 1
2
3
D**2 (CM**2)
*10⁻³
0.76
0.78
0.80
0.82
0.84
0.04
0.08
0.12
0.16
0.20
0.24
0.28
TIME (SEC)
*10⁻¹


RUN NO. CA126
Ta=860 C
Ua=205 CM/SEC. Ud=254 CM/SEC
① EXPERIMENTAL DATA
- REGRESSIONAL CURVE 1
2
3
D**2 (CM**2)
*10⁻³
0.66
0.68
0.70
0.72
0.74
0.04
0.08
0.12
0.16
0.20
0.24
0.28
TIME (SEC)
*10⁻¹


RUN NO. D0124
Ta =858 C
Ua =204 CM/SEC. Ud =268 CM/SEC
EXPERIMENTAL DATA
REGRESSIONAL CURVE 1
2
3
D**2 (CM**2)
*10**-3
0.96
0.92
0.88
0.84
0.80
0.04
0.08
0.12
0.16
0.20
0.24
0.28
TIME (SEC)
*10**-1

APPENDIX C

COMPUTER PROGRAM OF FROESSLING MODEL

The listing includes the main program and the constants used in read statements. Calculating procedures should be referred to in Chapter 4.3. Appropriate comments are given in the program.

```
//DRNO611 JOB (48041,070628,RMT2,T-3,L-5,R-128K),SUMING
// EXEC FORTGCLD,FORTREG=96K,GOREG=96K
//FORT.SYSIN DD *
C     THIS PROGRAM COMPUTES THE VAPORIZATION RATE OF SMALL DROPLETS IN
C     AN ELEVATED TEMPERATURE GASEOUS MEDIUM, BOTH WITH AND WITHOUT RAD-
C     IATION.  FIRST, THE DROPLET SURFACE TEMPERATURE, TS, IS COMPUTED
C     BY THE NEWTON-RAPHSON METHOD, NEGLECTING RADIATION. NEXT, THE MEAN
C     THERMAL CONDUCTIVITY OF THE VAPOR MIXTURE,AK, IS COMPUTED BETWEEN
C     TEMPERATURE LIMITS OF TS AND TO.  THE VAPORIZATION RATE, AM, WITH-
C     OUT RADIATION IS COMPUTED NEXT.  THE CASE WITH RADIATION IS CONSI-
C     DERED NEXT, USING THE ABOVE VALUES OF TS AS A STARTING POINT FOR A
C     TRIAL AND ERROR SOLUTION OF THE NONLINEAR SET OF ALGEBRAIC EQUA-
C     TIONS RELATING THE VAPORATION RATE, TM, SURFACE TEMPERATURE, TTS,
C     AND MEAN THERMAL CONDUCTIVITY,TTK. FINALLY, THE VAPOR RATE, TM, IS
C     THE ROOT OF THE FUNCTION, Y, VERSUS TTS, FOR A GIVEN TEMP., TO.
C
C     THE PRIMARY NONDIMENSIONAL PARAMENTERS ARE: MODIFIED LEWIS NUMBER,
C     AL; ALPHA,A,WHICH IS THE PRODUCT OF THE LIQUID BOILING TEMPERATURE
C     AND ITS VAPOR HEAT CAPACITY CPA DIVIDED BY THE LATENT HEAT; BETA,
C     B, WHICH IS THE LATENT HEAT DIVIDED BY THE PRODUCT OF THE GAS CON-
C     STANT AND THE BOILING TEMP; AND THE GAS TEMPERATURE, TO.
C
C     THE VAPORIZATION THEORY IS BASED ON THE CONSTANT PROPERTY MODEL,
C     BUT USING MEAN VALUES OVER THE TEMPERATURE RANGE OF INTEREST.
C
C     THIS PARTICULAR VERSION OF THE PROGRAM CONTAINS THE VAPOR PRES-
C     SURE VS T FUNCTION FOR WATER, FROM KEENAN AND KEYES.  CONSTANTS
C     CONTAINED IN THE PROGRAM FOR WATER ARE:  VAPOR PRESSURE PARAMETERS
C     ( C1,C2,C3,C4,PC,TC), SURFACE TENSION PARAMETER (GA), ABSORPTIVITY,
C     AB VS TO(I).
C
C

      DIMENSION TO(30),TS(30),YA(30),TOO(30)
      DIMENSION  AK(30), AM(30),TOC(30),CCD(30)
      DIMENSION  F(30),TM(30),BAL(30),DR1(25)
      DIMENSION  BM(35),TTS(25),Y(35),Z(35),TTT(35)
      DIMENSION  WVM(25), WVK(25), WGR(25), WPR(25), TCC(10)
      DIMENSION  CMR(35), XAOO(10), DEF(35), YMIN(35), CRMR(35)
      DIMENSION WMM(35),WKK(35),WGG(35),WPP(35),WRR(35)
      DIMENSION  R1(25),DDT(25),BMM(25),WRE(25),BRMM(25)
      DIMENSION VPS(30),TT(50),ANN1(50),ANN2(50)
      DIMENSION VAA(50),VBB(50),DD12(50),TTSS(30),DD2(25)
      DIMENSION WTK(25),WCP(25),WTT(35),WCC(35),BRMF(35)
C
C

      READ(5,10) N
      READ(5,10)  M
      READ(5,10) L
      READ(5,10) L1
      READ(5,10) L2
   10 FORMAT(I2)
      N=1
      DO 20 I=1,N
   20 READ(5,25) TOC(I),YA(I),XAOO(I)
   25 FORMAT(F11.3,F11.3,F11.3)
   30 FORMAT(F11.3)
      READ(5,30) A
      READ(5,30) B
      READ(5,30) AL1
      READ(5,30)  AMA
      READ(5,30)  AMB
      READ(5,30)  AKB
      READ(5,30)  BKB
```

```
      READ(5,30)  AE
      READ(5,30)  BE
      READ(5,30) AVB
      READ(5,30) BVB
      READ(5,30) AVE
      READ(5,30) BVE
      READ(5,30)  D
      READ(5,30) PT
      READ(5,30)  CPA
      READ(5,30)  CPB
      READ(5,30) DLH
      READ(5,30) TB
      READ(5,30) TBB
      READ(5,30)  GA
      READ(5,30) EA
      READ(5,30) EB
      READ(5,30) S1
      READ(5,30) S2
      READ(5,30)  SI
      READ(5,30) SS
      READ(5,30) ST
      READ(5,30) DST
      READ(5,30) DTT
C
C     CONSTANTS REQUIRED IN THE COMPUTATION OF THE VAPOR PRESSURE
C
      R=D/2.
      C1=7.7052
      C2=4.6178*TB/373.15
      C3=0.116692*(TB/373.15)**3
      C4=5.1474*TB/373.15
      C5=0.380334*(TB/373.15)**4
      PC=218.167
      TC=1.73456*373.15/TB
C
C     GAS CONSTANT AND MOLECULAR PARAMETERS
C
      RG    = 82.05
      EK    = (EA*EB)**(.5)
      S12   = (S1+S2)/2.
C
C     ERROR LIMIT ON SEARCH FOR SURFACE TEMP W/O RADIATION
      ER=10.**(-8)
C
C
      DO 1000  I=1,N
      SS=1.0
      DT=0.
      LL=0
      TOO(I)=TOC(I)+273.15
      TO(I)=TOO(I)/TB
      DO 1111 IJ=1,1
      TCC(I) = TO(I)*TB - 273.15
      AO =   0.7136E 01
      BO     = 0.2640E-02
      CO     = 0.4590E-07
      T1     = BO*TB*(TO(I)**2 - 1.0)/(2.*(TO(I) - 1.0))
      T2    = CO*TB**2*(TO(I)**3 - 1.0)/(3.*(TO(I) - 1.0))
      CPA    = (AO + T1 + T2)/AMA
      A      = CPA*TB/DLH
      DO 420 J2 = 1,L2
      AL  = AL1
C
C     COMPUTATION OF THE SURFACE TEMP WITHOUT RADIATION, TS
C
      IF(TO(I).GE.1.0) GO TO 100
```

```
      TS2=TO(I)
      GO TO 110
  100 TS2=1.0
  110 F2 = 1.+A*(TO(I)-TS2)
      FT1 =-C1*(TC/TS2-1.)
      DTS = TC-TS2
      FT2=1.+C2*DTS+C3*DTS**3+C5*DTS**4
      FT3 = 1.+C4*DTS
      FT  = FT1*FT2/FT3
      FT4 =-C1*(TC/TO(I)-1.)
      DTA = TC-TO(I)
      FT5 = 1.+C2*DTA + C3*DTA**3 +C5*DTA**4
      FT6 = 1.+C4*DTA
      FTA = FT4*FT5/FT6
      IF(TO(I)-1.)  115, 115, 120
  115 XA0 = PC*YA(I)*EXP(FTA)/PT
      GO TO 125
  120 XA0  = XA00(I)
  125 FTT  = GA/(R*TS2)
      Z2  =(1.-XA0)/F2**AL-1.+PC*EXP(FT+FTT)/PT
      FTP1= C4/FT3 - TC/(TS2*DTS)
      FTP2= (C2+3.*DTS**2)/FT3
      FTP = FTP1*FT-FT1*FTP2-FTT/TS2
      S   =(1.-XA0)*A*AL/F2**(AL+1.)+PC*EXP(FT+FTT)*FTP/PT
      TS1= (S*TS2-Z2)/S
      F1 = 1.+A*(TO(I)-TS1)
      FT11=-C1*(TC/TS1-1.)
      DTS1= TC-TS1
      FT22=1.+C2*DTS1+C3*DTS1**3+C5*DTS1**4
      FT33=1.+C4*DTS1
      FTF = FT11*FT22/FT33+GA/(R*TS1)
      Z1  =(1.-XA0)/F1**AL-1.+PC*EXP(FTF)/PT
      IF(Z1.LE.ER)  GO TO 200
      TS2= TS1
      GO TO 110
  200 TS(IJ)=TS1
C
C     COMPUTATION OF THE MEAN CONDUCTIVITY,AK, AND THE MEAN LEWIS NO.,AL
C     W/O RADIATION
C
      M=40
      SUM = 0.
      SUM1 = 0.
      DEL=(TO(I)-TS(IJ))/FLOAT(M)
  300 DO 400  J=1,M
      T   = TS(IJ)+DEL*FLOAT(J-1)+DEL/2.
      FK=(1.+A*(T-TS(IJ)))/(1.+A*(TO(I)-TS(IJ)))
      AN1 = AKB*T**AE
      AN2 = BKB*T**BE
      VA      = AVB*T**AVE
      VB      = BVB*T**BVE
      VF      = (VA/VB)*(AMB/AMA)**(.75)
      XAB     = FK**(-AL)-1.
      SAT     = 1.5/T
      SBT     = SAT*(TBB/TB)
      SABT    = 1.05*(TBB/TB)**(.5)/T
      SF1     = (1.+SAT)/(1.+SBT)
      SF2     = (1.+SABT)/(1.+SAT)
      SF3     = (1.+SABT)/(1.+SBT)
      AAB     = (1.+(VF*SF1)**(.5))**(2.)*SF2/4.
      ABA     = (1.+(VF*SF1)**(-0.5))**(2.)*SF3/4.
      D1      = 1.+AAB/XAB
      D2      = 1.+ABA*XAB
      DK      = AN1/D1+AN2/D2
      DA      = DK*DEL
      SUM     = SUM+DA
```

```
      TKE   = TB*T/EK
      DTKE = TKE-2.6
      IF(DTKE)  350,355,355
  350 W12 = 1.347*TKE**(-0.3259)
      GO TO 360
  355 W12 = 1.277*TKE**(-0.2697)
  360 AM12 = ((AMA+ AMB)/(2.*AMA*AMB))**(.5)
      DEN =  RG  *S12**2.*W12
      CD    = 0.002628*TB**(.5)*T**(.5)*AM12/DEN
      DA1 = CD*DEL
      SUM1 = SUM1 + DA1
400   CONTINUE
      CCD(IJ)=CD
      AK(IJ)=SUM/(TO(I)-TS(IJ))
      CD12=SUM1/(TO(I)-TS(IJ))
      AL1=AK(IJ)/(CD12*CPA*AMA)
      WRITE(6,411)AL1
  411 FORMAT(10X,'AL1=',F10.4)
      IF(ABS(AL1-AL).LE.1.0E-05) GO TO 421
  420 CONTINUE
  421 AL   =AL1
C
C     COMPUTATION OF THE VAPORIZATION RATE, AM, W/O RADIATION
C
      F(IJ)=ALOG(1.+A*(TO(I)-TS(IJ)))
      AM(IJ)=4.*3.1416*R*AK(IJ)*F(IJ)/CPA
      A1    = CPA/(4.*3.14*R)
      A2    = 4.*3.14*R**2/DLH
C
C     COMPUTATION OF THE MEAN CONDUCTIVITY, TK, WITH RADIATION, FOR A
C     SEQUENCE OF SURFACE TEMPERATURES, STARTING WITH TS
C
  501 KJ=0
      KY=1
      SN=1.0
      SP=1.0
500   DO 600 K=1,L
  506 BM(K)=SS*AM(IJ)
      WRITE(6,422) K,BM(K),SS
  422 FORMAT(2X,'BM(',I2,')=',E11.4,6X,'SS=',E14.7)
 510  DO 560 K1=1,L1
      ST=(0.95-TS(IJ))/L1
      TTS(K1)=TS(IJ)+ST*FLOAT(K1-1)
      SUM    = 0.
      SUM1   = 0.
      SUM2   = 0.
      SUM3   = 0.
      DEL    = (TO(I)-TTS(K1))/FLOAT(M)
 520  DO 539 J1=1,M
      T      = TTS(K1)+DEL*FLOAT(J1-1)+DEL/2.
      TT(J1)=T*TB
      AN1 = AKB*T**AE
      ANN1(J1)=AN1
      AN2 = BKB*T**BE
      ANN2(J1)=AN2
      VA     = AVB*T**AVE
      VAA(J1)=VA
      VB     = BVB*T**BVE
      VBB(J1)=VB
      AB     = 1.159-0.1167*TO(I)
      QR1   = AB*1.355*10.**(-12)*TB**4*(TO(I)**4-TTS(K1)**4)
      QR1=0.3143*QR1
      QR     = A2*QR1/BM(K)
      FK1    = 1.+A*(T-TTS(K1))
      FK2    = 1.+A*(TO(I)-TTS(K1))
      XXX=(QR-FK1)/(QR-FK2)
```

```
      IF(XXX.LE.0.) GO TO 206
      XAB  = XXX**(-AL)-1.
      IF(XAB.LE.0.) GO TO 206
      VF      = (VA/VB)*(AMB/AMA)**(.75)
      SAT     = 1.5/T
      SBT     = SAT*(TBB/TB)
      SABT    = 1.05*(TBB/TB)**(.5)/T
      SF1     = (1.+SAT)/(1.+SBT)
      SF2     = (1.+SABT)/(1.+SAT)
      SF3     = (1.+SABT)/(1.+SBT)
      AAB     = (1.+(VF*SF1)**(.5))**(2.)*SF2/4.
      ABA     = (1.+(VF*SF1)**(-0.5))**(2.)*SF3/4.
      D1      = 1.+AAB/XAB
      D2      = 1.+ABA*XAB
      DK      = AN1/D1+AN2/D2
      DA      = DK*DEL
      SUM     = SUM+DA
      TFK    = TB*T
      TKE   = TFK/EK
C     COMPUTATION OF THE COLLISION INTEGRALS, W12 AND A12
      DTKE = TKE - 2.6
      IF(DTKE)  525, 530, 530
  525 W12   = 1.347*TKE**(-0.3259)
      GO TO 535
  530 W12   = 1.277*TKE**(-0.2697)
  535 A12   = 1.095
C     COMPUTATION OF THE BINARY DIFFUSION COEFFICIENT, D12
      AM12 = ((AMA+ AMB)/(2.*AMA*AMB))**(.5)
      DEN   = PT*S12**2.*W12
      D12   = 0.002628*TFK**(1.5)*AM12/DEN
      DD12(J1)=D12
C     COMPUTATION OF THE MOLE FRACTIONS
      XA     = XAB/(1. + XAB)
      XB     = 1. - XA
      XA2    = XA**2.
      XB2    = XB**2.
      XP     = XA*XB
      CMF   = PT/(RG*TFK)
      FMM   = AMA*XA  + AMB*XB
      DF    = FMM*CMF
C     COMPUTATION OF THE MIXTURE VISCOSITY AT THE FILM CONDITIONS, VM
      SM    = AMA + AMB
      F1    = XA2/VA
      F2    = 2.*XP/SM
      F3    =RG*TFK/(PT*D12)
      F4    = 1. + 0.6*AMB*A12/AMA
      H11   = F1 + F2*F3*F4
      F5    = XB2/VB
      F6    = 1. + 0.6*AMA*A12/AMB
      H22   = F5 + F2*F3*F6
      F7    = 1. - 0.6*A12
      H12   = -F2*F3*F7
      T1    = XA2/H11
      T2    = XB2/H22
      T3    = 2.*XP      *H12/(H11*H22)
      T4    = 1./(1. - H12**2 /(H11*H22))
      VML   = (T1 + T2 - T3)*T4
      VKL    = VML/DF
      DVK    = VKL*DEL
      SUM1   = SUM1 + DVK
      CPL    = (XA*CPA*AMA + XB*CPB*AMB)/FMM
      DCP    = CPL*DEL
      SUM3   = SUM3 + DCP
      DVML   = VML*DEL
      SUM2   = SUM2 + DVML
  539 CONTINUE
```

```
      TTK     = SUM/(TO(I)-TTS(K1))
      VKM     = SUM1/(TO(I) - TTS(K1))
      VM      = SUM2/(TO(I) - TTS(K1))
      CPM     = SUM3/(TO(I) - TTS(K1))
      GR      = 980.*(2.*R)**3.*(TO(I) - TTS(K1))/(VKM**2.*TTS(K1))
      PR      = CPM*VM/TTK
      DSA=AMB*PT/(RG*TOO(I))
      UA=53.
      UD=234.
      UA=UA*TOO(I)/293.15
      UO=(UA**2.+UD**2.)**0.5
      RE=2.*R*UO*DSA/VM
      WVM(K1)= VM
      WVK(K1)= VKM
      WTK(K1)=TTK
      WCP(K1)=CPM
      WGR(K1)= GR
      WPR(K1)= PR
      WRE(K1)=RE
C     COMPUTATION OF THE FUNCTIONS Y AND Z
      YA2     = EXP(-A1*BM(K)/TTK)
      YB      = (1.-QR)/(FK2-QR)
      Y(K1)   = YA2-YB
      FT1F = -C1*(TC/TTS(K1)-1.)
      DTSF = TC - TTS(K1)
      FT2F=1.+C2*DTSF+C3*DTSF**3+C5*DTSF**4
      FT3F = 1. + C4*DTSF
      FTF   = FT1F*FT2F/FT3F
      GTF   = GA/(R*TTS(K1))
      YYY=(QR1-BM(K)/A2)/(QR1-BM(K)*FK2/A2)
      IF(YYY.LE.0.) GO TO 206
      Z3     =YYY**AL
      Z4    = PC*EXP(FTF+GTF)/PT
      VPP1=PC*EXP(FTF+GTF)
      Z(K1)=1.-(1.-XA0)*Z3-Z4
      BAL(IJ)=AL
      GRM = GR - 4.2/PR
      IF(GRM)  540, 545, 545
  540 FGR    =0.15*(GR*PR)**(.5)
      GO TO  550
  545 FGR    =0.215*(GR*PR)**(.25)
  550 CMR(K1)=BM(K)*(1.+AM(IJ)*FGR/BM(K))
      FRE=0.3*(RE**0.5*PR**(1./3.))
      CRMR(K1)=BM(K)*(1.+FRE)
      CRMR(K1)=BM(K)*(1.+AM(IJ)*FRE/BM(K))
      DEF(K1)=Y(K1)-Z(K1)
560   CONTINUE
      KJ=K
      DO 111 K1=1,L1
      KL1=K1
      IF(Y(K1).LT.0.) GO TO 112
  111 CONTINUE
      GO TO 206
  112 KL2=1
      IF(KL1.LE.1) GO TO 777
      DO 122 K1=1,L1
      KL2=K1
      IF(Z(K1).LE.0.) GO TO 776
  122 CONTINUE
      GO TO 206
  776 IF(KL2.LE.1) GO TO 777
      GO TO 997
  206 IF(KY-1) 6,6,7
    6 SP=SS
      SS=SP*5.
      GO TO 600
```

```
    7 SP=SS
      SS=(SP+SN)/2.0
      SMU=ABS(SS-SP)
      SMUR=SMU/SS
      IF(SMUR.LE.5.0E-04) GO TO 997
600   CONTINUE
  777 WRITE(6,996) KJ,BM(KJ),SS
      IF(KL1.GT.1.AND.KL2.GT.1) GO TO 997
      KY=KY+1
      SN=SS
      SS=(SP+SN)/2.0
      SMV=ABS(SS-SN)
      SMVR=SMV/SS
      IF(SMVR.LE.5.0E-04) GO TO 997
      GO TO 500
  996 FORMAT(9X,'BM(',I2,')=',E11.4,6X,'SS=',E14.7)
  997 WRITE(6,999)(K1,TTS(K1),K1,Z(K1),K1,Y(K1),K1,CMR(K1)
     C,K1,CRMR(K1),K1=1,L1)
  999 FORMAT(/(2X,'TTS(',I2,')=',E11.4,2X,'Z(',I2,')=',E11.4,2X,'Y(',
     CI2,')=',E11.4,2X,'CMR(',I2,')=',E11.4,2X,'CRMR(',I2,')=',E11.4))
      DMIN=ABS(DEF(1))
      K1=1
      DO 666 J=1,L1
      IF(ABS(DEF(J)).GT.DMIN) GO TO 666
      DMIN=ABS(DEF(J))
      K1=J
  666 CONTINUE
      YMIN(IJ)=Y(K1)
      TTSS(IJ)=TTS(K1)*TB-273.15
      TSWR=TS(IJ)*TB-273.15
      WMM(IJ)=WVM(K1)
      WKK(IJ)=WVK(K1)
      WTT(IJ)=WTK(K1)
      WCC(IJ)=WCP(K1)
      WGG(IJ)=WGR(K1)
      WPP(IJ)=WPR(K1)
      WRR(IJ)=WRE(K1)
      VPS(IJ)=VPP1
  555 BMM(IJ)=CMR(K1)
      BRMM(IJ)=CRMR(K1)
      BRMF(IJ)=BRMM(IJ)/(4.0*3.1416*(R**2.))
      WRITE(6,361)R,I,TOO(I),IJ,TTSS(IJ),IJ,VPS(IJ),IJ,BMM(IJ)
     C,IJ,BRMM(IJ)
  361 FORMAT(/,5X,'R=',E11.4,2X,'TOO(',I2,')=',F10.4,2X,'TTSS(',I2,
     C')=',E11.4,2X,'VPS(',I2,')=',E11.4,2X,'BMM(',I2,')=',E11.4,
     C2X,'BRMM(',I2,')=',E11.4,/)
      WRITE(6,362)
  362 FORMAT(11X,'TEMP.',6X,'STEAM COND.',4X,'GAS COND.',4X,'STEAM VIS.
     C',6X,'GAS VIS.',6X,'DIFFU.')
      WRITE(6,363)(J1,TT(J1),ANN1(J1),ANN2(J1),VAA(J1),VBB(J1),
     CDD12(J1),J1=1,40)
  363 FORMAT(3X,I2,6E14.4)
  567 WRITE(6,565) TCC(I)
  565 FORMAT(///,1X,76HTHE COMPUTED FUNCTIONS OVER A RANGE OF SURFACE TE
     1MPS. FOR A GAS TEMP. TO =  ,F10.3,'C')
      WRITE(6,570) BM(KJ)
  570 FORMAT(3X,42HTHE VAPORIZATION RATE WITH RAD.      MO =  ,E11.4)
      WRITE(6,575)
  575 FORMAT(/,2X,'SURFACE TEMP',2X,'Y FUNCTION',3X,'Z FUNCTION',3X,'VIS
     1COSITY',3X,'K VISCOSITY VKM',2X,'GRASHOF NO.',5X,'PR',9X,
     C'CMR',9X,'RE',8X,'CRMR')
  580 WRITE(6,585) TTSS(IJ),YMIN(IJ),Z(K1),WMM(IJ),WKK(IJ),WGG(IJ),
     CWPP(IJ),CMR(K1),WRR(IJ),CRMR(K1)
  585 FORMAT(2X,E11.4,2X,E11.4,2X,E11.4,2X,E10.3,5X,E10.3,4X,E10.3,2X,E1
     CO.3,1X,E11.4,1X,E10.3,1X,E11.4)
      WRITE(6,576)
```

```
  576 FORMAT(/,2X,'THERMAL COND. TTK',2X,'MIXTURE CP CPM',7X,'AIR VEL.')
      WRITE(6,586) WTT(IJ),WCC(IJ),UD
  586 FORMAT(7X,E11.4,3X,E11.4,2X,E11.4)
  650 WRITE(6,660)  TCC(I)
  660 FORMAT(//,3X,57HCOMPUTED RESULTS WITHOUT RADIATION FOR A GAS TEMP.
     1 TO =  ,E11.4)
      WRITE(6,670)
  670 FORMAT(/,3X,'REL. HUMIDITY',5X,'SURF. TEMP.',5X,'MEAN GAS COND.',5
     1X,'MEAN LEWIS NO.',5X,'VAPOR. RATE',5X,'BIN DIF CO',5X,'W V MOL FR
     1AC XAO')
      WRITE(6,680)YA(I),TSWR  ,AK(IJ),BAL(IJ),AM(IJ),CCD(IJ),XAOO(I)
  680 FORMAT((5X,E11.4,5X,E11.4,6X,E11.4, 8X,E11.4, 7X,E11.4,5X,E11.4,9X
     1,E10.3)///)
      R1(IJ)=R
      DR1(IJ)=R1(IJ)*2.
      DD2(IJ)=(R1(IJ)/R1(1))**2.
      DDT(IJ)=DT
      AF=(4./3.)*3.1416*DST
      R11=R1(IJ)**3-DTT*BMM(IJ)/AF
      LL=LL+1
      IF(R11.LE.0.) GO TO 146
      R12=R11**(1./3.)
      R=R12
      DT=DDT(IJ)+DTT
 1111 CONTINUE
  146 WRITE(6,147) (IJ,BRMM(IJ),IJ,BRMF(IJ),IJ,DR1(IJ),IJ,DD2(IJ),IJ,
     CDDT(IJ),IJ=1,LL)
  147 FORMAT(10X,'BRMM(',I2,')=',E11.4, 5X,'BRMF(',I2,')=',E11.4,5X,
     C'D(',I2,')=',E11.4,5X,'(D/DO)**2.(',I2,')=',F9.4,5X,'DDT(',I2,
     C')=',F10.4/)
 1000 CONTINUE
C
C
 1140 WRITE(6,1150)
 1150 FORMAT(//,3X,35HDATA TABLE FOR THIS SERIES OF CASES)
      WRITE(6,1250)
 1250 FORMAT(/,5X,'DROPLET RADIUS',5X,'ALPHA',11X,'BETA',11X,'VAP MOL WT
     1 AMA',5X,'GAS MOL WT AMB',5X,'TOT PRES PT')
      WRITE(6,1350)  R, A, B, AMA, AMB, PT
 1350 FORMAT(7X,E11.4,8X,E11.4,6X,E11.4,5X,E11.4,9X,E11.4,9X,E11.4)
      WRITE(6,1450)
 1450 FORMAT(/,5X,'CP VAPOR',11X,'CP GAS',10X,'LATENT HEAT',3X,'DROP BOI
     1L TEMP',5X,'GAS BOIL TEMP',6X,'NORM SURF TEN GA')
 1550 WRITE(6,1350) CPA, CPB, DLH, TB, TBB, GA
      WRITE(6,1660)
 1660 FORMAT(/,5X,'COND.PAR AKB',7X,'COND PAR BKB',4X,'COND.PAR AE',4X,'
     1COND.PAR BE',8X,'VISC.PAR AVB',7X,'VISC.PAR BVB')
      WRITE(6,1350) AKB, BKB, AE, BE, AVB, BVB
      WRITE(6,1750)
 1750 FORMAT(/,5X,'VISC.PAR AVE',7X,'VISC.PAR BVE',4X,'VAP CONST, EA',2X
     1,'GAS CONST, EB',6X,'VAP COL DIA.S1',5X,'GAS COL DIA.S2')
      WRITE(6,1350) AVE, BVE, EA, EB, S1, S2
      WRITE(6,1850)
 1850 FORMAT(/,5X,'STEP SIZE SI',7X,'STEP SIZE SS',7X,'STEP SIZE ST',
     C7X,'DROP DST',7X,'PT',7X,'DTT',7X,'DLH',7X,'AB')
      WRITE(6,1950) SI, SS, ST, DST, PT, DTT,DLH,AB
 1950 FORMAT(7X,E11.4,7X,E11.4,7X,E11.4,5X,F10.4,3X,F8.3,1X,F8.3,
     C2X,F8.2,2X,F8.3)
 2000 STOP
      END
```

```
//GO.SYSIN DD *
 4
40
15
15
 5
 502.0      0.0        0.0
  0.347E 00
  13.09
  0.660E 00
  0.180E 02
  0.288E 02
  0.575E-04
  0.763E-04
  0.116E 01
  0.766E 00
  0.125E-03
  0.218E-03
  1.055E 00
  0.683E 00
 0.2691E-01
  1.0
  0.485E 00
  0.250E 00
  0.539E+03
  0.373E+03
  0.800E 02
 8.4425E-08
  0.506E 03
  0.970E 02
  2.710E 00
  3.617E 00
  0.160E-06
  1.0
  0.150E-02
  0.986
  0.003
```

APPENDIX D

COMPUTER PROGRAM OF LARGE FLUX MODEL

Main program, constants and appropriate comments on the Large Flux model are included in the following pages. Calculating procedures should be referred to in Chapter 4.4.

```
//LRNO611 JOB (48041,C70628,RMT2,G-W),SUMING
$JOB
C     THIS PROGRAM IS DESIGNED TO COMPUTE THE VAPORIZATION RATES OF DROPLETS
C     MOVING UNDER FORCED CONVECTION IN A HIGH TEMPERATURE AIR STREAM,
C     ACCORDING TO THE LARGE FLUX MODEL.  THE SOLUTION FOR THE VAPORIZATION
C     RATE IS ACHIEVED WHEN THE NET HEAT FLUX TO THE DROPLET, FTS, IS ZERO.
C
C
      DIMENSION TSC(5),FTS(5)
      READ(5,30)  TOC
      READ(5,30)  XAO
      READ(5,35)  UA,UD
      READ(5,30)  D
      READ(5,30)  PT
      READ(5,30)  TBA
      READ(5,30)  TBB
      READ(5,30)  AMA
      READ(5,30)  AMB
      READ(5,30)  EA
      READ(5,30)  EB
      READ(5,30)  S1
      READ(5,30)  S2
      READ(5,30)  AKB
      READ(5,30)  BKB
      READ(5,30)  AE
      READ(5,30)  BE
      READ(5,30)  AVB
      READ(5,30)  BVB
      READ(5,30)  AVE
      READ(5,30)  BVE
      READ(5,35)  H, R2
   30 FORMAT(E11.4)
   35 FORMAT(E11.4,E11.4)
      TC    = 1.73456*373.15/TBA
      PC    = 218.167
      C1    = 7.7052
      C2    =4.6178*TBA/373.15
      C3    = 0.116692*(TBA/373.15)**3.
      C4    = 5.1474*TBA/373.15
      C5    = 0.380334*(TBA/373.15)**4.
      R     = 82.05
      SIG   = 1.355*10.**(-12)
      UO=(UA**2.+UD**2.)**0.5
      READ(5,30)  TSR
C
C     TEMPERATURE CONVERSIONS
C
      TSC(1)=TSR
      TSC(2)=90.
      DO 31 I=1,3
   32 TSC(3)=(TSC(1)+TSC(2))/2
      TSK   = TSC(I) + 273.15
      TOK   = TOC + 273.15
      TS    = TSK/TBA
      TO    = TOK/TBA
C
C     COMPUTATION OF THE VAPOR PRESSURE AT THE GIVEN SURFACE TEMP
C
      FT1   =-C1*(TC/TS - 1.)
      DTS   = TC - TS
      FT2    =1. + C2*DTS + C3*DTS**3. + C5*DTS**4.
      FT3   = 1. + C4*DTS
      FT    = FT1*FT2/FT3
      PAS   = PC*EXP(FT)
```

```
C
C     COMPUTATION OF THE VAPOR MOLE FRACTION AT THE SURFACE
C
      XAS  = PAS/PT
C
C     COMPUTATION OF THE FILM CONDITIONS
C
      XAF  = (XAS + XAO)/2.
      XBF  = 1. - XAF
      TFC  = (TSC(I) + TOC)/2.
      TFK  = (TSK + TOK)/2.
      TF   = TFK/TBA
C
C     COMPUTATION OF THE PURE COMPONENT PROPERTIES AT THE FILM CONDITIONS
C
      VA   = AVB*TF**AVE
      VB   = BVB*TF**BVE
      AN1  = AKB*TF**AE
      AN2  = BKB*TF**BE
      CMF  = PT/(R*TFK)
      FMM  = AMA*XAF + AMB*XBF
      DF   = FMM*CMF
      CPA  = (7.136+TFK*(2.640E-3+0.0459E-6*TFK))/AMA
      CPB  = (6.386+TFK*(1.762E-3-0.2656E-6*TFK))/AMB
      CPM  = (XAF*CPA*AMA + XBF*CPB*AMB)/FMM
      TC1  = (TC*TBA-TSK)**(0.38)
      TC2  = (TC*TBA-TBA)**(1.38)
      HV   = 1.987*TC*TBA**2*ALOG(PC)*TC1/TC2
C
C     COMPUTATION OF THE MIXTURE CONDUCTIVITY AT THE FILM CONDITIONS, AKF
C
      XAB  = XAF/XBF
      VF   = (VA/VB)*(AMB/AMA)**(.75)
      SAT  = 1.5/TF
      SBT  = SAT*(TBB/TBA)
      SABT = 1.05*(TBB/TBA)**(.5)/TF
      SF1  = (1. + SAT)/(1. + SBT)
      SF2  = (1. + SABT)/(1. + SAT)
      SF3  = (1. + SABT)/(1. + SBT)
      AAB  = (1. + (VF*SF1)**(.5))**2.*SF2/4.
      ABA  = (1. + (VF*SF1)**(-.5))**2.*SF3/4.
      D1   = 1. + AAB/XAB
      D2   = 1. + ABA*XAB
      AKF  = AN1/D1 + AN2/D2
C
C     COMPUTATION OF THE FORCE CONSTANTS AND REDUCED TEMPERATURE, EK,S12,AND TKE
C
      EK   = (EA*EB)**(.5)
      S12  = (S1 +S2)/2.
      TKE  = TFK/EK
C
C     COMPUTATION OF THE COLLISION INTEGRALS, W12 AND A12
C
      DTKE = TKE - 2.6
      IF(DTKE)  300,400,400
  300 W12  = 1.347*TKE**(-0.3259)
      GO TO 500
  400 W12  = 1.277*TKE**(-0.2697)
  500 A12  = 1.095
C
C     COMPUTATION OF THE BINARY DIFFUSION COEFFICIENT, D12
C
      AM12 = ((AMA+ AMB)/(2.*AMA*AMB))**(.5)
      DEN  = PT*S12**2.*W12
      D12  = 0.002628*TFK**(1.5)*AM12/DEN
C     COMPUTATION OF THE MIXTURE VISCOSITY AT THE FILM CONDITIONS, VM
```

```
      SM   = AMA + AMB
      F1   = XAF**2./VA
      F2   = 2.*XAF*XBF/SM
      F3   = R*TFK/(PT*D12)
      F4   = 1. + 0.6*AMB*A12/AMA
      H11  = F1 + F2*F3*F4
      F5   = XBF**2./VB
      F6   = 1. + 0.6*AMA*A12/AMB
      H22  = F5 + F2*F3*F6
      F7   = 1. - 0.6*A12
      H12  = -F2*F3*F7
      T1   = XAF**2./H11
      T2   = XBF**2./H22
      T3   = 2.*XAF*XBF*H12/(H11*H22)
      T4   = 1./(1. - H12**2 /(H11*H22))
      VM   = (T1 + T2 - T3)*T4
C
C     COMPUTATION OF THE AIR PROPERTIES
C
      VBO  = BVB*TO**BVE
      DBO  = AMB*PT/(R*TOK)
C
C     COMPUTATION OF THE  NONDIMENSIONAL GROUPS
C
      RE   = D*UO*DF/VM
      REO  = D*UO*DBO/VBO
      PR   = CPM*VM/AKF
      SC   = VM/(DF*D12)
C
C     COMPUTATION OF THE HEAT TRANSFER COEFFICIENT, HM
C
      RER  = RE**(.5)
      PRR  = PR**(1./3.)
      HM   = AKF *(2. + 0.6*RER*PRR)/D
C
C     COMPUTATION OF THE MASS TRANSFER COEFFICIENT, AKX
C
      SCR  = SC**(1./3.)
      AKX  = CMF*D12*(2.+ 0.6*RER*SCR)/D
C
C
C     COMPUTATION OF THE FROESSLING FACTOR
C
      FF1  = 0.276*RER*PRR
      FF2  = 0.276*REO**(.5)*PRR
C
C     COMPUTATION OF THE FLUXES  SNA, CQ, AND RQ
C
      DX   = (XAS - XAO)/(1. - XAS)
      SNA  = AKX*ALOG(1. + DX)
      VMR  = SNA*3.14159*D**2*AMA
      VMRF =VMR/(4.0*3.1416*(D/2.)**2.)
      CQN  = SNA*CPA*AMA*(TSC(I)-TOC)
      CQD  = EXP(SNA*CPA*AMA/HM) - 1.
      CQ   = CQN/CQD
C     F12  = (1. -  COS( ATAN( R2/H)))/2.
      F12=0.4
      RQ   = SIG*F12*TBA**4.*(TS**4. - TO**4.)
      ABP=1.159-0.1167*TO
      RQ =ABP*RQ
C
C     COMPUTATION OF THE HEAT BALANCE, FTS
C
      FTS(I)  = SNA*HV + CQ + RQ
      IF(I.LT.3)GO TO 31
      IF(ABS(FTS(3)).LT.1.0E-02)GO TO 33
```

```
      FTS13=FTS(1)*FTS(3)
      IF(FTS13.LT.0.)THEN
      TSC(2)=TSC(3)
      FTS(2)=FTS(3)
      ELSE
      TSC(1)=TSC(3)
      FTS(1)=FTS(3)
      ENDIF
      GO TO 32
   31 CONTINUE
C
   33 WRITE(6,1000)  TSC(3)
 1000 FORMAT(//,1X,50HRESULTS FOR THE TRIAL SURFACE TEMPERATURE, TSC =
     1,F10.2)
      WRITE(6,1100)
 1100 FORMAT(/,5X,'HEAT FLUX EXCESS',7X,'VAP MOLAR FLUX',7X,'COND HEAT F
     1LUX',7X,'RAD HEAT FLUX',7X,'HEAT XFER COEF')
      WRITE(6,1200) FTS(3),SNA,CQ,RQ,HM
 1200 FORMAT(8X,E11.4,12X,E11.4,10X,E11.4,10X,E11.4,9X,E11.4)
      WRITE(6,1300)
 1300 FORMAT(/,5X,'MASS XFER COEF',9X,'REYNOLDS NO.',9X,'PRANDTL NO.',10
     1X,'SCHMIDT NO.',9X,'VAPOR PRESSURE')
      WRITE(6,1200) AKX,RE,PR,SC,PAS
      WRITE(6,1400)
 1400 FORMAT(/,5X,'SURF MOLE FRAC',9X,'VAPOR VISC.',11X,'GAS VISCOSITY',
     18X,'MIXTURE VISC.',11X,'MIXTURE COND.')
      WRITE(6,1200) XAS,VA,VB,VM,AKF
      WRITE(6,1500)
 1500 FORMAT(/,5X,'DIFFUSION COEF',15X,'CP VAPOR',15X,'CP GAS',10X,
     1 'LATENT HEAT', 7X,'VAP MASS RATE')
      WRITE(6,1200) D12,CPA,CPB,HV,VMR
      WRITE(6,1501)
      WRITE(6,1201) VMRF,ABP
 1501 FORMAT(/,5X,'VAP MASS FLUX',8X,'DROPLET EMISS')
 1201 FORMAT(8X,E11.4,11X,E11.4)
 1650 WRITE(6,1700)
 1700 FORMAT(//,1X,24HDATA TABLE FOR THIS CASE)
      WRITE(6,1800)
 1800 FORMAT(/,5X,'GAS TEMP, TOC',10X,'REL VELOC, VO',8X,'DROPLET DIA, D
     1',7X,'TOT PRESSURE, PT',4X,'VAP MOLE FRAC, XAO')
      WRITE(6,1200) TOC,UO,D,PT,XAO
      WRITE(6,1900)
 1900 FORMAT(/,5X,'VAP MOLE WT, AMA',7X,'GAS MOLE WT, AMB',5X,'VAP FORCE
     1 CONST, EA',2X,'GAS FORCE CONST, EB',1X,'VAP COLL DIA, S1')
      WRITE(6,1200) AMA,AMB,EA,EB,S1
      WRITE(6,2000)
 2000 FORMAT(/,5X,'GAS COLL DIA, S2',7X,'RAD. FACTOR, F12',7X,'HEIGHT, H
     1',10X,'TUBE RADIUS',9X,'AIR REYNOLDS NO.')
      WRITE(6,1600) S2, F12, H, R2, REO
 1600 FORMAT(8X,E11.4,13X,E11.4,9X,E11.4,10X,E11.4,9X,E11.4)
      WRITE(6,2100)  FF1
 2100 FORMAT(/,1X,45HFROESSLING FACTOR BASED ON FILM PROP., FF1 = ,E11.4
     1)
      WRITE(6,2200)  FF2
 2200 FORMAT(/,1X,45HFROESSLING FACTOR BASED ON AIR PROP.,  FF2 = ,E11.4
     1)
      STOP
      END
```

```
$ENTRY
 5.0200E 02
 0.0000E 00
 1.4000E 02 2.3400E 02
 2.6910E-02
 0.1000E 01
 0.3731E 03
 0.8000E 02
 0.1800E 02
 0.2882E 02
 0.5060E 03
 0.9700E 02
 0.2710E 01
 0.3617E 01
  0.575E-04
  0.763E-04
  0.116E 01
  0.766E 00
  0.125E-03
  0.218E-03
  1.055E 00
  0.683E 00
0.2500E 00 0.1250E 01
0.6200E 02
```

APPENDIX E

PROPERTY VALUE EXPRESSIONS FOR THE AIR-WATER VAPOR SYSTEM

The property value expressions that have been employed in the calculations of both the Froessling model and the Large Flux model are summarized here.

1. Vapor Pressure

The vapor pressure of water is calculated from the following relation proposed by Keenan and Keyes(38):

$$\ln \frac{Pc}{P_A} = \frac{aX}{Ts} \left(\frac{1+bX+cX^3+eX^4}{1+dX} \right) \qquad \text{(E-1)}$$

where P_A: vapor pressure, atm

Pc: critical pressure, 218.167 atm

Ts: absolute droplet surface temperature, ^oK

X : (Tc-Ts)/Tb

Tc: absolute critical temperature, 647.27^oK

Tb: absolute water boiling temperature, ^oK

a : 7.7052

b : 4.6178(Tb/373.15)

c : $0.116692(Tb/373.15)^3$

d : 5.1474(Tb/373.15)

e : $0.380334(Tb/373.15)^4$

2. Thermal Conductivity and Viscosity

The thermal conductivity of the binary gas mixture of the air-water vapor system, Km, was approximated by Lindsay and Bromley(50) as in the following:

$$Km = \sum_{i=1}^{n} K_i \left(1 + \sum_{\substack{j=1 \\ j\neq i}}^{n} A_{ij} \frac{X_j}{X_i}\right)^{-1} \qquad \text{(E-2)}$$

where

$$A_{ij} = \frac{1}{4}\left(1+\left[\left(\frac{\mu_i}{\mu_j}\right)\left(\frac{M_j}{M_i}\right)^{3/4}\left(\frac{1+S_i/T}{1+S_j/T}\right)\right]^{1/2}\right)^2 \times (1+S_{ij}/T)/(1+S_i/T) \qquad \text{(E-3)}$$

S_i : constant, $1.5/Tb_i$

S_{ij}: constant, $0.7(S_i\ S_j)^{1/2}$ for nitrogen-water vapor mixture, $S_{ij}=S_{ji}$

K_i : thermal conductivity of component i, cal/cm,sec, ^oK

μ_i : viscosity of component i, g/cm,sec

T : absolute temperature, ^oK

Tb_i: normal boiling point of component i

M_i : molecular weight of component i

X_i : mole fraction of component i

The visocity of binary mixture of air-water vapor system, μ_m is calculated by the equation proposed by Mason and Monchick(55), which is written in the following form:

$$\mu_m = \left(\frac{X_1^2}{H_{12}} + \frac{X_2^2}{H_{22}} - \frac{2X_1 X_2 H_{12}}{H_{11} H_{22}}\right)\left(1 - \frac{H_{12}^2}{H_{11} H_{22}}\right)^{-1} \qquad \text{(E-4)}$$

$$\text{where } H_{11} = \frac{X_1^2}{\mu_1} + \frac{2X_1 X_2}{M_1+M_2} \frac{R\,T}{P\,D_{12}} \left(1 + \frac{3M_2}{5M_1} A_{12} \right)$$

$$H_{12} = - \frac{2X_1 X_2}{M_1+M_2} \frac{R\,T}{Pt\,D_{12}} \left(1 - \frac{3}{5} A_{12} \right)$$

Pt : total pressure, atm

R : gas constant, cm^3-atm/mole-^oK

D_{12} : binary diffusion coefficient

A_{12} : $\Omega_{v12}/\Omega_{D12}$, 1.095

The following forms are used for the temperature dependence of thermal conductivities and viscosities of both water vapor and air:

$$K_i = a\,\theta^b \qquad \text{(E-5)}$$

$$\mu_i = c\,\theta^d \qquad \text{(E-6)}$$

where θ : normalized temperature, T/Tb

The parameters in Eq.(E-5) and (E-6) are evaluated by fitting the data collected by Eckert(14) and Perry(61). The values are listed in the following:

	Air	Water
a	0.763×10^{-4}	0.575×10^{-4}
b	0.766	1.16
c	0.218×10^{-3}	0.125×10^{-3}
d	0.683	1.055

The mean thermal conductivity and the mean viscosity of the air-water vapor mixture are both taken as integrated means, according to the form:

$$\overline{Km}(\text{or } \overline{\mu}_m) = \int_{\theta_s}^{\theta_a} \overline{Km}(\text{or } \overline{\mu}_m)\, d\theta \,/(\, \theta_a - \theta_s) \qquad \text{(E-7)}$$

3. Heat Capacity

Heat capacity of water vapor is calculated as:

$$Cp_A = C_0 + C_1 T + C_2 T^2 \qquad \text{(E-8)}$$

where

Cp_A: heat capacity of water vapor, cal/g-mol

T : absolute temperature, ^oK

C_0 : 7.136

C_1 : 0.264×10^{-2}

C_2 : 0.459×10^{-7}

Integrated mean values are used according to the form in Eq.(E-7).

4. Diffusion Coefficient

The air-water diffusion coefficient is computed according to the method suggested by Mason and Monchick(55):

$$D_{AB} = \frac{2.628 \times 10^{-3} T^{3/2}}{Pt\, \sigma_{AB}^2\, \Omega_{AB}^{(1,1)^*}} \left(\frac{M_A + M_B}{2 M_A M_B} \right)^{1/2} \qquad \text{(E-9)}$$

where $\Omega_{AB}^{(1,1)^*}$ is the reduced collision integral for diffusion taken from tabulated values for the 12-6 potential. σ_{AB} is the collision diameter for molecules of type A and B. The unit of D_{AB} is cm^2 /sec when Pt and T are expressed in atmosphere and ^oK, respectively.

APPENDIX F

RAW VAPORIZATION DATA

The following tables contain the raw data of each individual run reduced from photographs. The asterisk, *, indicates the data points which were excluded in regression analysis.

RUN NO. N0609

Ttc=515 C Ta=522 C
Ua=144 Cm/Sec Ud=266 Cm/Sec
Distance above Furnace Tube=0.64 cm

DROPLET NO.	FLIGHT DISTANCE, Cm	DIAMETER, Cm
1	1.8900	0.2708E-01
2	1.9500	0.2748E-01
3	2.0100	0.2741E-01
4	2.0700	0.2741E-01
5	2.3200	0.2726E-01
6	2.3800	0.2736E-01
7	2.4400	0.2726E-01
8	2.5000	0.2726E-01
9	2.8300	0.2745E-01
10	2.8800	0.2712E-01
11	2.9400	0.2736E-01
12	3.0000	0.2707E-01
13	3.0600	0.2745E-01
14	3.3700	0.2733E-01
15	3.4300	0.2752E-01
16	3.4900	0.2719E-01
17	3.5400	0.2742E-01
18	3.6000	0.2714E-01
19	3.9000	0.2733E-01
20	3.9500	0.2718E-01
21	4.0000	0.2746E-01
22	4.0600	0.2737E-01
23	4.1200	0.2737E-01
24	4.4300	0.2720E-01
25	4.4900	0.2749E-01
26	4.5400	0.2711E-01
27	4.6100	0.2744E-01
28	4.6500	0.2711E-01
29	4.9100	0.2740E-01
30	4.9700	0.2713E-01
31	5.0200	0.2727E-01
32	5.0800	0.2708E-01
33	5.1300	0.2732E-01

RUN NO. N0610

Ttc=495 C Ta=501 C
Ua=140 Cm/Sec Ud=252 Cm/Sec
Distance above Furnace Tube=0.64 cm

DROPLET NO.	FLIGHT DISTANCE, Cm	DIAMETER, Cm
1	1.9000	0.2719E-01
2	1.9500	0.2709E-01
3	2.0000	0.2719E-01
4	2.0600	0.2688E-01
5	2.1100	0.2717E-01
6	2.3700	0.2717E-01
7	2.4200	0.2713E-01
8	2.4700	0.2699E-01
9	2.5200	0.2722E-01
10	2.5800	0.2696E-01
11	2.8400	0.2725E-01
12	2.8900	0.2691E-01
13	2.9400	0.2730E-01
14	3.0000	0.2695E-01
15	3.0900	0.2715E-01
16	3.3700	0.2713E-01
17	3.4200	0.2706E-01
18	3.4700	0.2688E-01
19	3.5200	0.2728E-01
20	3.5700	0.2705E-01
21	3.6200	0.2715E-01
22	3.8600	0.2711E-01
23	3.9100	0.2724E-01
24	3.9600	0.2715E-01
25	4.0100	0.2693E-01
26	4.0700	0.2724E-01
27	4.1100	0.2688E-01
28	4.4400	0.2723E-01
29	4.4900	0.2688E-01
30	4.5400	0.2714E-01
31	4.5800	0.2688E-01
32	4.8700	0.2711E-01
33	4.9100	0.2702E-01
34	4.9600	0.2702E-01
35	5.0100	0.2720E-01
36	5.0600	0.2688E-01
37	5.1000	0.2706E-01
38	5.1500	0.2688E-01

RUN NO. N0611

Ttc=496 C Ta=502 C
Ua=140 Cm/Sec Ud=234 Cm/Sec
Distance above Furnace Tube=0.64 cm

DROPLET NO.	FLIGHT DISTANCE, Cm	DIAMETER, Cm
1	1.8600	0.2702E-01
2	1.9100	0.2686E-01
3	1.9700	0.2722E-01
4	2.0200	0.2686E-01
5	2.0700	0.2707E-01
6	2.2200	0.2680E-01
7	2.2700	0.2712E-01
8	2.3300	0.2712E-01
9	2.3800	0.2717E-01
10	2.6400	0.2686E-01
11	2.6800	0.2702E-01
12	2.7400	0.2712E-01
13	2.7900	0.2712E-01
14	3.2900	0.2692E-01
15	3.3400	0.2686E-01
16	3.3900	0.2699E-01
17	3.4400	0.2723E-01
18	3.4900	0.2681E-01
19	3.5500	0.2712E-01
20	3.6000	0.2697E-01
21	3.7100	0.2704E-01
22	3.7600	0.2679E-01
23	3.8100	0.2714E-01
24	3.8600	0.2705E-01
25	4.1900	0.2708E-01
26	4.2400	0.2693E-01
27	4.9500	0.2688E-01
28	5.0000	0.2699E-01
29	5.0500	0.2708E-01
30	5.0900	0.2683E-01
31	5.1400	0.2688E-01
32	5.1900	0.2683E-01

RUN NO. N0924

Ttc=550 C Ta=574 C
Ua=136 Cm/Sec Ud=189 Cm/Sec
Distance above Furnace Tube=0.64 cm

DROPLET NO.	FLIGHT DISTANCE, Cm	DIAMETER, Cm
1	1.9100	0.3233E-01
2	1.9700	0.3275E-01
3	2.0500	0.3278E-01
4	2.4100	0.3264E-01
5	2.4700	0.3278E-01
6	2.8900	0.3233E-01
7	2.9600	0.3279E-01
8	3.0300	0.3231E-01
9	3.1000	0.3229E-01
10	3.1600	0.3274E-01
11	3.8900	0.3271E-01
12	3.9600	0.3210E-01
13	4.0300	0.3251E-01
14	4.0900	0.3237E-01
15	4.1600	0.3239E-01
16	4.2300	0.3257E-01
17	4.4300	0.3257E-01
18	4.5000	0.3210E-01
19	4.5800	0.3200E-01
20	4.6200	0.3262E-01
21	4.6600	0.3201E-01
22	4.9100	0.3233E-01
23	5.1000	0.3223E-01
24	5.4100	0.3242E-01

RUN NO. C1001

Ttc=555 C Ta=580 C
Ua=137 Cm/Sec Ud=203 Cm/Sec
Distance above Furnace Tube=0.64 cm

DROPLET NO.	FLIGHT DISTANCE, Cm	DIAMETER, Cm
* 1	1.8800	0.2980E-01
2	1.9400	0.3023E-01
3	2.0600	0.3003E-01
* 4	2.1200	0.2981E-01
5	2.4300	0.3018E-01
6	2.5500	0.3009E-01
7	2.6100	0.3023E-01
8	2.8400	0.2992E-01
9	2.9000	0.3011E-01
10	2.9500	0.3013E-01
11	3.0100	0.2993E-01
12	3.0700	0.3018E-01
13	3.3300	0.3014E-01
14	3.3800	0.2984E-01
15	3.4400	0.3000E-01
16	3.5500	0.3002E-01
* 17	3.6000	0.2967E-01
18	3.6600	0.2999E-01
19	4.3500	0.2989E-01
20	4.4100	0.2982E-01
21	4.4600	0.2983E-01
22	4.5100	0.2997E-01
23	4.5600	0.3003E-01
24	4.6200	0.2990E-01
25	4.8300	0.2976E-01
26	4.8900	0.2982E-01
27	4.9400	0.2982E-01
28	4.9900	0.2994E-01
29	5.0400	0.2965E-01
30	5.0900	0.2978E-01
31	5.4300	0.2979E-01
32	5.4800	0.2969E-01
33	5.5300	0.2964E-01
34	5.5800	0.2972E-01

RUN NO. D0911

Ttc=552 C Ta=576 C
Ua=136 Cm/Sec Ud=176 Cm/Sec
Distance above Furnace Tube=0.64 cm

DROPLET NO.	FLIGHT DISTANCE, Cm	DIAMETER, Cm
* 1	2.3900	0.2961E-01
2	2.4500	0.3032E-01
3	2.5000	0.3029E-01
4	2.5500	0.3045E-01
5	2.6100	0.3045E-01
6	2.9000	0.3000E-01
7	2.9500	0.3046E-01
8	3.0000	0.3035E-01
9	3.0500	0.3034E-01
10	3.1100	0.3042E-01
11	3.1600	0.3019E-01
12	3.4100	0.3031E-01
13	3.4600	0.3008E-01
14	3.5200	0.3044E-01
15	3.5600	0.3010E-01
16	3.6200	0.3019E-01
17	4.4800	0.3035E-01
18	4.5300	0.3011E-01
19	5.4100	0.2995E-01
20	5.4600	0.3015E-01
21	5.5100	0.3024E-01
22	5.6000	0.3011E-01

RUN NO. N1122

Ttc=620 C Ta=652 C
Ua=167 Cm/Sec Ud=253 Cm/Sec
Distance above Furnace Tube=0.64 cm

	DROPLET NO.	FLIGHT DISTANCE, Cm	DIAMETER, Cm
	1	1.8300	0.2856E-01
	2	1.8700	0.2843E-01
	3	1.9000	0.2851E-01
	4	1.9300	0.2838E-01
*	5	1.9600	0.2866E-01
	6	2.0000	0.2823E-01
	7	2.0300	0.2861E-01
	8	2.0600	0.2843E-01
	9	2.3800	0.2848E-01
	10	2.4400	0.2828E-01
	11	2.5600	0.2828E-01
	12	2.3900	0.2856E-01
	13	2.4500	0.2835E-01
	14	2.5100	0.2856E-01
	15	2.5700	0.2840E-01
	16	2.8500	0.2853E-01
	17	2.9000	0.2828E-01
	18	2.9600	0.2843E-01
	19	3.0300	0.2833E-01
	20	3.0800	0.2853E-01
	21	3.8800	0.2836E-01
	22	3.9400	0.2826E-01
	23	3.9900	0.2846E-01
	24	4.3600	0.2835E-01
	25	4.4200	0.2820E-01
	26	4.4700	0.2835E-01
	27	5.3900	0.2802E-01
	28	5.4500	0.2815E-01
	29	5.5000	0.2832E-01
	30	5.5600	0.2812E-01

RUN NO. N1121

Ttc=620 C Ta=652 C
Ua=167 Cm/Sec Ud=240 Cm/Sec
Distance above Furnace Tube=0.64 cm

DROPLET NO.	FLIGHT DISTANCE, Cm	DIAMETER, Cm
* 1	1.8700	0.2822E-01
* 2	1.9300	0.2812E-01
* 3	1.9800	0.2826E-01
* 4	2.0500	0.2812E-01
5	2.4000	0.2803E-01
6	2.4600	0.2816E-01
7	2.5200	0.2796E-01
8	2.5700	0.2785E-01
9	2.8400	0.2815E-01
10	2.9000	0.2782E-01
11	2.9600	0.2801E-01
12	3.0200	0.2811E-01
13	3.3300	0.2785E-01
14	3.3900	0.2794E-01
15	3.4400	0.2819E-01
16	3.4900	0.2794E-01
* 17	3.5500	0.2824E-01
18	3.6000	0.2784E-01
19	3.8700	0.2807E-01
20	3.9300	0.2792E-01
21	3.9800	0.2787E-01
22	4.0300	0.2802E-01
23	4.0900	0.2805E-01
24	4.8700	0.2764E-01
25	4.9200	0.2804E-01
26	4.9700	0.2784E-01
27	5.0300	0.2794E-01
28	5.0800	0.2764E-01
29	5.3900	0.2784E-01
30	5.4400	0.2754E-01
31	5.4900	0.2789E-01
32	5.5400	0.2754E-01

RUN NO. N1120

Ttc=614 C Ta=645 C
Ua=166 Cm/Sec Ud=254 Cm/Sec
Distance above Furnace Tube=0.64 cm

DROPLET NO.	FLIGHT DISTANCE, Cm	DIAMETER, Cm
1	1.8200	0.2829E-01
2	1.8500	0.2837E-01
* 3	1.8900	0.2854E-01
4	1.9100	0.2823E-01
* 5	1.9500	0.2854E-01
6	1.9800	0.2828E-01
7	2.0100	0.2839E-01
8	2.0400	0.2823E-01
9	2.0800	0.2844E-01
10	2.3900	0.2830E-01
11	2.4500	0.2840E-01
12	2.5200	0.2830E-01
13	2.5700	0.2835E-01
14	2.8600	0.2830E-01
15	2.9200	0.2830E-01
16	2.9800	0.2840E-01
17	3.0400	0.2840E-01
18	3.1000	0.2830E-01
19	3.4800	0.2817E-01
20	3.5400	0.2817E-01
21	3.6000	0.2832E-01
22	3.9100	0.2817E-01
23	3.9700	0.2821E-01
24	4.0300	0.2817E-01
25	4.3600	0.2817E-01
26	4.4200	0.2827E-01
27	4.4800	0.2803E-01
* 28	4.5400	0.2842E-01
29	4.9300	0.2803E-01
30	4.9500	0.2817E-01
31	5.0000	0.2793E-01
32	5.0600	0.2813E-01

RUN NO. C1122

Ttc=608 C Ta=638 C
Ua=165 Cm/Sec Ud=205 Cm/Sec
Distance above Furnace Tube=0.64 cm

DROPLET NO.	FLIGHT DISTANCE, Cm	DIAMETER, Cm
1	1.8300	0.2710E-01
2	1.8800	0.2730E-01
3	1.9300	0.2715E-01
4	1.9800	0.2715E-01
5	2.0300	0.2710E-01
6	2.0800	0.2705E-01
7	2.3100	0.2719E-01
8	2.3600	0.2709E-01
9	2.4100	0.2729E-01
10	2.4600	0.2709E-01
11	2.5100	0.2709E-01
12	2.5600	0.2701E-01
13	2.6100	0.2729E-01
* 14	2.7900	0.2741E-01
* 15	2.8400	0.2736E-01
* 16	2.8900	0.2739E-01
17	2.9400	0.2713E-01
18	2.9800	0.2710E-01
19	3.0400	0.2700E-01
20	3.3300	0.2715E-01
21	3.3800	0.2703E-01
22	3.4300	0.2713E-01
23	3.4800	0.2726E-01
24	3.9300	0.2709E-01
25	3.9800	0.2719E-01
26	4.0200	0.2707E-01
27	4.0700	0.2705E-01
28	4.3500	0.2704E-01
29	4.4000	0.2699E-01
30	4.4400	0.2715E-01
31	4.4900	0.2697E-01
32	4.5300	0.2711E-01
33	4.5800	0.2711E-01
34	4.8000	0.2717E-01
35	4.8400	0.2705E-01
36	4.8900	0.2705E-01
37	4.9400	0.2691E-01
38	4.9800	0.2690E-01
39	5.0300	0.2705E-01
40	5.0700	0.2695E-01

RUN NO. C1123

Ttc=608 C Ta=638 C
Ua=165 Cm/Sec Ud=256 Cm/Sec
Distance above Furnace Tube=0.64 cm

DROPLET NO.	FLIGHT DISTANCE, Cm	DIAMETER, Cm
1	2.3500	0.2734E-01
2	2.4100	0.2712E-01
3	2.4600	0.2734E-01
4	2.5200	0.2734E-01
5	2.5800	0.2719E-01
6	2.6300	0.2734E-01
7	2.8400	0.2728E-01
8	2.8900	0.2718E-01
9	2.9500	0.2728E-01
* 10	3.0000	0.2697E-01
11	3.0600	0.2723E-01
12	3.1100	0.2706E-01
* 13	3.1700	0.2749E-01
14	3.4100	0.2719E-01
15	3.4600	0.2709E-01
16	3.5200	0.2730E-01
17	3.5700	0.2719E-01
* 18	3.8400	0.2674E-01
19	3.9000	0.2711E-01
20	3.9500	0.2700E-01
21	4.0000	0.2727E-01
22	4.0500	0.2706E-01
23	4.3600	0.2724E-01
24	4.4100	0.2706E-01
25	4.4600	0.2698E-01
26	4.5100	0.2717E-01
27	4.5700	0.2719E-01
28	5.3500	0.2679E-01
29	5.4000	0.2679E-01
30	5.4500	0.2700E-01
31	5.4900	0.2700E-01
32	5.5500	0.2711E-01
33	5.6000	0.2690E-01

RUN NO. D0107

Ttc=610 C Ta=641 C
Ua=165 Cm/Sec Ud=227 Cm/Sec
Distance above Furnace Tube=0.64 cm

DROPLET NO.	FLIGHT DISTANCE, Cm	DIAMETER, Cm
1	1.9400	0.2696E-01
2	2.0000	0.2728E-01
3	2.0500	0.2700E-01
4	2.1000	0.2745E-01
5	2.1600	0.2700E-01
6	2.4400	0.2721E-01
7	2.5000	0.2699E-01
8	2.5500	0.2744E-01
9	2.6000	0.2699E-01
10	2.6900	0.2730E-01
11	2.9800	0.2694E-01
12	3.0300	0.2721E-01
13	3.0800	0.2699E-01
14	3.1300	0.2726E-01
15	4.6900	0.2695E-01
16	5.0000	0.2711E-01
17	5.0500	0.2711E-01
18	5.1000	0.2702E-01
19	5.4100	0.2702E-01
20	5.5000	0.2688E-01
21	5.5500	0.2698E-01
22	5.6000	0.2684E-01
23	5.6400	0.2688E-01
24	5.6900	0.2688E-01

RUN NO. NO108

Ttc=679 C Ta=719 C
Ua=179 Cm/Sec Ud=214 Cm/Sec
Distance above Furnace Tube=0.64 cm

DROPLET NO.	FLIGHT DISTANCE, Cm	DIAMETER, Cm
1	1.8500	0.2664E-01
2	1.9000	0.2660E-01
3	1.9500	0.2687E-01
4	2.0000	0.2687E-01
* 5	2.0600	0.2651E-01
6	2.1100	0.2673E-01
7	2.1600	0.2660E-01
8	2.3600	0.2660E-01
9	2.4200	0.2673E-01
10	2.4700	0.2673E-01
11	2.5100	0.2678E-01
12	2.5700	0.2678E-01
13	2.6200	0.2655E-01
14	2.6700	0.2669E-01
15	3.2100	0.2682E-01
16	3.2600	0.2682E-01
17	3.3100	0.2660E-01
18	3.8000	0.2669E-01
19	3.8500	0.2678E-01
20	3.9000	0.2664E-01
21	3.9400	0.2651E-01
22	3.9900	0.2651E-01
23	4.0400	0.2673E-01
24	4.0800	0.2655E-01
25	4.1300	0.2664E-01
26	4.3900	0.2663E-01
27	4.4300	0.2644E-01
28	4.4800	0.2637E-01

RUN NO. NA108

Ttc=679 C Ta=719 C
Ua=179 Cm/Sec Ud=194 Cm/Sec
Distance above Furnace Tube=0.64 cm

DROPLET NO.	FLIGHT DISTANCE, Cm	DIAMETER, Cm
1	1.8400	0.2640E-01
2	1.8900	0.2613E-01
3	1.9400	0.2640E-01
4	1.9800	0.2600E-01
5	2.0400	0.2631E-01
6	2.0900	0.2600E-01
7	2.3900	0.2623E-01
8	2.4400	0.2614E-01
9	2.4800	0.2632E-01
10	2.5300	0.2601E-01
11	2.5800	0.2614E-01
12	2.9200	0.2604E-01
13	2.9700	0.2606E-01
14	3.0100	0.2622E-01
15	3.0600	0.2626E-01
16	3.9100	0.2598E-01
17	3.9600	0.2620E-01
18	4.0000	0.2584E-01
19	4.0500	0.2602E-01
20	4.3900	0.2582E-01
21	4.4300	0.2586E-01
22	4.4800	0.2586E-01
23	4.5200	0.2595E-01
24	4.5700	0.2595E-01
25	4.9300	0.2607E-01
26	4.9700	0.2607E-01
27	5.0600	0.2582E-01
28	5.1000	0.2595E-01
29	5.4300	0.2582E-01
30	5.4800	0.2586E-01
31	5.5200	0.2565E-01
32	5.5600	0.2582E-01
33	5.6000	0.2582E-01

RUN NO. C0111

Ttc=679 C Ta=719 C
Ua=179 Cm/Sec Ud=254 Cm/Sec
Distance above Furnace Tube=0.64 cm

DROPLET NO.	FLIGHT DISTANCE, Cm	DIAMETER, Cm
1	1.8100	0.2738E-01
2	1.8700	0.2763E-01
3	1.9200	0.2738E-01
4	1.9800	0.2738E-01
5	2.0300	0.2738E-01
6	2.0900	0.2763E-01
* 7	2.4000	0.2713E-01
8	2.4600	0.2763E-01
9	2.5100	0.2753E-01
* 10	2.5700	0.2773E-01
11	2.7300	0.2720E-01
12	2.7800	0.2755E-01
13	2.8400	0.2745E-01
14	3.2200	0.2728E-01
15	3.2700	0.2728E-01
16	3.3300	0.2758E-01
17	3.3800	0.2738E-01
18	3.8200	0.2710E-01
19	3.8700	0.2725E-01
20	3.9200	0.2720E-01
21	3.9700	0.2737E-01
22	4.0200	0.2720E-01
23	4.0700	0.2748E-01
24	4.1200	0.2720E-01
25	4.8600	0.2719E-01
26	4.9100	0.2715E-01
27	4.9600	0.2741E-01
28	5.0100	0.2715E-01
29	5.0600	0.2714E-01
30	5.1000	0.2703E-01
31	5.2900	0.2693E-01
32	5.3400	0.2708E-01
33	5.3800	0.2698E-01
34	5.4300	0.2733E-01
35	5.4800	0.2703E-01
36	5.5300	0.2733E-01
37	5.5700	0.2698E-01
38	5.6200	0.2698E-01
39	5.6700	0.2698E-01

RUN NO. CA111

Ttc=679 C Ta=719 C
Ua=179 Cm/Sec Ud=270 Cm/Sec
Distance above Furnace Tube=0.64 cm

DROPLET NO.	FLIGHT DISTANCE, Cm	DIAMETER, Cm
1	2.4300	0.2715E-01
2	2.4800	0.2670E-01
3	2.5300	0.2750E-01
4	2.5900	0.2720E-01
5	2.9100	0.2752E-01
6	2.9600	0.2707E-01
7	3.0200	0.2727E-01
8	3.0700	0.2707E-01
9	3.1200	0.2737E-01
10	3.3600	0.2645E-01
11	3.4200	0.2660E-01
12	3.4700	0.2635E-01
13	3.5200	0.2684E-01
14	3.5700	0.2635E-01
15	3.8000	0.2726E-01
16	3.8500	0.2691E-01
17	3.9000	0.2726E-01
18	3.9500	0.2716E-01
19	4.0500	0.2716E-01
20	4.1100	0.2741E-01
21	4.3600	0.2686E-01
22	4.4100	0.2681E-01
23	4.4600	0.2651E-01
24	4.5100	0.2681E-01
25	4.5600	0.2641E-01
26	4.6100	0.2691E-01
27	4.9100	0.2676E-01
28	4.9600	0.2691E-01
29	5.0000	0.2670E-01
30	5.0500	0.2681E-01
31	5.1000	0.2681E-01

RUN NO. D0113

Ttc=680 C Ta=720 C
Ua=179 Cm/Sec Ud=243 Cm/Sec
Distance above Furnace Tube=0.64 cm

DROPLET NO.	FLIGHT DISTANCE, Cm	DIAMETER, Cm
1	2.8100	0.2634E-01
2	2.9100	0.2658E-01
3	3.3500	0.2648E-01
4	3.4000	0.2638E-01
5	3.4500	0.2654E-01
6	3.5000	0.2643E-01
7	3.5500	0.2638E-01
8	3.6000	0.2638E-01
9	3.6500	0.2628E-01
10	3.9100	0.2638E-01
11	3.9500	0.2623E-01
12	4.0000	0.2638E-01
13	4.0500	0.2643E-01
14	4.4100	0.2621E-01
15	4.4500	0.2626E-01
16	4.5000	0.2631E-01
17	4.5500	0.2631E-01
18	4.6000	0.2641E-01
19	4.6500	0.2631E-01
20	4.6900	0.2646E-01
21	4.8900	0.2611E-01
22	4.9400	0.2624E-01
23	4.9900	0.2645E-01
24	5.0300	0.2629E-01
25	5.0800	0.2645E-01
26	5.1200	0.2619E-01
27	5.3400	0.2627E-01
28	5.3900	0.2617E-01
29	5.4400	0.2617E-01
30	5.4800	0.2627E-01
31	5.5300	0.2622E-01
32	5.5700	0.2622E-01
33	5.6200	0.2607E-01

RUN NO. NO109

Ttc=727 C Ta=774 C
Ua=189 Cm/Sec Ud=252 Cm/Sec
Distance above Furnace Tube=0.64 cm

DROPLET NO.	FLIGHT DISTANCE, Cm	DIAMETER, Cm
1	2.3700	0.2711E-01
2	2.4300	0.2720E-01
3	2.4900	0.2734E-01
4	2.5400	0.2705E-01
5	2.6000	0.2734E-01
6	2.6500	0.2692E-01
7	2.8700	0.2734E-01
8	2.9200	0.2698E-01
9	2.9800	0.2721E-01
10	3.0300	0.2695E-01
11	3.0800	0.2725E-01
12	3.1400	0.2701E-01
13	3.4500	0.2715E-01
14	3.9400	0.2703E-01
15	4.0000	0.2712E-01
16	4.0500	0.2708E-01
17	4.0900	0.2698E-01
18	4.8800	0.2692E-01
19	4.9300	0.2707E-01
20	4.9800	0.2707E-01
21	5.0300	0.2703E-01
22	5.0800	0.2698E-01
23	5.1300	0.2703E-01
24	5.3600	0.2693E-01
25	5.4100	0.2679E-01
26	5.4500	0.2696E-01
27	5.5000	0.2703E-01
28	5.5600	0.2695E-01
29	5.6000	0.2675E-01

RUN NO. NO121

Ttc=727 C Ta=774 C
Ua=189 Cm/Sec Ud=240 Cm/Sec
Distance above Furnace Tube=0.64 cm

DROPLET NO.	FLIGHT DISTANCE, Cm	DIAMETER, Cm
1	2.3800	0.2754E-01
2	2.4400	0.2786E-01
3	2.5000	0.2754E-01
4	2.5600	0.2772E-01
5	2.6100	0.2786E-01
6	3.8300	0.2744E-01
7	3.8800	0.2767E-01
8	3.9400	0.2753E-01
9	4.0000	0.2776E-01
10	4.0600	0.2753E-01
11	4.3200	0.2726E-01
12	4.3800	0.2768E-01
13	4.4400	0.2759E-01
14	4.5000	0.2773E-01
15	4.5500	0.2754E-01
16	4.6100	0.2782E-01
17	4.8000	0.2717E-01
18	4.8500	0.2754E-01
19	4.9100	0.2740E-01
20	4.9600	0.2778E-01
21	5.0200	0.2754E-01
22	5.0800	0.2749E-01
23	5.3400	0.2707E-01
24	5.4000	0.2749E-01
25	5.4500	0.2731E-01
26	5.5000	0.2754E-01
27	5.5600	0.2731E-01
28	5.6200	0.2759E-01

RUN NO. C0110

Ttc=721 C Ta=767 C
Ua=188 Cm/Sec Ud=255 Cm/Sec
Distance above Furnace Tube=0.64 cm

	DROPLET NO.	FLIGHT DISTANCE, Cm	DIAMETER, Cm
	1	1.9300	0.2748E-01
	2	1.9800	0.2729E-01
	3	2.0400	0.2734E-01
	4	2.1000	0.2744E-01
*	5	2.3900	0.2688E-01
	6	2.4500	0.2712E-01
*	7	2.5000	0.2683E-01
	8	2.5600	0.2712E-01
	9	2.8700	0.2707E-01
	10	2.9200	0.2741E-01
	11	2.9700	0.2727E-01
	12	3.0900	0.2727E-01
	13	3.1400	0.2717E-01
	14	3.3900	0.2727E-01
*	15	3.4400	0.2678E-01
*	16	3.4900	0.2678E-01
	17	3.8400	0.2717E-01
	18	3.8900	0.2703E-01
	19	3.9400	0.2722E-01
	20	3.9900	0.2703E-01
	21	4.0500	0.2722E-01
	22	4.1000	0.2693E-01
	23	4.3800	0.2720E-01
	24	4.4300	0.2715E-01
	25	4.4800	0.2691E-01
	26	4.5400	0.2701E-01
	27	4.5900	0.2691E-01
	28	5.4000	0.2678E-01
	29	5.4500	0.2688E-01
	30	5.5000	0.2674E-01
	31	5.5500	0.2703E-01
	32	5.6000	0.2685E-01

RUN NO. CA110

Ttc=721 C Ta=767 C
Ua=188 Cm/Sec Ud=249 Cm/Sec
Distance above Furnace Tube=0.64 cm

DROPLET NO.	FLIGHT DISTANCE, Cm	DIAMETER, Cm
1	1.9000	0.2703E-01
2	1.9600	0.2727E-01
3	2.0100	0.2741E-01
* 4	2.0700	0.2684E-01
5	2.1200	0.2736E-01
6	2.4000	0.2719E-01
7	2.4500	0.2714E-01
8	2.5000	0.2719E-01
9	2.5600	0.2709E-01
10	2.8700	0.2714E-01
11	2.9300	0.2709E-01
12	2.9800	0.2714E-01
13	3.0300	0.2699E-01
14	3.4900	0.2720E-01
15	3.8800	0.2710E-01
16	3.9400	0.2711E-01
17	3.9900	0.2701E-01
18	4.0300	0.2729E-01
19	4.3800	0.2709E-01
20	4.4300	0.2704E-01
21	4.4800	0.2709E-01
22	4.5300	0.2704E-01
23	4.5800	0.2714E-01
24	4.8300	0.2714E-01
25	4.8800	0.2719E-01
26	4.9300	0.2704E-01
27	4.9800	0.2723E-01
28	5.0300	0.2714E-01
29	5.1300	0.2699E-01
30	5.3700	0.2710E-01
31	5.4200	0.2686E-01
32	5.4600	0.2710E-01
33	5.5200	0.2686E-01
34	5.5700	0.2686E-01
35	5.6100	0.2681E-01

RUN NO. D0112

Ttc=725 C Ta=771 C
Ua=189 Cm/Sec Ud=232 Cm/Sec
Distance above Furnace Tube=0.64 cm

	DROPLET NO.	FLIGHT DISTANCE, Cm	DIAMETER, Cm
	1	3.4100	0.2690E-01
	2	3.4600	0.2664E-01
	3	3.5100	0.2679E-01
	4	3.5500	0.2659E-01
*	5	3.6100	0.2638E-01
	6	3.6600	0.2664E-01
	7	3.7100	0.2659E-01
	8	3.9300	0.2679E-01
*	9	3.9800	0.2638E-01
	10	4.0300	0.2679E-01
	11	4.1300	0.2664E-01
	12	4.1800	0.2674E-01
	13	4.2200	0.2674E-01
	14	4.4500	0.2665E-01
	15	4.4900	0.2660E-01
	16	4.5400	0.2660E-01
	17	4.5900	0.2660E-01
	18	4.6800	0.2660E-01
	19	4.9000	0.2643E-01
	20	4.9500	0.2674E-01
	21	4.9900	0.2643E-01
	22	5.0400	0.2633E-01
	23	5.0900	0.2659E-01
	24	5.1300	0.2638E-01
	25	5.1800	0.2643E-01

RUN NO. D0122

Ttc=732 C Ta=779 C
Ua=190 Cm/Sec Ud=265 Cm/Sec
Distance above Furnace Tube=0.64 cm

DROPLET NO.	FLIGHT DISTANCE, Cm	DIAMETER, Cm
1	2.4000	0.2771E-01
2	2.4600	0.2745E-01
3	2.5200	0.2769E-01
4	2.5800	0.2745E-01
5	2.8000	0.2794E-01
6	2.8500	0.2760E-01
7	3.3300	0.2755E-01
8	3.3900	0.2755E-01
9	3.4500	0.2769E-01
10	3.5000	0.2755E-01
11	3.5700	0.2779E-01
12	3.6200	0.2755E-01
13	3.7700	0.2748E-01
14	3.8200	0.2748E-01
15	3.8800	0.2782E-01
16	3.9400	0.2748E-01
17	4.0000	0.2762E-01
18	4.1100	0.2772E-01
19	4.2800	0.2769E-01
20	4.3400	0.2754E-01
21	4.4000	0.2730E-01
22	4.4500	0.2749E-01
23	4.5100	0.2745E-01
24	4.5700	0.2745E-01
25	4.8100	0.2726E-01
26	4.8600	0.2760E-01
27	5.0300	0.2755E-01
28	5.3400	0.2731E-01
29	5.3900	0.2706E-01
30	5.4400	0.2745E-01
31	5.5000	0.2716E-01
32	5.5500	0.2755E-01
33	5.6100	0.2745E-01

RUN NO. NO115

Ttc=728 C Ta=775 C
Ua=150 Cm/Sec Ud=265 Cm/Sec
Distance above Furnace Tube=0.64 cm

DROPLET NO.	FLIGHT DISTANCE, Cm	DIAMETER, Cm
1	1.8900	0.2679E-01
2	1.9500	0.2660E-01
3	2.0000	0.2684E-01
4	2.0600	0.2675E-01
5	2.1100	0.2699E-01
6	2.4700	0.2673E-01
7	2.5200	0.2668E-01
8	2.5800	0.2686E-01
9	2.6400	0.2673E-01
10	2.9000	0.2692E-01
11	2.9600	0.2692E-01
12	3.0000	0.2673E-01
13	3.0600	0.2649E-01
14	3.1100	0.2663E-01
15	3.3400	0.2654E-01
16	3.3900	0.2682E-01
17	3.4500	0.2668E-01
18	3.6100	0.2649E-01
19	3.8200	0.2649E-01
20	3.8800	0.2682E-01
21	3.9300	0.2673E-01
22	3.9800	0.2682E-01
23	4.0300	0.2673E-01
24	4.0800	0.2663E-01
25	4.3400	0.2653E-01
26	4.4000	0.2644E-01
27	4.4500	0.2682E-01
28	4.5000	0.2645E-01
29	4.5500	0.2673E-01
30	4.9000	0.2630E-01
31	5.0000	0.2649E-01
32	5.0500	0.2673E-01
33	5.1000	0.2668E-01
34	5.4000	0.2643E-01
35	5.4500	0.2650E-01
36	5.5000	0.2637E-01
37	5.5500	0.2635E-01
38	5.6000	0.2649E-01

RUN NO. NO114

Ttc=725 C Ta=771 C
Ua=167 Cm/Sec Ud=290 Cm/Sec
Distance above Furnace Tube=0.64 cm

DROPLET NO.	FLIGHT DISTANCE, Cm	DIAMETER, Cm
1	1.9000	0.2680E-01
2	1.9600	0.2707E-01
3	2.0100	0.2697E-01
4	2.0700	0.2697E-01
5	2.4600	0.2693E-01
6	2.5100	0.2683E-01
7	2.5700	0.2678E-01
8	2.6300	0.2711E-01
9	2.6900	0.2697E-01
10	2.8700	0.2669E-01
11	2.9300	0.2693E-01
12	2.9900	0.2697E-01
13	3.0400	0.2697E-01
14	3.1000	0.2683E-01
15	3.1500	0.2688E-01
16	3.4300	0.2699E-01
17	3.4900	0.2685E-01
18	3.5400	0.2699E-01
19	3.6000	0.2666E-01
20	3.6500	0.2695E-01
21	4.0100	0.2659E-01
22	4.0600	0.2692E-01
23	4.1700	0.2663E-01
24	4.3900	0.2666E-01
25	4.4400	0.2680E-01
26	4.5000	0.2657E-01
27	4.5500	0.2676E-01
28	4.6000	0.2671E-01
29	4.6600	0.2662E-01
30	4.7100	0.2666E-01

RUN NO. NA114

Ttc=725 C Ta=771 C
Ua=167 Cm/Sec Ud=271 Cm/Sec
Distance above Furnace Tube=0.64 cm

DROPLET NO.	FLIGHT DISTANCE, Cm	DIAMETER, Cm
1	2.3800	0.2706E-01
2	2.4300	0.2685E-01
3	2.4900	0.2722E-01
4	2.6000	0.2701E-01
5	2.9000	0.2682E-01
6	2.9500	0.2701E-01
7	3.0000	0.2710E-01
8	3.0600	0.2724E-01
9	3.1200	0.2701E-01
10	3.1700	0.2701E-01
11	3.4100	0.2685E-01
* 12	3.4600	0.2653E-01
13	3.5100	0.2662E-01
* 14	3.5700	0.2648E-01
* 15	3.6200	0.2653E-01
16	3.6700	0.2662E-01
17	3.8200	0.2706E-01
18	3.8800	0.2701E-01
19	3.9300	0.2701E-01
20	3.9900	0.2701E-01
21	4.0400	0.2701E-01
22	4.0900	0.2677E-01
23	4.1400	0.2692E-01
24	4.3800	0.2661E-01
25	4.4200	0.2684E-01
26	4.4600	0.2661E-01
27	4.5200	0.2679E-01
28	4.5700	0.2661E-01
29	4.6200	0.2661E-01
30	4.6700	0.2661E-01
31	4.8900	0.2675E-01
32	4.9500	0.2650E-01
33	5.0000	0.2683E-01
34	5.0500	0.2664E-01
35	5.1000	0.2652E-01
36	5.1500	0.2660E-01
37	5.3700	0.2655E-01
38	5.4200	0.2667E-01
39	5.5100	0.2667E-01

RUN NO. NA113

Ttc=732 C Ta=779 C
Ua=212 Cm/Sec Ud=267 Cm/Sec
Distance above Furnace Tube=0.64 cm

DROPLET NO.	FLIGHT DISTANCE, Cm	DIAMETER, Cm
1	1.9100	0.2652E-01
2	1.9700	0.2652E-01
* 3	2.0200	0.2678E-01
4	2.0800	0.2626E-01
5	2.1300	0.2663E-01
* 6	2.1800	0.2611E-01
7	2.4700	0.2642E-01
8	2.5200	0.2626E-01
9	2.5800	0.2652E-01
10	2.6300	0.2637E-01
11	2.9500	0.2652E-01
12	3.0000	0.2642E-01
13	3.0500	0.2647E-01
14	3.1000	0.2642E-01
15	3.1500	0.2627E-01
16	3.4100	0.2652E-01
17	3.4600	0.2626E-01
18	3.5200	0.2652E-01
19	3.5700	0.2626E-01
20	4.0200	0.2611E-01
21	4.0700	0.2642E-01
22	4.3900	0.2638E-01
23	4.4400	0.2621E-01
24	4.4900	0.2626E-01
25	4.5400	0.2617E-01
26	4.5900	0.2626E-01
27	4.6400	0.2634E-01
28	4.8100	0.2623E-01
29	4.9100	0.2618E-01

RUN NO. NA116

Ttc=728 C Ta=775 C
Ua=150 Cm/Sec Ud=542 Cm/Sec
Distance above Furnace Tube=0.64 cm

DROPLET NO.	FLIGHT DISTANCE, Cm	DIAMETER, Cm
1	1.9400	0.2944E-01
2	2.0300	0.2969E-01
3	2.1200	0.2994E-01
4	2.5200	0.2965E-01
5	2.6000	0.2944E-01
6	2.8700	0.2960E-01
7	2.9600	0.2994E-01
8	3.0400	0.2942E-01
9	3.1300	0.2998E-01
10	3.4000	0.2944E-01
11	3.4800	0.2959E-01
12	3.5600	0.2944E-01
13	3.6500	0.2984E-01
14	3.8800	0.2944E-01
15	3.9600	0.2949E-01
16	4.0500	0.2994E-01
17	4.1300	0.2944E-01
18	4.4100	0.2994E-01
19	4.4900	0.2944E-01
20	4.5700	0.2984E-01
21	4.6500	0.2930E-01
22	4.8400	0.2979E-01
23	4.9200	0.2935E-01
24	5.0000	0.2964E-01
25	5.0900	0.2935E-01
26	5.1700	0.2964E-01

RUN NO. NO116

Ttc=728 C Ta=775 C
Ua=150 Cm/Sec Ud=427 Cm/Sec
Distance above Furnace Tube=0.64 cm

DROPLET NO.	FLIGHT DISTANCE, Cm	DIAMETER, Cm
* 1	2.5100	0.3054E-01
2	2.6000	0.3034E-01
3	2.9500	0.3025E-01
4	3.0500	0.3029E-01
5	3.1400	0.3025E-01
6	3.4500	0.3015E-01
7	3.9800	0.3015E-01
8	4.0700	0.3029E-01
9	4.1600	0.3005E-01
* 10	4.4600	0.2983E-01
* 11	4.5400	0.3047E-01
12	4.6300	0.3008E-01
13	4.9900	0.3008E-01
14	5.1700	0.3025E-01
15	5.4600	0.2990E-01
16	5.5500	0.3021E-01
17	5.6400	0.2988E-01

RUN NO. NO124

Ttc=799 C Ta=858 C
Ua=204 Cm/Sec Ud=272 Cm/Sec
Distance above Furnace Tube=0.64 cm

DROPLET NO.	FLIGHT DISTANCE, Cm	DIAMETER, Cm
1	2.3900	0.2776E-01
2	2.4500	0.2797E-01
3	2.5100	0.2756E-01
4	2.5700	0.2802E-01
5	2.6300	0.2787E-01
6	2.6900	0.2807E-01
7	2.8300	0.2756E-01
8	2.9000	0.2807E-01
9	2.9600	0.2781E-01
10	3.0200	0.2787E-01
11	3.0800	0.2761E-01
12	3.1400	0.2797E-01
13	3.2000	0.2787E-01
14	3.3500	0.2771E-01
15	3.4100	0.2776E-01
16	3.4700	0.2781E-01
17	3.5300	0.2781E-01
18	3.6400	0.2776E-01
19	3.7000	0.2781E-01
20	3.8800	0.2756E-01
21	3.9400	0.2766E-01
22	4.0000	0.2771E-01
23	4.0500	0.2787E-01
24	4.1100	0.2766E-01
25	4.1700	0.2781E-01
26	4.4000	0.2761E-01
27	4.4600	0.2771E-01
28	4.5100	0.2766E-01
29	4.5700	0.2766E-01
30	4.6200	0.2756E-01
31	4.6800	0.2756E-01
32	4.8700	0.2766E-01
33	4.9200	0.2756E-01
34	4.9700	0.2756E-01
35	5.0300	0.2746E-01
36	5.0900	0.2756E-01
37	5.1400	0.2746E-01
38	5.4000	0.2759E-01
39	5.4600	0.2736E-01
40	5.5100	0.2746E-01
41	5.5700	0.2751E-01

RUN NO. NA124

Ttc=799 C Ta=858 C
Ua=204 Cm/Sec Ud=268 Cm/Sec
Distance above Furnace Tube=0.64 cm

DROPLET NO.	FLIGHT DISTANCE, Cm	DIAMETER, Cm
1	1.8600	0.2792E-01
2	1.9200	0.2843E-01
3	1.9800	0.2823E-01
4	2.0500	0.2843E-01
5	2.1100	0.2792E-01
6	2.1700	0.2838E-01
7	2.3400	0.2805E-01
8	2.4000	0.2817E-01
9	2.4600	0.2807E-01
10	2.5200	0.2807E-01
* 11	2.5900	0.2766E-01
12	2.6500	0.2833E-01
13	2.8600	0.2802E-01
14	2.9200	0.2828E-01
* 15	2.9800	0.2777E-01
16	3.0400	0.2818E-01
17	3.1000	0.2807E-01
18	3.1600	0.2833E-01
19	3.3900	0.2812E-01
20	3.4500	0.2807E-01
21	3.5000	0.2833E-01
22	3.5600	0.2802E-01
23	3.6200	0.2807E-01
24	3.8700	0.2799E-01
25	3.9300	0.2819E-01
26	3.9800	0.2830E-01
27	4.0400	0.2789E-01
28	4.1000	0.2809E-01
29	4.1600	0.2830E-01
30	4.3500	0.2801E-01
31	4.4000	0.2812E-01
32	4.4600	0.2807E-01
33	4.5200	0.2817E-01
34	4.5700	0.2790E-01
35	4.6300	0.2780E-01
36	5.3200	0.2807E-01
37	5.3800	0.2771E-01
38	5.4400	0.2812E-01
39	5.4900	0.2775E-01
40	5.5500	0.2785E-01
41	5.6000	0.2807E-01

RUN NO. CA126

Ttc=801 C Ta=860 C
Ua=205 Cm/Sec Ud=254 Cm/Sec
Distance above Furnace Tube=0.64 cm

DROPLET NO.	FLIGHT DISTANCE, Cm	DIAMETER, Cm
1	1.8900	0.2652E-01
2	1.9500	0.2673E-01
3	2.0000	0.2678E-01
4	2.0500	0.2668E-01
5	2.1100	0.2648E-01
6	2.3300	0.2668E-01
7	2.3800	0.2648E-01
8	2.4400	0.2658E-01
9	2.4900	0.2658E-01
10	2.5400	0.2646E-01
* 11	2.5900	0.2617E-01
12	2.6400	0.2673E-01
13	2.8700	0.2663E-01
14	2.9200	0.2673E-01
15	2.9700	0.2643E-01
16	3.0200	0.2648E-01
17	3.0700	0.2658E-01
18	3.1200	0.2663E-01
19	3.4000	0.2658E-01
20	3.4500	0.2632E-01
21	3.5000	0.2658E-01
22	3.5500	0.2612E-01
23	3.6000	0.2643E-01
24	3.6500	0.2648E-01
25	3.9900	0.2652E-01
26	4.0400	0.2621E-01
27	4.0900	0.2636E-01
28	4.1400	0.2605E-01
29	4.3400	0.2643E-01
30	4.3900	0.2637E-01
31	4.8600	0.2596E-01
32	4.9100	0.2607E-01
33	4.9600	0.2643E-01
34	5.0000	0.2612E-01
35	5.0500	0.2643E-01
36	5.1600	0.2612E-01

RUN NO. D0124

Ttc=799 C Ta=858 C
Ua=204 Cm/Sec Ud=268 Cm/Sec
Distance above Furnace Tube=0.64 cm

DROPLET NO.	FLIGHT DISTANCE, Cm	DIAMETER, Cm
* 1	1.3900	0.2945E-01
* 2	1.4600	0.2921E-01
* 3	1.5400	0.2960E-01
* 4	1.6100	0.2931E-01
* 5	1.6800	0.2941E-01
6	1.8800	0.2930E-01
7	1.9500	0.2944E-01
8	2.0200	0.2958E-01
9	2.0900	0.2936E-01
10	2.1700	0.2954E-01
11	2.4200	0.2921E-01
12	2.4800	0.2921E-01
13	2.5600	0.2931E-01
14	2.6300	0.2951E-01
15	2.6900	0.2935E-01
16	2.8200	0.2921E-01
17	2.8800	0.2941E-01
18	3.3800	0.2937E-01
19	3.4400	0.2916E-01
20	3.5100	0.2918E-01
21	3.5800	0.2926E-01
22	3.6500	0.2937E-01
23	3.8700	0.2934E-01
24	3.9400	0.2934E-01
25	4.0100	0.2944E-01
26	4.0700	0.2924E-01
27	4.1400	0.2914E-01
28	4.2100	0.2934E-01
29	4.3200	0.2924E-01
30	4.3800	0.2934E-01
31	4.4500	0.2913E-01
32	4.9000	0.2904E-01
33	4.9700	0.2924E-01
34	5.0300	0.2910E-01
35	5.1000	0.2898E-01
36	5.1600	0.2912E-01
37	5.3500	0.2913E-01
38	5.4200	0.2895E-01
39	5.4800	0.2908E-01
40	5.5400	0.2897E-01
41	5.6100	0.2893E-01

VITA

The author was born on April 1, 1949, in Taipei, Taiwan. He attended elementary schools in that city and was graduated from the High School affiliated with National Taiwan Normal University in Taipei in June 1967. The following September he entered Feng Chia University, and in June 1971 he received a Bachelor of Science degree in Chemical Engineering.

After a two-year service in the army, he entered the Graduate School of Georgia Institute of Technology in September 1974. He was awarded a Master of Science degree in June 1976.

In September 1976 he was admitted in the Graduate School of The University of Tennessee, Knoxville, studying toward a Ph.D. degree in Chemical Engineering.

The author has been employed by Burlington Industries since 1981.